CHEMICAL REVIEWS

pubs.acs.org/CR

Review

Ab Initio Simulations of Water/Metal Interfaces

Axel Groß* and Sung Sakong

Cite This: https://doi.org/10.1021/acs.chemrev.1c00679

Read Online

ACCESS | Metrics & More | Article Recommendations

ABSTRACT: Structures and processes at water/metal interfaces play an important technological role in electrochemical energy conversion and storage, photoconversion, sensors, and corrosion, just to name a few. However, they are also of fundamental significance as a model system for the study of solid−liquid interfaces, which requires combining concepts from the chemistry and physics of crystalline materials and liquids. Particularly interesting is the fact that the water−water and water−metal interactions are of similar strength so that the structures at water/metal interfaces result from a competition between these comparable interactions. Because water is a polar molecule and water and metal surfaces are both polarizable, explicit consideration of the electronic degrees of freedom at water/metal interfaces is mandatory. In principle, ab initio molecular dynamics simulations are thus the method of choice to model water/metal interfaces, but they are computationally still rather demanding. Here, ab initio simulations of water/metal interfaces will be reviewed, starting from static systems such as the adsorption of single water molecules, water clusters, and icelike layers, followed by the properties of liquid water layers at metal surfaces. Technical issues such as the appropriate first-principles description of the water−water and water−metal interactions will be discussed, and electrochemical aspects will be addressed. Finally, more approximate but numerically less demanding approaches to treat water at metal surfaces from first-principles will be briefly discussed.

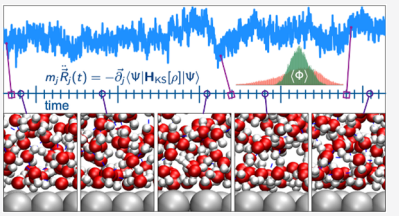

CONTENTS

1. INTRODUCTION

Water with its chemical formula H_2O is a seemingly simple inorganic molecule that is transparent, tasteless, odorless, and nearly colorless. At the same time it is one of the most mysterious liquids on our planet due to a large number of anomalies compared to simple liquids.[1,2] Water is not only essential for all known forms of life, but its interaction with interfaces also plays a critical technological role.[2,3] For example, fuel cells and electrolyzers, but also many photocatalysts, are based on electrocatalytic processes at the interface between an aqueous electrolyte and an electrode.[4] Yet, processes that one would rather like to avoid, such as corrosion, also occur at water/metal interfaces.[5] Thus, it is

Special Issue: Computational Electrochemistry

Received: August 1, 2021

no surprise that the interaction of water with solid surfaces, in particular metal surfaces, has been the subject of many experimental and theoretical studies, which have been covered in a number of reviews.[2,3,5−13]

Surface scientists have also been interested in the atomistic study of water−metal interfaces for a rather long time.[6,8,11] From a fundamental point of view, it is interesting to note that the water−metal interaction is of similar strength as the water−water interaction.[14−16] Hence, the water structures at water/metal interfaces result from a balance of these comparable and competing attractive interactions. Furthermore, these interfaces also serve as model systems for the study of liquid/solid interfaces. However, ultrahigh-vacuum (UHV) chambers are required in order to apply the rigor of surface science techniques in the structure determination of water layers on metal surfaces by employing experimental tools with atomistic resolution such as scanning tunneling microscopy (STM). Due to the relatively low water adsorption energies on metal surfaces, the water molecules already start to desorb at temperatures around 150 K in ultrahigh-vacuum conditions.[11]

It might be likely that in general at such low temperatures only icelike layers exist. Hence, first-principles electronic structure studies based on density functional theory (DFT) concentrated on the structure of either adsorbed isolated water molecules and clusters[16] or thin icelike layers.[5] These theoretical studies provided valuable insights into the subtle balance between water−metal and water−water interactions governing the structure formation of adsorbed water. Still, most of the technically relevant applications including water/metal interfaces involve liquid water. Unfortunately, the modeling of liquid water requires taking the statistical nature of liquids into account through, e.g., appropriate averaging along sufficiently long molecular dynamics trajectories. In spite of the ever-increasing computer power and the development of more efficient first-principles codes, ab initio molecular dynamics (AIMD) simulations are still computationally rather demanding.[17−21] Still, computationally less expensive methods typically cannot faithfully capture important aspects of the water−metal interaction such as, e.g., the strong polarization effects occurring at these interfaces.[22−24] Hence, ab initio simulations are compulsory for a true fundamental understanding of the scientifically interesting and technologically important structures and processes at water/metal interfaces.[22,25,26] At the same time, they are essential to benchmark more approximate but numerically less demanding theoretical approaches.[27,28]

Here we will review ab initio simulation studies addressing structures and processes at water/metal interfaces. However, before discussing these structures, one first needs to address technical aspects related to the choice of the proper method for an appropriate description of the water−water and water−metal interaction. We will then start with the description of first-principles studies of adsorbed water molecules, clusters, and icelike layers. We will continue with AIMD simulations of liquid water layers on metal surfaces. Macroscopic liquid water always contains solvated ions, already through the autionization of water, that can adsorb rather strongly on metal surfaces. These ions are also essential in electrochemistry, which is concerned with structures and processes at the interface between an electron conductor, e.g., a metal electrode, and an ion conductor, e.g., an aqueous electrolyte. Hence, we will also address ab initio studies that are concerned with adsorbate-covered metal surfaces in the presence of water. Finally, we will discuss approximate models of water/metal interfaces using implicit solvent models. It should be noted that the first AIMD simulations of water/metal interfaces were done only 20 years ago;[29,30] hence, this is still a relatively young field. This Review shall illustrate the progress that has been made in our understanding of water/metal interfaces based on ab initio simulations of water/metal interfaces in these last 20 years.

Furthermore, water/metal interfaces also play an important role in electrochemical devices and processes, for example, in electrocatalysis or fuel cells. Hence, theoretical studies of metal interfaces are relevant for, e.g., a better understanding of the structure of electric double layers at electrochemical interfaces.[25] Continuum-based concepts to analyze the structure of an electric double layer were developed more than 100 years ago,[31−34] and they are still used nowadays in the discussion of electrochemical interfaces. Hence, we will also briefly touch electrochemical topics, for example, the structure of water/metal interfaces under electrochemical control, and see whether the traditional concepts are still valid. However, electrochemistry is not the focus of this Review. For more detailed information on electrochemical aspects derived from simulations of water/metal interfaces, we refer the reader to the large number of corresponding reviews.[21,25,35−39]

2. THEORETICAL DESCRIPTION OF THE WATER−WATER AND WATER−METAL INTERACTIONS

This Review focuses on studies providing an atomistic understanding of structures and processes at water/metal interfaces. Because of the high computational effort associated with an appropriate consideration of the liquid nature of water, numerically inexpensive approaches such as force-field methods appear to be the natural choice. Indeed, there are well-suited parametrized classical interaction potentials that faithfully describe the water−water interaction and reproduce structural properties of water rather satisfactorily.[40−42] These reliable water interaction potentials have also been used in molecular dynamics studies addressing the structure of the metal−water interface at finite temperatures.[43−47] Such studies have certainly provided the basis for a fundamental understanding of the properties of water/metal interfaces. Still, it needs to be noted that classical parametrized interaction potentials typically only describe one family of materials reliably. However, there is no interpolation scheme based on physical and chemical concepts that reproduces water and metal properties satisfactorily at the same time. Force fields are well-suited to describe covalently and weakly bonded systems, but they do not really capture the essence of metal bonding. Besides, force fields typically fail to describe bond-breaking and bond-making processes. Reactive force fields based on bond-order concepts[48] are free from this restriction, but they require a considerable fitting effort and are therefore typically restricted to a small number of elements.[49,50] On the other hand, interpolation schemes including many-body effects such as the embedded atom method (EAM)[51,52] are appropriate for simple metals but cannot appropriately reproduce covalent bonding.

Recently, techniques based on machine learning such as artificial networks have become rather popular as a tool to represent interaction potentials.[27,28,53−58] They are very versatile and in principle can reproduce any multidimensional potential energy surface. In fact, they have already been

https://doi.org/10.1021/acs.chemrev.1c00679
Chem. Rev. XXXX, XXX, XXX−XXX

successfully applied to address structural properties of liquid water,[57] water/metal interfaces,[27] and water/oxide interfaces.[59] However, because their construction procedure is not based on any chemical insights, their fitting usually requires large training sets.[53] Furthermore, similar to many other interpolation schemes, the effort to obtain neural-network interaction potentials often scales exponentially with the number of atom types considered in the potential.

Instead of classical interaction potentials, semiempirical methods taking the quantum nature of the atomic interaction into account to a certain extent might be suitable for the description of water/metal interfaces. For example, the empirical valence-bond (EVB) model[60] has been used to describe the dynamics of the proton transfer from an electrolyte to metal electrodes.[61−64] The EVB method can be regarded as an extension of the force-field approach by including a region that is treated quantum mechanically in the spirit of hybrid quantum mechanical/molecular mechanics (QM/MM) methods.[65] Because of its relative simplicity, EVB methods allow one to treat systems of several thousands of atoms over long time scales. Still it suffers from the problem of all empirical interaction models: taking into account a new element in the simulation that has not been parametrized before requires a considerable additional fitting effort.

First-principles methods avoid this problem as they are in principle universal and capable of treating all chemical systems of interest. The only inputs needed are the element numbers of the considered atoms. In the fields of surface, interface, and condensed matter science, periodic DFT calculations represent the method of choice for first-principles electronic structure calculations.[66−68] Although there are first implementations of ab initio wave function-based quantum chemistry into periodic codes,[69] they are still much too time-consuming to address such extended systems. In the periodic DFT calculations, electron exchange and correlation are typically treated in the generalized gradient approximation (GGA) using functionals such as Perdew−Wang 1991 (PW91),[70] Perdew−Burke−Ernzerhof (PBE),[71] or its revised form (RPBE) in the implementation introduced by Hammer, Hansen, and Nørskov.[72] Hybrid DFT functionals including exact exchange are rather popular for bulk water simulations.[73] However, they are not appropriate for metal surfaces because they are still computationally very demanding for periodic systems and, even more importantly, they do not properly reproduce the properties of metals.[74]

However, for a reliable description of water/metal interfaces, it is important that the chosen functionals reliably reproduce metal properties, and they should also yield a good description of water properties. Unfortunately, AIMD simulations of liquid water using the PBE functional showed that PBE water is overstructured.[77−79] This overstructuring is illustrated in Figure 1, where the radial distribution functions g of the H−H, O−H, and O−O distances r derived from DFT liquid water simulations for several selected functionals[76] are compared to the results of neutron-scattering experiments.[75] With regard to the neutron-scattering data, the PBE results exhibit much higher peaks, i.e., PBE water exhibits a more crystalline structure than natural water. As a simple workaround, PBE water simulations have been run at a higher temperature of 350 K[77−79] at which the calculated radial distribution functions resemble the experimentally measured ones at 300 K.[80] However, this is not a satisfactory solution, as the dynamics

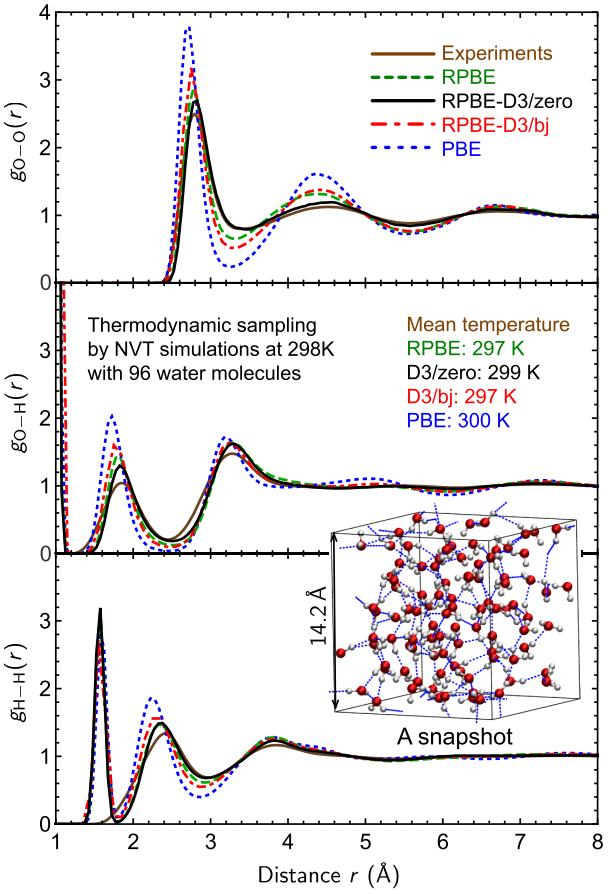

Figure 1. Radial distribution functions g of the H−H, O−H, and O−O distances r according to DFT liquid water simulations for different functionals compared to the results of neutron-scattering experiments.[75] Reprinted with permission from ref 76. Copyright 2016 AIP Publishing.

of the metal and the interface are sampled under wrong thermodynamic conditions.

The failure of the PBE functional to correctly describe the liquid water properties has been traced back to the lack of dispersive interactions in GGA functionals.[55,81−89] Including dispersion interactions in DFT liquid water simulations, either through semiempirical dispersion corrections[90,91] or through van der Waals functionals,[82,92,93] leads to a much better agreement with the experiment[84−88,94−96] for a variety of GGA and hybrid functionals. Still, for the PBE functional the addition of dispersion corrections does not lead to a significant improvement in the radial distribution functions of liquid water.[89,94] The overestimated directional hydrogen bonding of PBE does not vanish upon the addition of dispersion corrections. Water radial distributions very close to the experiment are obtained in AIMD simulations,[76,89,97] as Figure 1 demonstrates, only when the nondirectional dispersion interaction replaces this overestimated directional hydrogen bonding by replacing the PBE functional with the less-attractive RPBE functional together with the D3 dispersion corrections. The RPBE-D3 functional is not only successful in reproducing liquid water properties but also yields satisfactory results for the energetics and structures of small water clusters and bulk ice phases,[76] for molecular adsorption energies,[98] and even for the properties of supercritical water.[99,100] Still, the RPBE-D3 functional does not yield the proper relative

https://doi.org/10.1021/acs.chemrev.1c00679
Chem. Rev. XXXX, XXX, XXX−XXX

densities between the liquid and ice phases of water,[76] as is also the case for other GGA functionals including the van der Waals interaction.[86] This deficiency is corrected for when the strongly constrained and appropriately normed (SCAN) meta-GGA functional[101] is used.[102] Still, the RPBE-D3 functional represents a good choice for a reasonable trade-off between accuracy and computational performance in the first-principles description of liquid water and water/metal interfaces, as the consideration of dispersion interactions does not only improve the DFT treatment of liquid water. It also leads to a more accurate description of the metal−water interaction.[103−105]

Yet, there is another field of concern with respect to the simulation of water. Due to the light mass of hydrogen, quantum nuclear effects[106] might play a role in the water dynamics with respect to its thermodynamic quantities and structural properties.[12,107] For example, by applying quantum statistics for the occupation of the water O−H vibrations, a quantum correction of ∼0.04 eV per water molecule is obtained.[108] Furthermore, the influence of the quantum nuclear effects in water is also reflected by the fact that there is a nuclear isotope effect in the autoionization of water.[12] Quantum delocalization effects on the structural properties of water, for example, can be taken into account using path-integral methods.[109] Indeed, for proton transfer in liquid water according to the Grotthus mechanism, quantum-delocalization effects are non-negligible.[110] Still, there are conflicting results based on path-integral Car−Parrinello molecular dynamics studies on whether nuclear quantum effects soften[111] or harden[112] the structure of liquid water. Furthermore, path-integral studies also found that the O−O radial distribution function is hardly affected by nuclear quantum effects,[113] which could be due to the fact that there are competing quantum, tunneling, and zero-point effects that can cancel to a large extent.[113−115] In first-principles simulations of water/metal interfaces, nuclear quantum effects are typically neglected as their consideration is numerically rather demanding. Still, effects of the nuclear quantum delocalization on the ionization of water at aqueous electrode interfaces have been found,[116] as will be discussed later.

In the following, there will be some figures illustrating the structure of an adsorbed water monomer, dimer, and hexamer, as well as of different bilayer structures, on Pt(111). These static water structures have been recalculated for this Review using the setup described in ref 98, i.e., by RPBE-D3 calculations, in order to have a consistent structure determination. Furthermore, we have redesigned the presentation of other water structures determined in previous studies of our group in order to have a consistent presentation of these structures so that the comparison is not hampered by varying designs.

3. ADSORPTION OF WATER MOLECULES, CLUSTERS, AND BILAYERS ON METAL SURFACES

From a surface science point of view, the adsorption of water on metal surfaces is rather interesting as the strengths of the water−metal and water−water interactions are of comparable magnitude so that any resulting water−adsorbate structure is the result of a subtle balance between these two interactions. As this balance also plays a crucial role for the structure of liquid water layers on metal surfaces, we will first consider the adsorption of water molecules, clusters, and bilayers on metal surfaces in detail, which will allow us to analyze the strengths of these two competing interactions.

3.1. Adsorption of Isolated Water Molecules and Small Water Clusters

The adsorption of single water molecules is illustrated in Figure 2. The typical adsorption configuration of isolated water molecules on a close-packed metal surface is demonstrated in Figure 2A. They preferentially bind through their oxygen atom to the metal at a top site in a flat-lying geometry.[14,118−128]

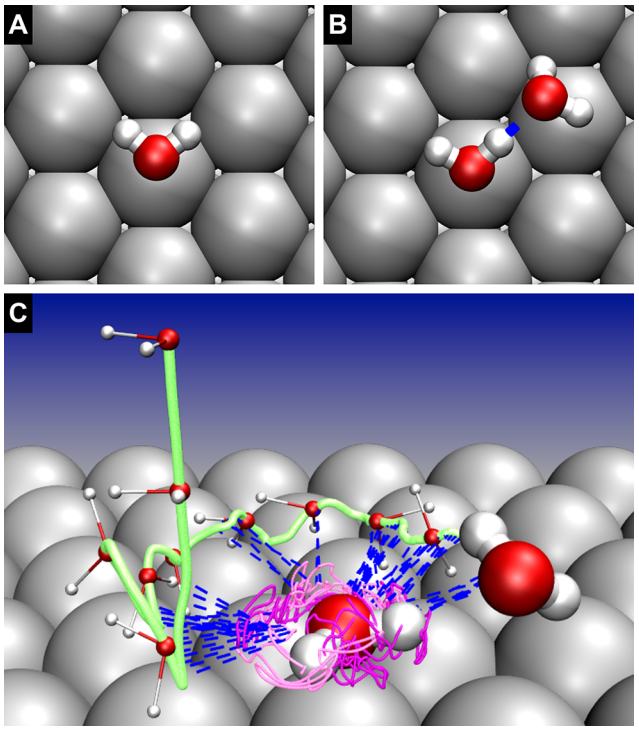

Figure 2. Adsorption of water molecules on a metal surface. (A) Top view of the typical adsorption configuration of a water monomer on a close-packed metal surface. (B) Top view of the adsorption configuration of a water dimer on a close-packed metal surface. (C) AIMD trajectory of water molecule impinging on a Pt(111) surface with one adsorbed water molecule already present within a 3 × 3 geometry. The periodic images of the water molecules are omitted for the sake of clarity. The green line indicates the trace of the oxygen atom of the impinging water molecule, and the purple lines trace the hydrogen atoms of the adsorbed water molecule. Some snapshots of the impinging water molecule are included with its atoms imaged in a small size; the final position is plotted in the regular size. The blue-dashed lines indicate configurations along the trajectory in which the impinging and adsorbed molecules are interacting via hydrogen bonds. This panel corresponds to a reanalysis of the AIMD simulation presented in ref 117.

On some typical late transition metals, the adsorption energies calculated with the Perdew−Wang 91 functional[70] for single water molecules on (111) metal surfaces are between −0.1 and −0.4 eV with the binding strength ordered according to Au < Ag < Cu < Pd < Pt < Ru < Rh, as summarized by Michaelides.[16] The binding energies are relatively small, which is also reflected in the rather large distances between the water oxygen atom and the topmost metal atoms: 2.25 Å (Cu) and 3.02 Å (Au).

As already mentioned earlier, the water−metal and water−water attractions are of comparable magnitude. Hence, on a partially water-covered metal surface, impinging water molecules will find adsorption sites with a higher adsorption energy than on the clean metal surface, as both the water−

https://doi.org/10.1021/acs.chemrev.1c00679
Chem. Rev. XXXX, XXX, XXX−XXX

water and water−metal interactions contribute to the binding. This notion is consistent with the experimental observation that the sticking probability of water molecules impinging on a Pt(111) surface increases with increasing water coverage.[11,129,130] Indeed, these experimental findings have been reproduced in AIMD simulations of water impinging on Pt(111) by summing up over 100 trajectories with random initial conditions as a function of water coverage and initial kinetic energy.[117] Figure 2B illustrates one trajectory of an impinging water molecule with an initial kinetic energy of 50 meV on a Pt(111) surface with one water molecule already adsorbed per (3×3) surface unit cell, i.e., with an initial water coverage of $\Theta_{H_2O} = 1/9$.[17,117] For the sake of clarity, in Figure 2B the periodic images of the two water molecules are omitted.

The traces of the oxygen atoms of the two water molecules indicate that the impinging water molecule orbits around the preadsorbed water molecule before the two molecules bind to each other. The dimer formation occurs after the initial kinetic energy and the additional energy gain through the attractive water−metal and water−water have been dissipated to surface phonons and internal water degrees of freedom.[117] During this phase, due to their high initial kinetic energy, the two water molecules constantly change their orientation, as illustrated by the traces of the preadsorbed water molecules and the formation and breaking of hydrogen bonds illustrated by the blue dashed line. Still they remain close to each other due to their mutual attraction. In the final adsorption configuration, the two adsorbed water molecules are connected through a hydrogen bond, with both being in a rather flat configuration.

The binding energies per water molecule of the adsorbed dimer on Pt(111),[117,131] Pd(111),[132] and Pd/Au(111)[15] are ∼50% larger than the binding energies of a single water molecule, indicating the significant influence of the water−water attraction for the resulting water adsorption structures. It is also interesting to look at the change of the dimer formation energy upon adsorption. On Pt(111) the dimer binding is slightly stronger,[131] and on Pd/Au(111) it is slightly weaker,[15] than in the gas phase. However, these changes are in the range of typical DFT uncertainties.[133] These small changes confirm that the electronic properties of the water molecules are only slightly changed upon adsorption due to the still relatively weak water−metal bonding. Note that in a simple bond-order picture[17] one would expect that the interaction between two molecules becomes weaker if these molecules are already bonded to a surface.

Several other small water clusters adsorbed on metal surfaces have been found to be particularly stable in a number of STM experiments,[134−136] which motivated corresponding first-principles calculations. Of particular interest is the adsorbed water hexamer illustrated in Figure 3. The water hexamer has been regarded as "the smallest piece of ice".[137] As Figure 3 depicts, in the adsorption structure the oxygen atoms are approximately located at the on-top positions over the metal atoms. Note that the oxygen−oxygen distance in water of ∼2.7 Å (see the upper panel of Figure 1) is rather close to the nearest-neighbor distance d_{nn} of late transition metals such as Ru (d_{nn} = 2.68 Å), Pt (d_{nn} = 2.77 Å), or Au (d_{nn} = 2.86 Å).[138] Hence, the hexagonal ring of the oxygen atoms in ice fits rather nicely on the hexagonal arrangement of the metal atoms in close-packed surfaces such as Ru(0001), Pt(111), or Au(111), in particular considering the fact that the strength of hydrogen bonding between the water molecules depends only rather weakly on small changes in the distance.[14,16]

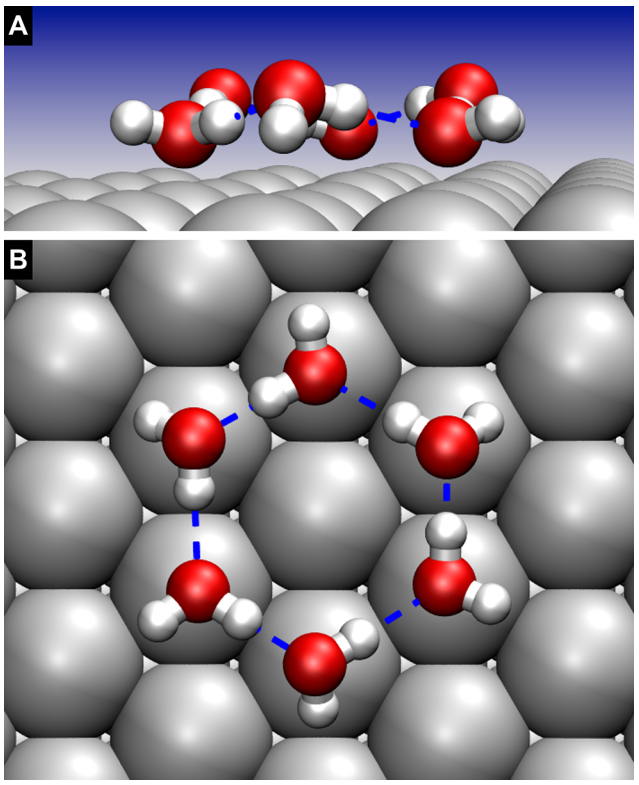

Figure 3. Adsorption structure of a water hexamer on Pt(111) calculated with the setup described in ref 98.

Figure 3 shows the adsorption structure of the water hexamer on Pt(111) calculated with the setup described in ref 98. It becomes apparent that this structure is buckled, as already found in previous studies.[136] This has been associated with the fact that this buckled structure resembles the tetrahedral configuration of ice.[136] However, in contrast to the isolated water hexamer,[139] in the adsorbed hexamer all the hydrogen atoms are approximately at the same height. This indicates that in spite of the buckling the structure-determining factor is the interaction of the oxygen atom of the water hexamer with the metal atoms. The water hexamer is arranged in such a way as to optimize the oxygen−metal interaction by keeping all of the water molecules rather flat with respect to the metal surface. In a bilayer of the ice Ih(0001) water bilayer, in contrast, the water molecules are oriented differently, as will be shown later. In fact, the hexamer shown in Figure 3 does not correspond to a structural element of an extended hydrogen-bonded water bilayer. Thus, the notion that the water hexamer should be considered as the basic structural unit that is interlinked to make up an ice Ih(0001) water bilayer[11] does not capture the structural properties of adsorbed water bilayers.

3.2. Icelike Water Bilayers on Close-Packed Hexagonal Metal Surfaces

The structural elements of icelike water bilayers on close-packed metal surfaces are illustrated in Figure 4A and B. Its geometry is similar to that of the densest layer of ice Ih[6] and corresponds to a $\sqrt{3} \times \sqrt{3}R30°$ structure with respect to the surface unit cell of the hexagonally close-packed surface. Every second water molecule binds with its oxygen atom to the metal

https://doi.org/10.1021/acs.chemrev.1c00679
Chem. Rev. XXXX, XXX, XXX−XXX

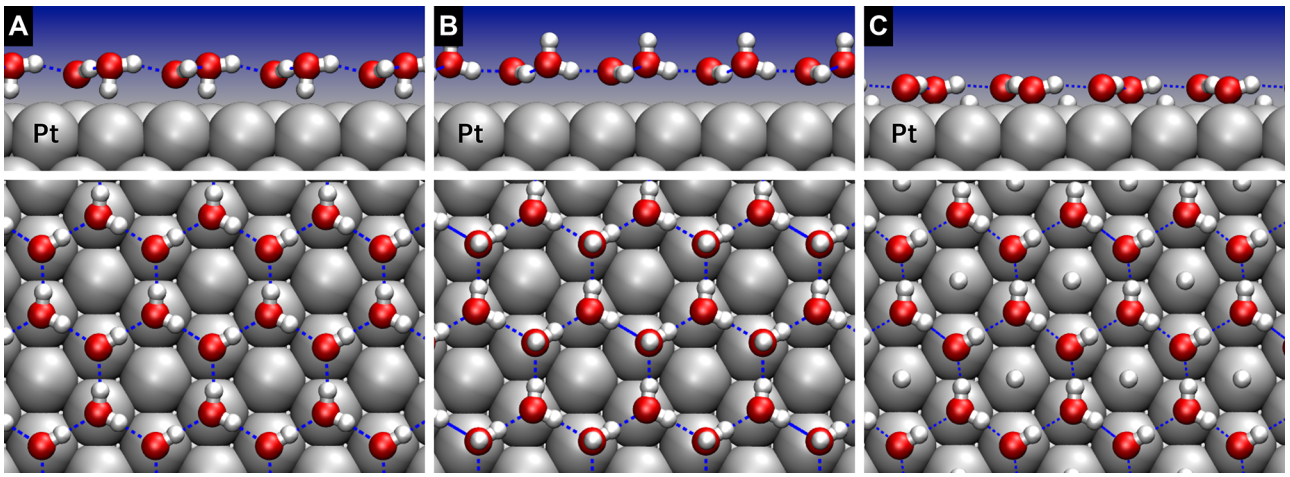

Figure 4. Side and top views of water bilayer structures on Pt(111): (A) H-down bilayer, (B) H-up water bilayer, and (C) half-dissociated water−OH bilayer with the additional hydrogen atoms at the center of the hexagonal rings.

surface in a flat configuration similar to the one of the adsorbed water monomer shown in Figure 2. However, the icelike bilayer structure can only be completed when every second water molecule is oriented with one hydrogen atom either pointing toward or away from the surface, resulting in the so-called H-down and H-up structures, respectively. These water bilayers have been very intensively studied using periodic DFT calculations.[14−17,22,104,119,127,131,138,140−142]

According to periodic DFT calculations using the PBE functional,[16,140] the energy gain upon formation of the icelike water layers on various late transition metals with respect to the free water molecule is between −0.42 and −0.56 eV per water molecule with respect to the free molecule. Interestingly, the energy difference between the H-up and H-down layers is rather small, and the energetic preference varies from metal to metal. On Ni(111), Cu(111), and Ru(0001), the H-up structure is more stable, whereas on Rh(111), Ag(111), Pt(111), Pd(111),[16] and Pd/Au(111),[15] the H-down structure is energetically favorable. In fact, these PBE results indicate that the adsorption of the water molecules in the bilayer structures is energetically less favorable than the sublimation of ice-Ih that is associated with an energy gain of E_{sub} = −0.666 eV.[15] This is at variance with the experimental observation that water wets the close-packed surfaces of Pt, Ru, Ni, Pd, and Rh.[6,8,11,143] This obvious failure of a popular DFT-GGA functional was discussed at length in the literature in the first decade of the century.[11,123,144,145] One additional aspect of this discussion was whether the also observed $\sqrt{39} \times \sqrt{39}$R16.1° or $\sqrt{37} \times \sqrt{37}$R25.3° water structures[129,146] are more stable on Pt(111) than the $\sqrt{3} \times \sqrt{3}$R30° bilayer.[145,147]

As far as the wetting is concerned, the erroneous DFT description of the PBE functional has been traced back to its lack of nonlocal correlations.[103,104] Taking into account van der Waals (vdW) dispersion interactions either through nonlocal vdW functionals[92,103,105] or via dispersion-corrected functionals[90] leads to the correct wetting behavior.[103,104] This has been attributed to the fact that, because of the higher polarizability of the surface metal atoms, the vdW dispersion interaction between water and the metal is stronger than that between the water molecules.[103] Thus, the inclusion of the vdW interaction strengthens the water−metal interaction more than the water−water interaction. Note that the appropriate consideration of the vdW dispersion interaction is also necessary in order to correct for the overstructuring of PBE water[77−79] and leads to a correct energetic ordering of water structures.[55,57,76,133] This demonstrates that only DFT calculations that appropriately take the vdW dispersion interaction into account can yield a reliable description of the properties of water and its interaction with surfaces.

Another intensively discussed issue regarding the water interaction with metal surfaces was whether water adsorbs dissociatively on metal surfaces or not.[148,149] Experimentally, it is a significant challenge to detect hydrogen atoms as they scatter electrons very weakly. Hence, the observed water structures on Ru(0001) at a temperature of 80 K were interpreted to result from a bilayer structure.[150] However, this was not consistent with the results of low-energy electron diffraction (LEED) IV experiments, which showed that the height of the oxygen atoms above the Ru surface in the water layer only varies within 0.1 Å,[151] whereas in water bilayers they should differ by >0.5 Å, as illustrated in parts A and B of Figure 4. This discrepancy was resolved by Feibelman.[148] He showed using DFG-GGA calculations that on Ru(0001) a half-dissociated water layer, where every second water molecule is dissociated to OH, is energetically more stable than the intact water bilayer. In this half-dissociated water layer, all oxygen atoms are close to the metal atoms, as shown in Figure 4C. These findings were later confirmed in further DFT studies.[14,22,149,152] In fact, Ru is not the only metal where water should adsorb dissociatively; on Rh and Ni also, half-dissociated water layers are energetically favorable.[16]

In electrocatalysis, bimetallic electrodes are of great interest as they allow one to tailor the catalytic activity of the electrode by a variation of the composition and structure of the catalyst.[153−155] Hence, the study of the structure of water layers on bimetallic surfaces is also of interest. The structure and stability of water layers on a PtRu/Pt(111) surface has been systematically studied for varying compositions of the PtRu surface alloy.[127] Due to so-called ligand interaction and geometric strain effects, the electronic properties, and thus also the reactivity of the constituents of the bimetallic systems, will be modified with respect to the isolated systems.[154] Still, in the PtRu surface alloys, the Ru atoms more strongly interact with the water molecules. As a consequence, those water bilayers are energetically more favorable on PtRu/Pt(111), whose strongly bound water molecules are located at Ru sites. Short AIMD

https://doi.org/10.1021/acs.chemrev.1c00679
Chem. Rev. XXXX, XXX, XXX−XXX

runs were performed for the water bilayers at room temperature. Most of the water bilayers quickly dissolved except for those that were adsorbed on a PtRu surface alloy that provided a hexagonal pattern allowing all water molecules to directly interact only with Ru atoms.[127]

Up to now, we have concentrated on icelike layers on the hexagonal close-packed surfaces of late d-band metals. Their nearest-neighbor distance is close to the O−O distance in ice Ih so that the icelike hexagonal water bilayers fit nicely to the underlying hexagonal structure of the close-packed metal surfaces. However, there are many other interesting and important metals and also many other stable surface terminations with nonhexagonal symmetry. First of all, we will stay with a hexagonal surface but see what happens when the nearest-neighbor distance is increased substantially. For example, the nearest-neighbor distance d_{nn} = 3.50 Å in Pb[142] is 22% larger than the corresponding distance d_{nn} = 2.86 Å in Au.[138] Figure 5A shows the water structure that results

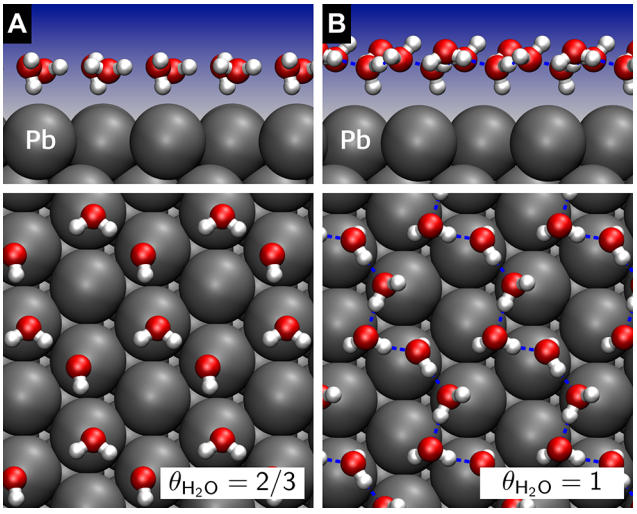

Figure 5. Optimized water structures of a water layer on Pb(111) for water coverages of (A) Θ_{H_2O} = 2/3 and (B) Θ_{H_2O} = 1 (replotted using the results presented in ref 17). The blue dashed lines indicate the presence of hydrogen bonds.

according to DFT calculations when an icelike water bilayer is initially deposited on Pb(111).[17,142] Upon relaxation of the water bilayer, the hexagonal rings break apart due to the larger distance, and instead water dimers are formed that are arranged in a chainlike structure. Due to the reduced direct water−water interaction between these dimers, the adsorption energies of the water layer of −0.254 eV per water molecule at a nominal coverage of 2/3 are also significantly smaller compared to, e.g., the water bilayer adsorption energy on Au(111).[142]

In fact, it is energetically favorable to add one more water molecule per $\sqrt{3} \times \sqrt{3}$ surface unit cell, resulting in a water structure with the nominal coverage of one. This structure with an adsorption energy of −0.350 eV is illustrated in Figure 5B. Still, no true two-dimensional water network forms, but instead, a chainlike structure is created. The overall lower coordination of the water molecules in this structure is the reason the binding energy per water molecule is still smaller than that in the hexagonal bilayer on late transition metals.

3.3. Adsorption of Water Layers on Low-Index Metal Surfaces with Nonhexagonal Symmetry

As far as the other low-index (100) and (110) metal surfaces are concerned, due to the fact that their symmetry is different from that of the icelike bilayer, it is not easy to form commensurate water structures. That might be the reason the number of both experimental and theoretical studies addressing an icelike water layer on (100) and (110) metal surfaces is somewhat limited. Apart from the (111) surfaces, mainly the (110) surfaces of Ni, Cu, and Ag have been studied experimentally.[11] As the (110) termination corresponds to a relatively open surface, they are more reactive than the close-packed surfaces. Indeed, mixed OH/H_2O layers have been observed or deduced from the experiment.[11]

In the following, we will focus on the icelike structures on Cu(110) as quite a number of experimental and theoretical studies have addressed this particular system.[156−162] At low water coverages, one-dimensional ice structures across the troughs of the (110) surface have been observed.[156] The comparison of STM images and measured vibrational spectra with the results of periodic DFT calculations indicates that these one-dimensional ice structures consist of a face-sharing arrangement of pentagons.[156,157] Water hexagons are too large to be favorably accommodated on the Cu(100) surface. In contrast, the pentagons can adsorb on the Cu(110) surface in a structure in which two-thirds of the water molecule bind directly through their oxygen atoms to the underlying Cu atoms in a flat geometry, as illustrated in Figure 2, while still forming a tight hydrogen-bonded network. So again the most favorable icelike structure results from an optimal combination of the water−metal and water−water interactions.

As far as the structure of extended icelike layers on Cu(110) is concerned, LEED studies observed a $c(2 \times 2)$ pattern that was assumed to be consistent with an adsorbed bilayer structure.[158,159] The combination of X-ray photoelectron spectroscopy (XPS), X-ray absorption (XAS), and reflection absorption infrared spectroscopy (RAIRS) and LEED experiments together with DFT calculations showed that water adsorbs nondissociatively on Cu(110) at low temperatures.[160] This can be explained by the relatively high water dissociation barrier on Cu(110).[162] In fact, the combined experiments[160] also revealed intact water adsorption in a (7×8) superstructure with a 2:1 ratio with respect to the occurrence of H-down and H-up water molecules. This has been associated with the more open structure of Cu(110), which provides adsorption sites at which the H-up and H-down configurations are nearly energetically degenerate. Furthermore, upon electron exposure the (7×8) LEED pattern changes to a $c(2 \times 2)$ pattern, which has been related to the presence of OH groups created by the electron-induced dissociation of water.[160,161]

The preadsorption of oxygen also leads to the formation of H_2O−OH structures on Cu(110).[163,164] STM experiments revealed a distorted hexagonal $c(2 \times 2)$ structure (see Figure 6) with a composition of $2H_2O$/OH, as derived from the analysis of temperature-programmed desorption (TPD) data.[164] DFT calculations showed that the energetically most favorable structure consistent with the experimental observations is a partially dissociated overlayer structure containing so-called Bjerrum defects[165] in the hydrogen-bonding network. These defects are characteristic to ice and correspond to either two protons (D defect) or no proton (L defect) per hydrogen bond instead of the usual one proton per hydrogen bond. The

https://doi.org/10.1021/acs.chemrev.1c00679
Chem. Rev. XXXX, XXX, XXX−XXX

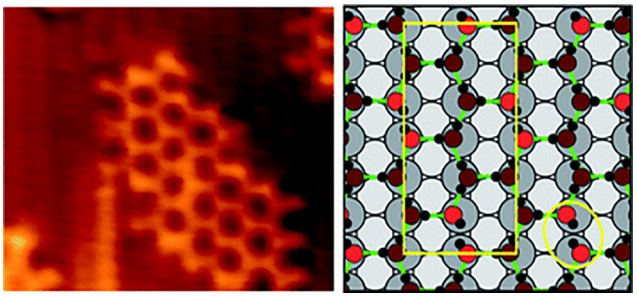

Figure 6. Comparison of an STM image and the calculated structure of the H_2O−OH $c(2 \times 2)$ phase on Cu(110). Reprinted with permission from ref 163. Copyright 2012 Royal Society of Chemistry. The yellow box indicates the unit cell used in the calculations, and the circle highlights the D-type Bjerrum defect (see text).

calculated energy minimum structure is also illustrated in Figure 6. In fact, each hydroxyl group is part of a D-type Bjerrum defect. The structure can be regarded as an arrangement of H_2O−OH−H_2O trimers with each H_2O molecule of the trimers still forming two other hydrogen bonds with further water molecules, leading to an extended hexagonal network. Hence, the driving force for this structure is the maximization of strong hydrogen bonds at the expense of forming D-type Bjerrum defects.[164]

3.4. Water Layers on Stepped Metal Surfaces

Note that the number of studies addressing water layers on higher index surfaces such as stepped surfaces is rather limited. Experimentally, Ibach studied monolayer water structures on Au(511)[166] and Ag(511)[167] using vibrationally spectroscopy. These studies found that the O−H vibrations of the adsorbed water layer split up into three separate peaks, two of which have been assigned to the O−H vibrations of hydrogen-bonded H atoms, whereas the peak with the highest frequency was associated with the vibrations of non-hydrogen-bonded H atoms. On the basis of the observed vibrational spectra and the particular structure of the (511) surface, Ibach proposed an adsorbed water network structure consisting of tetragons, hexagons, and octagons.[166]

Interestingly enough, DFT calculations confirmed that this structure, which corresponds to a compromise between the creation of a hydrogen-bonded network and the best-suited arrangement on the stepped (511) surface, is indeed the energetically most favorable one. This arrangement is surprisingly stable as a function of temperature, as AIMD simulations of water on Au(511) at T = 140 K and T = 300 K have shown.[168] Figure 7 provides snapshots of the AIMD simulations performed at these two temperatures. Figure 7A illustrates the water structure formed by the tetragons, hexagons, and octagons at T = 140 K, and it remains intact even at T = 300 K (see Figure 7B). The side views of the water structures in Figure 7 show that only the water molecules directly at the step sites are close to the metal atoms. Thus, the water layer is pinned to the metal step atoms, whereas the water molecules above the small (100)-like terrace only very weakly interact with the metal substrate. This leads to a stronger water−water interaction above the terraces that stabilizes the water network. The reliability of the computational results is confirmed by the fact that vibrational spectra derived from the AIMD simulation through the Fourier transform of the velocity autocorrelation function[169] nicely reproduce the measured vibrational spectra of water on

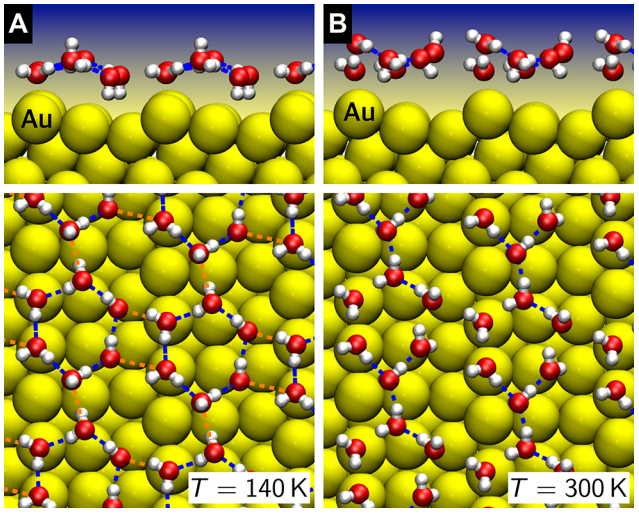

Figure 7. Top and side views of snapshots of an AIMD run of a water layer on Au(511) at (A) T = 140 K and (B) T = 300 K redesigned using the data presented in ref 168. The blue dashed lines indicate the hydrogen bonds, whereas the orange dashed lines in (A) are added in order to emphasize the water structure consisting of tetragons, hexagons, and octagons.

Au(511). Stronger binding of water molecules to step sites has also been found in DFT calculations for the (100) steps of Pt(533) and the (111) steps of Pt(553).[170]

The fact that the complex structure of the water layer on Au(511) is surprisingly stable has been explained by a bond-order argument.[168] Because the water film is pinned to the surface at the step atoms and the water molecules above the terraces are not directly bonded to the metal, the binding between the water molecules is stronger compared to a situation in which all water molecules are directly interacting with the metal surface. Similar arguments have also been employed[17] to explain the higher structural stability of icelike layers on hydrogen-covered Pt(111).[171] The adsorption of a dense layer of hydrogen on Pt(111), which occurs at low electrode potentials,[172−176] passivates the surface and reduces the water−surface interaction significantly, which, at the same time, increases the order within the water layer compared to a water layer on clean Pt(111),[171] as revealed from a comparison of AIMD simulations for both situations.

We will close the presentation of the geometric structure of icelike water layers on metal surfaces with a short discussion of free-standing water layers. Recently, high-resolution electron microscopy experiments identified a square ice structure confined between two graphene sheets.[177] Because graphene interacts only weakly with water molecules[178,179] and should not impose any square structure on the water layer, this was a rather surprising result.[180] Although it was soon suggested that this structure could have been an artifact of the presence of salt contaminants,[181] these observations motivated a number of DFT studies addressing the structure and properties of free-standing two-dimensional water layers.[182−186] Indeed these simulations found stable square ice monolayers[184,185] resulting from a compromise between high coordination and optimum tetrahedral bonding geometry. However, besides the square structures, two-dimensional layers based on rhombus, truncated-square, and secondary-prism motifs were found to be more stable than the standard hexagonal structures.[185] This demonstrates that water indeed exhibits a broad variety of

https://doi.org/10.1021/acs.chemrev.1c00679
Chem. Rev. XXXX, XXX, XXX−XXX

possible structural motifs, which should also be relevant for the interpretation of the local water structures found in liquid water.

3.5. Electronic Properties of Water Monolayers on Metal Surfaces

Turning back to the nondissociative adsorption of water on metal surfaces, we will now discuss the electronic properties of water/metal interfaces. As mentioned earlier, the adsorption energies of single water molecules on typical metal surfaces are relatively small; they bind by less than ~0.5 eV with respect to free water molecules.[16] Water bilayers bind a little more strongly to metal surfaces than single water molecules,[104] which is caused by the additional attractive water−water interaction.[15,16] These adsorption energies reflect the rather weak interaction between water molecules and metal surfaces. One indicator of the adsorption strength is the change of the local density of states (LDOS) of the surface upon the adsorption. This LDOS of the Pt(111) electrode in the absence and presence of water was derived from periodic DFT calculations.[141] The calculations showed that upon the adsorption of a H-down water bilayer the height of the peaks in the LDOS slightly changed. However, the corresponding peak positions hardly shifted upon the water adsorption. In the case of the adsorption of a water monomer on Pt(111), the changes in the LDOS peak heights of the Pt atom directly beneath the oxygen atom of the adsorbed water monomer are a little bit larger than those for the adsorption of the water bilayer, but still the peak positions remain basically the same. These results are consistent with the observation that the interaction of water molecules with metal surfaces is rather weak. One of the consequences of this weak interaction is the fact that the adsorption energies of atoms and small chemisorbed molecules are only weakly altered in the presence of a water layer,[15] as we will discuss in more detail later.

Furthermore, the adsorption energies of water bilayers in the H-up and H-down structures are rather similar.[16] For example, on Pt(111), they differ only by 0.03 eV per water molecule.[22] Still, there is one property that differs very strongly between these two orientations of the water bilayer, namely, the work function change of the metal surface upon depositing the icelike bilayers.[22,24] On Pt(111), the H-up layer lowers the work function by $\Delta\Phi = -2.34$ eV, whereas the H-down only lowers it by $\Delta\Phi = -0.22$ eV.[22] Note that the electrode potential of an electrochemical cell can be related to the work function of the water-covered metal surface.[187] A work function difference of 2 eV thus translates to a difference in the corresponding electrode potentials of 2 eV, which is much larger than the water stability window of 1.23 eV. This illustrates how dramatic is this difference.

It is relatively easy to understand why the H-up and H-down water bilayers cause work function changes that differ so significantly. Water molecules are strongly polar, and the H-up and the H-down water bilayers have opposite orientations of the OH bond, thus leading to opposite dipole moments, which causes the large work function difference. Naively, one would expect that the one bilayer configuration lowers the work function and the other one increases it by roughly the same amount. Thus, it is indeed surprising that both water orientations lower the work function of Pt(111).

To analyze the origins of this trend, the laterally averaged charge density difference $\Delta\rho$,

$$\Delta\rho = \rho(H_2O/Pt(111)) - (\rho(H_2O) + \rho(Pt(111))) \quad (1)$$

has been determined for the H-up and H-down water bilayers on Pt(111),[22] which is plotted in Figure 8 as a function of the

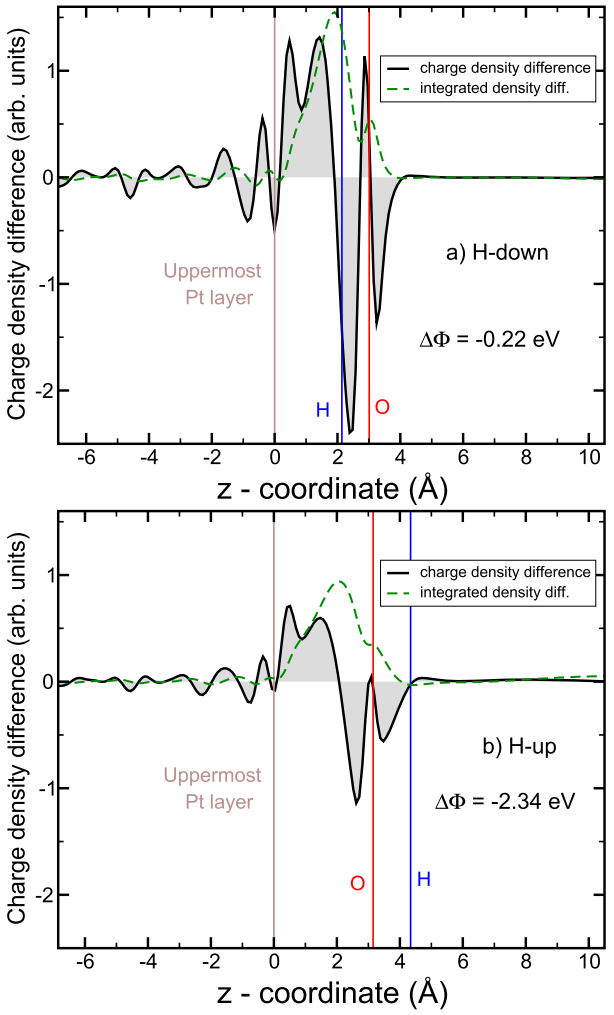

Figure 8. Laterally averaged electron density difference upon the adsorption of a H-down (a) and a H-up (b) water bilayer on Pt(111) as a function of the vertical height. The heights of the uppermost Pt layer and the hydrogen and oxygen atoms of the oppositely oriented water molecules are indicated by vertical lines. In addition, the integrated charge density difference is plotted. Note that the same scale for the charge density difference has been used in both figures. Reprinted from ref 22, published under a CC BY license.

height above the surface. $\Delta\rho$ can be interpreted as the interaction-induced charge rearrangement upon the adsorption in this case. Interestingly enough, for both orientations of the water bilayer there is a net transfer of electronic charge from the water bilayer toward the metal atoms of the Pt(111) surface. This charge transfer leads to an additional induced dipole at the surface that lowers the work function. Thus, there is a combination of two effects. The charge transfer toward the metal surface causes an interface dipole moment that even overcompensates the contribution of the dipole moment of the H-down layer to the work function change on Pt(111), whereas for the H-up layer the two dipole moments add up, leading to a substantial reduction of the work function.

However, this charge transfer depends on the strength of the interaction of the water bilayer with the metal surface. On the Au(111) surface, the charge transfer is relatively small so that

https://doi.org/10.1021/acs.chemrev.1c00679
Chem. Rev. XXXX, XXX, XXX−XXX

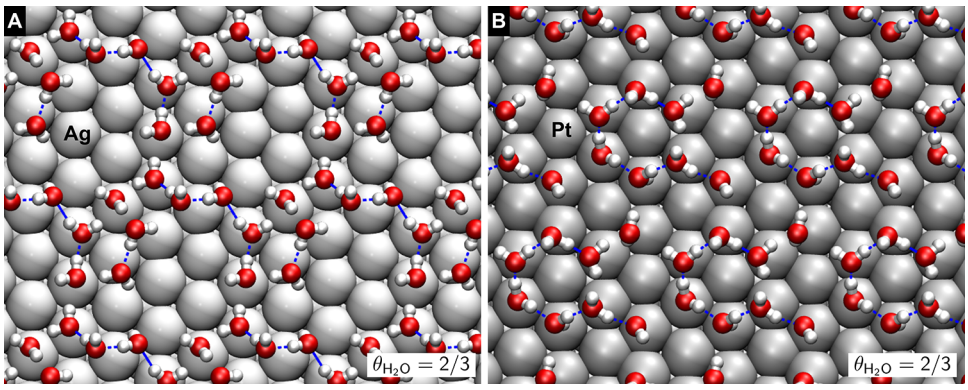

Figure 9. Snapshots of AIMD simulations of two water layers on (A) Ag(111) and (B) Pt(111) at 300 K after 7.5 ps of simulation time based on the trajectories presented in ref 22. Only the first water layer is shown.

the H-down water bilayer overall increases the work function by ~0.5 eV, whereas the H-up bilayer lowers it by ~1.5 eV.[22] In contrast, Ru is more reactive than Pt, so the water H-down and H-up bilayers lower the work function even more strongly than that on Pt by about 0.8 and 3.6 eV, respectively.[22,152]

The strong dipole moment associated with the H-up and H-down water bilayers in fact makes their energetic stability dependent on an applied field.[15,188] Still, the question remains whether water layers on close-packed surfaces except for very low temperatures are really icelike or already liquid-like. Structural studies of adsorbed water layers have been performed in UHV chambers in which, as mentioned earlier, water starts to desorb at temperatures above ~150 K.[11] Typically it was assumed that adsorbed water bilayers are still rather icelike at such temperatures.[6,8,189] On the other hand, work functions of water bilayers measured in UHV experiments on Au(111),[190] Pt(111),[191,192] and Ru(0001)[193,194] showed values between the calculated values for the adsorbed H-up and H-down bilayers.[138] This should not be due to intrinsic DFT errors, which typically do not result in work function errors of up to 1 eV.

This issue has in fact been resolved based on AIMD simulations of two water layers on Ag(111), Au(111), Pt(111), Pd/Au(111), and Ru(0001) within a $2\sqrt{3} \times 2\sqrt{3}$R30° surface unit cell at room temperature.[22] These simulations with a total run time of 10 ps each were started with initial icelike H-up and H-down bilayer structures, and the work function along the AIMD trajectories was monitored. After ~4 ps in the simulations, the mean work functions on a particular metal surface became rather similar for both H-up and H-down initial conditions,[22] approximately corresponding to the mean value of the work functions for the H-up and H-down layers.

Figure 9 shows snapshots of the AIMD trajectories of water layers on Ag(111) and Pt(111) after 7.5 ps simulation time. Their inspection allows one to analyze the reasons behind the change of the work function. First of all, there are significant structural differences between the two water layers. On the weakly interacting Ag(111) surface, the water structure has become rather disordered, and no indication of the initial hexagonal geometry is left. Some clustering can be observed, but still most of the water molecules bind through their oxygen atom to the metal atoms of the substrate. Otherwise, there is no preferential ordering visible, which explains the fact that the resulting work functions are in between the work function of the icelike H-up and H-down water bilayers.

In contrast, on Pt(111), there is still a hexagonal water arrangement visible. This might be due to the fact that Pt(111) more strongly interacts with water than Ag(111) and therefore still imposes a hexagonal ordering on the water layer. It should be noted that the chosen $2\sqrt{3} \times 2\sqrt{3}$ surface unit cell is rather small and also favors the hexagonal ordering. Yet, the work function of the water structure on Pt(111), as shown in Figure 9B, acquires an intermediate value between those of the two types of water bilayer. A closer inspection of the water orientation reveals that the water molecules are still positioned in a hexagonal structure, but their orientation has become disordered with no preferential alignment corresponding to either an H-up or H-down structure. Thus, these simulations yield averaged work function values close to those measured in the experiment. This provides a strong indication that the water bilayers observed in the experiment at ~150 K are already rather disordered.

4. AIMD STUDIES OF WATER FILMS ON METAL SURFACES

Up to now, we have considered the first-principles description of isolated water molecules, water clusters, and water layers on surfaces. The studies described earlier provide substantial insights into the interaction of water with metal surfaces. The electronic structure calculations demonstrate that the minimum energy structures of isolated water molecules and clusters and of water monolayers on metal surfaces result from a compromise between the water−metal and water−water interactions.

Still, from a technological point of view, the interest in water/metal interfaces is triggered by its ubiquitous role in practical matters such as electrochemistry, electrocatalysis, or corrosion. These processes typically occur at room temperature, i.e., at interfaces between some metal surface and liquid bulk water. The liquid nature of water in these systems leads to the fact that the standard tool of first-principles total energy calculations, structure optimization, is no longer applicable. Instead, appropriate statistical averages have to be performed, and instead of total energies, free energies determine the stability of these systems. As the theoretical studies presented in the previous sections show, there are strong polarization effects in the interaction of water at metal surfaces. Such effects are still hard to reproduce using parametrized interaction potentials. Hence, a quantum chemical treatment of water/metal interfaces is required to allow a free redistribution of electrons across the water/metal interfaces. However, even

https://doi.org/10.1021/acs.chemrev.1c00679
Chem. Rev. XXXX, XXX, XXX−XXX

with the constant improvements in first-principle codes and the ever-increasing computer power,[66] the required ab initio molecular dynamics simulations are computationally rather demanding. Still, such studies are required in order to get reliable insights into the structural, electronic, chemical, and catalytic properties of water/metal interfaces. Moreover, recently there has been an increasing number of AIMD studies that progressively provide new insights into these interfaces. In the following, we will try to review the advancements made through such studies.

4.1. Structure of Water Films on Clean Metal Surfaces

To the best of our knowledge, the first attempts to systematically study the structure of water layers on metal surfaces using AIMD simulations were performed by Izvekov and co-workers, who studied the water structures on both Cu(110)[29] and Ag(111)[30] at room temperature. In the first study, Cu(110) was modeled by a seven-layer slab and nine Cu atoms per surface unit cell covered by 12 water molecules. The initial configuration was chosen from a classical molecular dynamics simulation. In the AIMD simulations done within the Car−Parrinello MD approach,[195] the system was equilibrated at a temperature of 300 K for 1.34 ps, followed by a 2.52 ps long microcanonical ab initio run used for sampling. In this run, the initial one-layer water geometry was found to be unstable already during the equilibration run. Seven water molecules were identified to form the first water layer in a kind of bilayer structure. As far as the electronic degrees of freedom are concerned, the water molecules were found to be strongly coupled to the slab bulk electronic states, whereas the metal surface states were only weakly affected by the presence of the water layer.

In the second AIMD study by Izvekov and Voth, already 48 water molecules were considered on Ag(111) on a rectangular surface unit cell with 16 silver atoms per layer.[30] Otherwise, the computational setup and the run times were very similar to the those used in the water/Cu(110) study.[29] The electronic coupling between the metal and the water layers turned out to be very similar for both studied noble metal surfaces. The average surface coverage of the first water layer was ∼0.63 water molecules per Ag atom, which is close to the value of 2/3 for an icelike water bilayer. However, water molecules in the first layer were not arranged in a hexagonal pattern, but still the adsorbed water molecules stayed close to the Ag on-top sites within the 2.1 ps of the AIMD production run. This might be a consequence of the relatively short simulation time, as the snapshot of the water/Ag(111) AIMD simulations after 7.5 ps runtime derived from a more extended AIMD sampling[22] shown in Figure 9a indicates quite a number of water molecules that are no longer located above on-top sites.

AIMD simulations can be used to monitor structural data of water layers on metal surfaces, and also their vibrational spectra can be derived from the Fourier transform of the velocity autocorrelation function.[169] Short AIMD simulations with a runtime of 2 ps at a temperature of ∼100 K were used to determine the vibrational spectra of water bilayers on Pt(111), Rh(111), Au(111), and Ru(0001).[119,131] These spectra typically exhibit three distinct regions: Frequencies below 1000 cm^{-1} belong to translational and librational motions of the water molecules, at ∼1600 cm^{-1} HOH bending modes appear, and >3000 cm^{-1} O−H stretch vibrations become visible. The AIMD simulations at low temperatures[119,131] yielded a good agreement with experimental observations for icelike adsorbed water structures.[196] Compared to these simulations at low temperature, vibrational spectra of water layers on Ag(111), Au(111), Pt(111), Pd/Au(111), and Ru(0001) derived from AIMD simulations at room temperature yielded much broader spectra,[22] in agreement with the experiment,[189,197] in particular in the region of the O−H vibrations. This broadening is, first of all, caused by the fact that isolated water molecules have symmetric and antisymmetric OH stretching modes ν(OH) at 3720 and 3660 cm^{-1}, respectively. These frequencies are furthermore strongly affected by whether the O−H groups are hydrogen-bonded to other water molecules or not, as already discussed in the context of the water layers adsorbed on Au(511).[166,168] In addition, in the spectra derived from the AIMD simulations, the water vibrations on Pt(111), Pd/Au(111), and Ru(0001) exhibit a larger shift to lower frequencies than those on Au(111) and Ag(111). This has been explained by the stronger interaction between water and the more reactive substrates Pt, Pd/Au, and Ru, which weakens the binding within the adsorbed water molecules,[22] in agreement with the corresponding experimental results for Pt(111) and Au(111)[197] and more recent AIMD studies.[18]

The early AIMD simulations[22,29,30,119,131,138,168] focused on the properties of a single water layer adsorbed on the metal surface. This was caused by the high computational demand of AIMD simulations to model thick water layers for sufficiently long times. In recent years, the AIMD simulation of water films on metal surfaces consisting of several layers became possible and now corresponds to the standard approach for the modeling of water/metal interfaces.[20,23,76,198−202]

As mentioned earlier, molecular dynamics simulations of water/metal interfaces need to be performed in order to take the liquid nature of water adequately into account. This requires an appropriate statistical sampling over the microstates of the corresponding thermodynamic ensemble. In practice, observables then correspond to mean values of water properties along the MD run, but also the width of the distribution is of interest. Before discussing these properties, we first want to address the question of the appropriate system size. Figure 10 compares the work function of a water film consisting of six water layers on Pt(111) as a function of the AIMD run time in a 3 × 3 surface unit cell with 36 water molecules[76] and in a 6 × 6 surface unit cell with 144 water molecules.[23] Snapshots of the AIMD simulations in the larger unit cell are shown in Figure 11. This work function is of particular interest in electrochemistry, as the so-called potential of zero charge (pzc) is related to the work function of the clean metal surface covered by an ion-free water film.[187,203]

In passing, we note that the pzc is typically defined as the potential at which no excess charge exists on metal surfaces.[204] The underlying concept of a surface charge density, however, is only strictly valid in a purely classical continuum picture in which any excess charge at a metal surface is located in an infinitely thin surface layer. In any atomistic quantum chemical approach, surface charge is an ill-defined entity, as its determination would require the definition of a surface region of a certain thickness, which introduces some arbitrariness in its definition. Furthermore, there is also a certain arbitrariness in any charge partition scheme because there is no strict definition of which electrons belong to a particular ion core and which belong to adjacent atoms. As far as water/metal surfaces with a delocalized charge distribution across the interface are concerned, it is therefore fundamentally

https://doi.org/10.1021/acs.chemrev.1c00679
Chem. Rev. XXXX, XXX, XXX−XXX

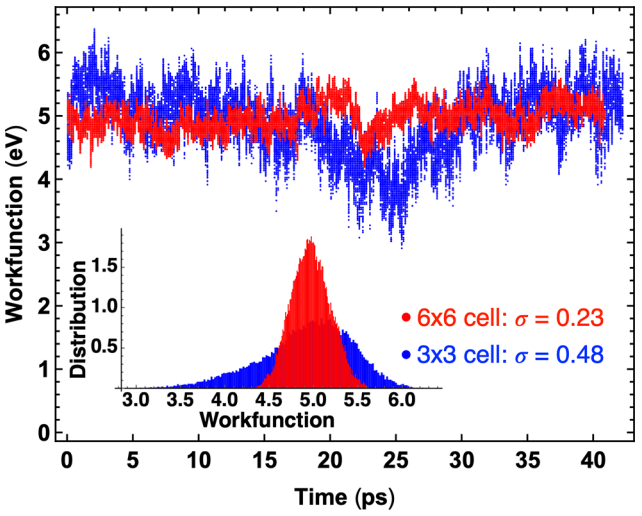

Figure 10. Comparison of the work function of a water film on Pt(111) as a function of the AIMD run time with six water layers in a 3 × 3 surface unit cell with 36 water molecules[76] and in a 6 × 6 surface unit cell with 144 water molecules.[23] The inset shows the distribution of the work function values.

impossible to establish any strict definition about which electronic charge belongs to the metal and which belongs to the water. This is also the reason no charge-partition scheme can yield an integer number of excess electrons in the metal electrode when, e.g., a proton is created from a hydrogen atom placed into the water film.[23,205] Still, it should also be noted that charge-partition schemes can be rather helpful in identifying trends in the charge rearrangement of a system upon some changes, for example, upon adding a water layer at a surface, as illustrated in Figure 8.

The mean values of the work function with respect to the electronic vacuum level are relatively similar in both trajectories shown in Figure 10: 5.01 eV for the smaller unit cell[76] and 4.96 eV for the larger unit cell.[23] Considering the rather large variances σ, 0.48 and 0.23 eV, respectively, the difference in the mean values does not appear to be statistically relevant. These results lead to pzc values of 0.57 and 0.52 V versus the standard hydrogen electrode (SHE), taking the generally accepted value of 4.44 eV[26,187] for the absolute value of the SHE. Within the statistical uncertainty, the values also agree reasonably well with the experimentally derived values,[203,206,207] although it needs to be stated that more recent results suggest a pzc of Pt(111) close to 0.3 V.[206,207]

Note again that there is a significant reduction of the variance σ from 0.48 to 0.23 eV by increasing the number of considered water molecules by a factor of 4. In fact, the work functions sampled along the AIMD trajectory spread over a range of about 2 and 1 eV in the smaller and larger unit cells, respectively. Included in the sampled canonical ensemble are water structures with a broad range of work functions corresponding to microstates that do not yield the pzc.

One can have two different points of view with regard to this. One can assume that along the trajectory the different configurations that are visited correspond to a sampling over various electrode potentials. Hence, one long run is sufficient to obtain results for a range of different electrochemical conditions. One then only needs to collect the configurations that belong to one particular work function (or rather, one small interval of work functions) to obtain mean values for

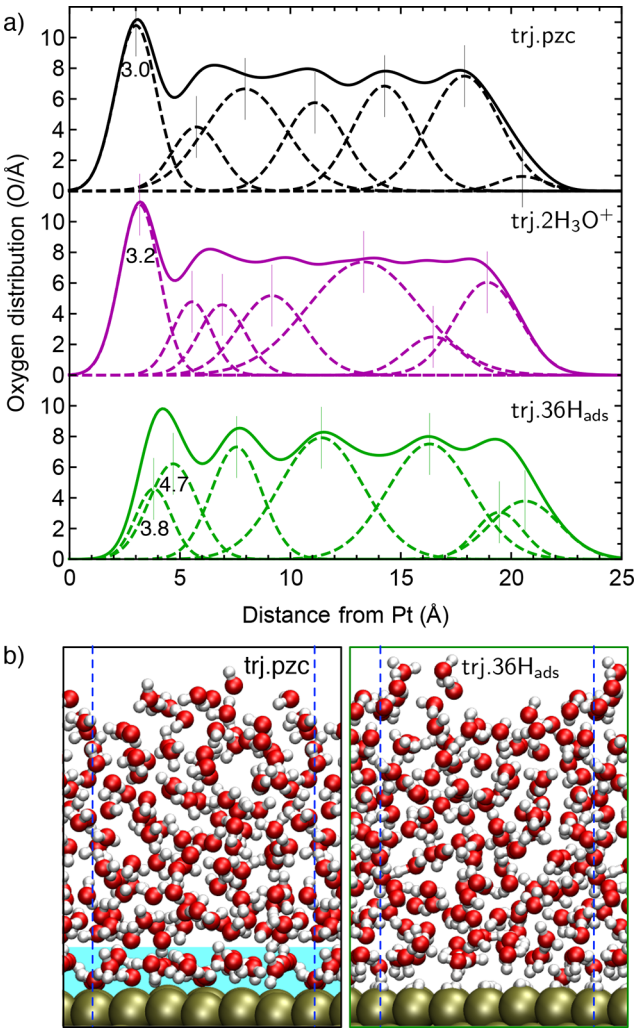

Figure 11. AIMD simulations of water on Pt(111) with 144 water molecules within a 6 × 6 surface unit cell.[23] (a) Distribution of oxygen atom in the water film in simulations with slightly different conditions: pure water film (trj.pzc, black line, upper panel), water film with two hydrogen atoms added (trj.2H_3O^+, blue line, middle panel), and pure water film on Pt(111) fully covered by hydrogen atoms (trj.36H_{ads}, red line, lower panel). A deconvolution of oxygen distributions in terms of Gaussian functions is shown as dashed lines. (b) Snapshots of the trj.pzc and trj.36H_{ads} AIMD trajectories. Reprinted from ref 23 with permission. Copyright 2018 AIP Publishing.

different electrochemical conditions. This is the basis of the so-called generalized computational hydrogen electrode (GCHE).[208,209] Using this approach, Hansen et al. ran AIMD simulations with 24 water molecules in about three water layers on Au(111) within a 3 × 4 orthogonal surface unit cell[210] for a range of different hydrogen concentrations. Thus, they could sample both potential dependent properties and pH effects. Within this ansatz, small unit cells are advantageous because they lead to a broad range of sampled electrode potentials.

However, one has to consider that, upon using a small unit cell size, only a limited set of possible water configurations will be explored. This might lead to a sampling that is not really representative with respect to the possible water structures it might contain, e.g., overstructured water configurations forced by the periodic boundary condition[76] or configurations

https://doi.org/10.1021/acs.chemrev.1c00679
Chem. Rev. XXXX, XXX, XXX−XXX

corresponding to work functions beyond the stability window of liquid water.[208,209] In addition, larger unit cells are also needed to faithfully model complex extended adsorbate structures and solvation layer configurations.[23,202] As far as the assignment of the ensemble to a particular electrode potential is concerned, one has to take into account that the work function is a macroscopic property in the micrometer range, and the appropriate ensemble will contain electrode/electrolyte structures that locally lead to a range of work functions in the nanometer range. Thus, by including structures with different work functions, one effectively samples over these local structures that together would yield a structure with the average work function.[20,23,76]

A large 6 × 6 surface unit cell was also used by Le et al.[199] in the AIMD simulations with a total of 151 water molecules in the unit cell to determine the pzc values of Pt(111) and Au(111); for additional simulations of water films on Pd(111) and Ag(111), smaller unit cells were used. However, instead of determining the electrode potential through the work function above the water film, the authors used the concept of the computational standard hydrogen electrode (CSHE).[36,211] In this approach, the electrode potential within the electrolyte can be derived by comparing the reference deprotonation free energies of a solvate hydronium ion at the interface and in a pure water model.[199] This involves a thermodynamic integration scheme to derive the deprotonation free energy of H_3O^+, but no vacuum region is needed in the supercell to determine the work function. The corresponding setup is illustrated in Figure 12a, which shows a snapshot of the Pt(111)−water simulation cell (note that at the right-hand side the periodic system is continued by the Pt(111) slab).

To analyze the water structure at the metal−water interface in more detail, the water molecules have been characterized in terms of their interaction with the metal surface and divided into watA, watB, and watC molecules.[199] Originally, watA and watB water molecules were characterized according to their dipole moment with respect to the surface:[199,200] watA molecules have a dipole pointing away to the surface, i.e., they correspond to O-down water molecules, whereas the dipole moment of watB molecules points toward the surface. However, it was also recognized at the same time that the watA molecules are those that directly bond to the metal surface through the oxygen atom in the same fashion that a water monomer binds to a metal surface, as illustrated in Figure 2A. The watB molecules, on the other hand, are slightly further away from the surface. They can even be further subdivided into watB-down and watB-up configurations,[199,200] which would correspond to the H-down and H-up water molecules in the icelike water bilayer structures shown in parts A and B of Figure 4, respectively. These two different species had already been identified in a preceding AIMD study.[212] Water molecules at a distance of >7 Å from the metal surface have been characterized as watC molecules.[200] They are already rather similar to bulk liquid water, their density is close to the liquid water bulk value of 1 g/mL, and they have no obvious net orientation. The bulk liquid water-like nature of these molecules can also be deduced from their relatively flat and smooth distribution, as illustrated in Figure 11a.

According to the AIMD simulations, the watA molecules are found to be more frequent on Pt(111) and Pd(111) than on Au(111) and Ag(111), i.e., their occurrence scales with the strength of the water monomer adsorption energy. Furthermore, the watA molecules on Pt(111) and Pd(111) exhibit a more narrow angular distribution than those on Au(111) and Ag(111).[200] Figure 12b shows the Pt and water density of states at the interface and in bulk water averaged over the AIMD trajectory. First of all, it is very obvious that the water DOS of the watA molecules differs significantly from those of the watB and watC molecules, which are rather similar. This appears to reflect the strong interaction of the watA molecules with the Pt surface atoms. On the other hand, a closer look at the Pt density of states reveals that, upon adding the water film, the Pt DOS is shifted to higher energies, but its shape remains basically the same. This indicates a charge transfer toward the Pt states, consistent with the charge density difference plotted in Figure 8 for the icelike water layers on Pt(111). The absence of new features in the Pt DOS suggests that there is no strong hybridization between Pt and water orbitals upon water adsorption, as already found before for the adsorption of icelike water layers on Pt(111).[141] The strongly modified DOS of the watA molecules compared to the watB and watC molecules thus might be a simple consequence of their distinctively different coordinations.

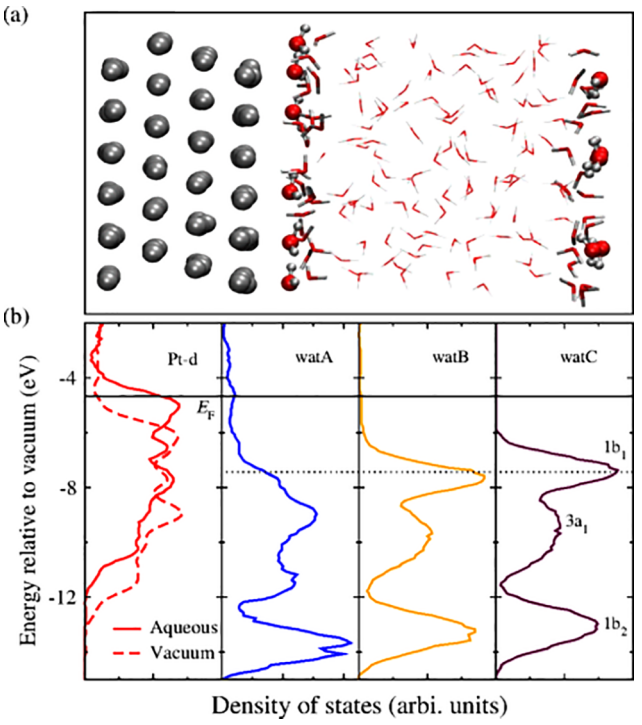

Figure 12. (a) Illustration of the Pt(111)−water interface model used in AIMD simulations. Pt, O, and H atoms are in silver, red, and white, respectively. Depending on the positions, watA, watB, and watC are distinguished and represented by balls, bonds, and lines, respectively. (b) Projected local density of states (DOS) plots of Pt and water at the interface averaged over an AIMD trajectory. Reprinted with permission from ref 199. Copyright 2017 American Physical Society.

By integrating the water density distribution for distances below 7 Å, the water surface coverage on the (111) metal surfaces was estimated.[200] For all considered metal surfaces, Pt(111), Pd(111), Au(111), and Ag(111), a coverage close to 0.8 ML (monolayer) was obtained. This value is clearly higher than the value of 2/3 ML for the icelike water bilayers. This shows that the already rather disordered structure of the first water solvation layers has a higher density than ice, which is characteristic for liquid water. Furthermore, a value of ∼1:3 was obtained for the ratio of watA to watB molecules, which is

https://doi.org/10.1021/acs.chemrev.1c00679
Chem. Rev. XXXX, XXX, XXX−XXX

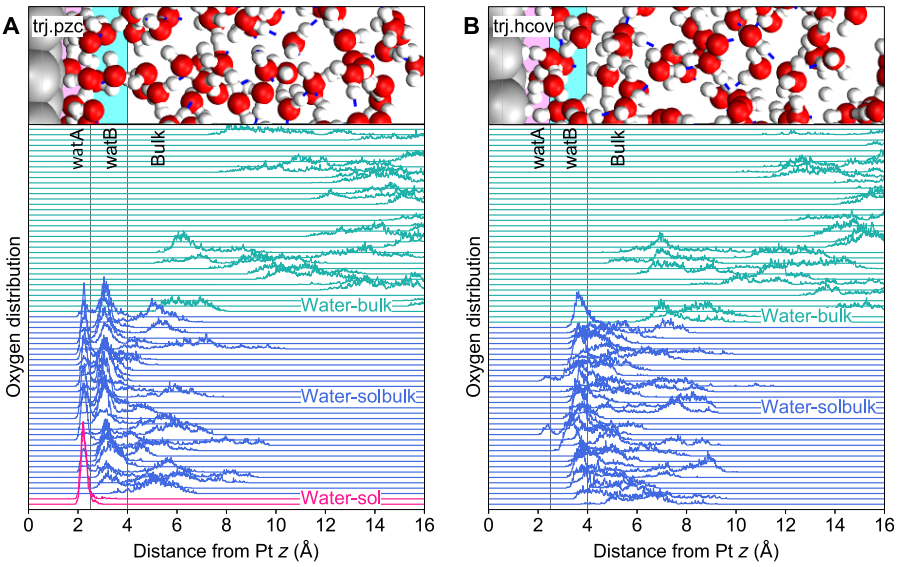

Figure 13. Distribution of the oxygen atoms of selected water molecules on Pt(111) along two 40 ps AIMD trajectories with 144 water molecules within a 6 × 6 surface unit cell.[20] (A) AIMD simulations of a pure water film on clean Pt(111). (B) AIMD simulations on a fully hydrogen-covered Pt(111) surface. The illustration is based on the data presented in ref 20.

1:1 for the icelike water bilayer. Obviously, the water coverage of liquid water on the metal surfaces is higher than those of icelike water layers, but the number of more strongly bound water molecules is lower.

In fact, the structure of the liquid water layers on the metal surfaces is obviously very dynamic. This is demonstrated in Figure 13, where the oxygen distribution in the first water layers on Pt(111) along two 40 ps AIMD trajectories with 144 water molecules within a 6 × 6 surface unit cell is shown.[20] Figure 13A displays the oxygen distribution of watA and watB water molecules staying for a certain amount of time within the solvation layer of a pure water film on clean Pt(111). In addition, some water molecules from the water bulk region above the metal surface have been selected.

The distributions in Figure 13A demonstrate that there was a constant exchange of the water molecules between the different water layers. Only two water molecules denoted by "water-sol" remained bound through the oxygen atom to the Pt(111) surface along the 40 ps of the AIMD run. All other water molecules that entered the watA region stayed there only temporarily and moved back and forth between the different water layers. These frequent exchanges ensured that the adsorbed water molecules were in equilibrium with the bulk liquid water. The water molecules that remained in the liquid water bulk regions also exhibited a wide distribution of distances from the Pt surfaces, demonstrating the high mobility of these water molecules.

Note that this Review in principle is not concerned with electrochemistry. However, it is not possible to discuss water/metal interfaces without addressing calculations and simulations under potential control. There have been a number of approaches to achieve that goal, as shown in refs 22 and 214−219, just to name a few, but it is fair to say that, in spite of considerable efforts, there is still no generally accepted scheme to realize this potential control. Some of these approaches try to achieve the potential control by varying the charge of the electrode. However, one has to note that the full electrochemical electrode/electrolyte interface has to be overall charge-neutral; otherwise, electric fields within the electrolyte would arise. Thus, any excess charge on the electrodes needs to be compensated by an opposite charge in the electric double layer (EDL) in the electrolyte. There are approaches that ensure this charge neutrality by explicitly allowing for charge compensation.[216] They are based on the idea of placing atoms into the electrolyte near the surfaces that then become either cations or anions, depending on their nature, and either transfer electrons to the Fermi energy of the electrode or attract electrons from there. For example, by adding hydrogen or alkali atoms into the water layer, cations become created and the electrode becomes negatively charged. Conversely, by adding halogen atoms or by removing hydrogen atoms from the water, anions are created, and the electrode becomes positively charged. Thus, the electrode potential effectively becomes altered, which, for example, can be monitored by the work functions of the water-covered electrode.

This approach to add or remove hydrogen atoms from the water layers in order to change the effective electrode potential has been used in a number of AIMD studies.[20,23] For example, adding or removing one hydrogen atom in the water layer in a simulation with a (6 × 6)Pt(111) surface unit cell lowers or raises the electrode potential, respectively, by ∼0.1 V.[20,23] Alternatively, sodium atoms also have been added to the water layers in order to modify the electrode potential.[58]

In Figure 14, the number of hydrogen-bond donors derived from AIMD simulations of the Au(111)/water interface is compared with the measured Raman water O−H frequencies as a function of the applied electrode potential.[213] In the simulations, the electrode potential has been varied by adding between zero and five sodium atoms to the water film. Furthermore, typical water structures in three potential regions are illustrated in the insets. Upon inserting atoms that then become cations in the aqueous electrolyte, the electrode potential can only be lowered, and the Au(111) surface becomes more negatively charged due to the transfer of the electron from the inserted Na atoms to the electrode. In region I, the number of hydrogen-bond donors at the interface decreases from ∼1.5 to ∼1. This indicates that the water molecules in the solvation layers at the interface gradually

https://doi.org/10.1021/acs.chemrev.1c00679
Chem. Rev. XXXX, XXX, XXX−XXX

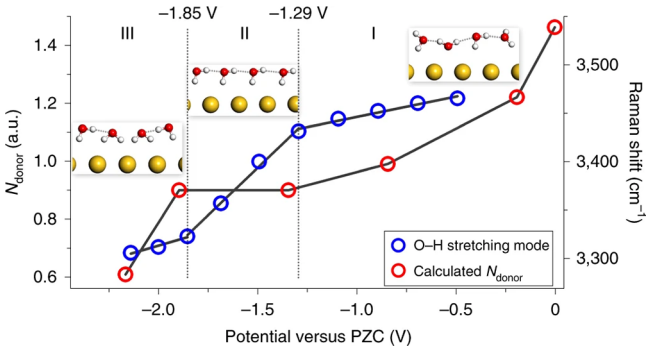

Figure 14. Properties of the Au(111)/water interface derived from AIMD simulations as a function of the electrode potential varied through the addition of Na atoms.[213] The calculated number of hydrogen-bond donors (red circles) and the experimental Raman O–H frequencies are plotted as a function of potential with respect to the potential of zero charge. In addition, structural models of the water in the corresponding potential regions are shown. Reprinted with permission from ref 213. Copyright 2019 Springer Nature.

become reoriented from a preferentially parallel configuration to a H-down configuration. The reorientation can be well-understood by the fact that the Au surface becomes more negatively charged for decreasing potential so that it is electrostatically more favorable when the positively charged hydrogen atoms of the water molecules turn toward the metal surface. Upon further decreasing the electrode potential, the water molecules even turn into a 2-H-down configuration because of the increased electrostatic attraction.

As already mentioned earlier, upon adding or removing one hydrogen atom in the water layer, the electrode potential can be lowered and raised, respectively, by ∼0.1 V with respect to the potential of zero charge for water above a (6 × 6)Pt(111) surface unit cell. Thus, the concentration of strongly bound watA molecules at the Pt(111) surface has been determined along AIMD simulations.[20] In fact, upon increasing the electrode potential, a higher number of watA molecules is observed. This can again be understood based on electrostatic arguments. At higher potentials, the metal electrode becomes more positively charged, which leads to a higher attraction of the negatively charged oxygen atoms of the water molecules. As far as the watB molecules are concerned, they are spread over a large area and diffuse rather freely within the layer at the lowest potential considered. Interestingly, they become more localized upon increasing the potential. This is related to the fact that at these higher potentials a larger number of strongly bound and highly localized watA molecules is present, which reduces the mobility of the watB molecules and makes their distribution pattern more structured.[20]

The effective electrode potential can also be changed by explicitly adding charge to the electrode region, which in a periodic setup then needs to be compensated by a corresponding countercharge[138,220] in order to keep the whole unit cell charge-neutral. In a hybrid AIMD explicit/implicit study combining explicit water molecules with an implicit solvent model to address voltage effects at the water/Au(111) interface,[220] the counter charge has been located in the implicit solvent region. These AIMD simulations confirmed the findings illustrated in Figure 14, namely, that the water molecules in the first layer above Au(111) orient toward or away from the electrode depending on the sign of the charge added to the electrode.

Another option to apply a bias to an interface is to use nonequilibrium Green's function (NGEF) techniques. Such an NGEF approach has been used to study the bias-dependent local structure of a water molecule at Au(111).[221] This study yielded qualitatively similar findings for the water/Au(111) structure as the AIMD studies under potential control.[213,220] However, because the NGEF study focused on one single water molecule above Au(111), it could show that a positive bias resulted in an unbound water molecule on Au(111) because of a combination of Pauli repulsion with electrostatic effects, whereas a negative bias led to a stronger oxygen–metal bond and a slightly rotated water molecule.[221]

4.2. Polarization Effects at Water–Metal Interfaces

After discussing the structural properties of water/metal interfaces obtained from AIMD simulations, we now turn to a closer look at the electronic properties of these interfaces. As Figure 8 has already demonstrated, the interaction of icelike water bilayers with Pt(111) leads to a strong polarization effect. Independent of whether the water bilayer is in the H-up or H-down configuration, there is a net charge transfer from the water layer toward the Pt(111) surface, leading to strong polarization effects and work function changes of the metal surface.[22] Of course, the question arises whether there are also such strong polarization effects at the interface of liquid water with metal surfaces. In fact, this issue has been addressed in several AIMD studies of water–metal interfaces.[23,199,202]

Figure 15 shows the averaged electronic charge density difference, the oxygen distribution profile, and snapshots derived from AIMD simulations at room temperature with 60 explicit water molecules above an orthogonal (5 × 4) Pt(111) surface unit cell and 48 explicit water molecules above an

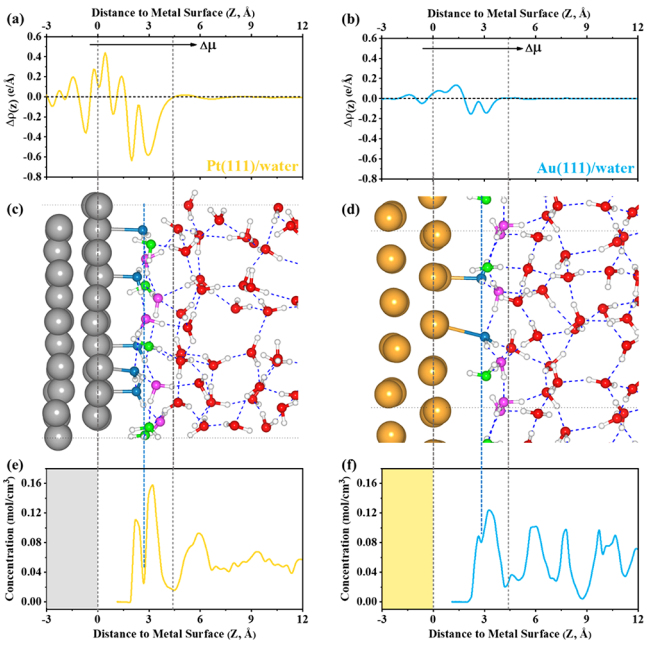

Figure 15. Electronic and atomic structures at Pt(111)/water and Au(111)/water interfaces derived from AIMD simulations. (a, b) Electronic charge density difference averaged along the AIMD trajectories. (c, d) Typical AIMD snapshot. The water molecules at the interface are colored differently to distinguish them from bulk water molecules. (e, f) Oxygen atom concentration distribution profiles. Reprinted with permission from ref 202. Copyright 2021 American Chemical Society.

https://doi.org/10.1021/acs.chemrev.1c00679
Chem. Rev. XXXX, XXX, XXX–XXX

Table 1. Summary of the Properties of the AIMD Simulations of Water Layers on Clean Metal (111) Surfaces Together with a Comparison of the Calculated and Measured Potential of Zero Charge (pzc) with Respect to the Standard Hydrogen Electrode (SHE)[a]

surface	unit cell	no. water mol.	functional, method	pzc_{theory} (V_{SHE})	pzc_{exp} (V_{SHE})
Pt(111)[76]	(3 × 3)	36	RPBE-D3, WF	0.57	
Pt(111)[23]	(6 × 6)	144	RPBE-D3, WF	0.52	0.1−0.5,[203] 0.35[222]
Pt(111)[199]	(6 × 6)	151	PBE-D3, CSHE	0.2	0.28,[206] 0.3[207]
Pt(111)[202]	(5 × 4)	60	PBE-D3, WF	0.23	
Pt(111)[223]	c(2 × 4)	52	PBE-D3, WF	0.43	
Pt(111)[223]	c(2 × 4)	52	PBE-D3, CSHE	0.21	
Pt(111)[223]	c(2 × 4)	52	rVV10,[224] WF	0.56	
Pt(111)[223]	c(2 × 4)	52	rVV10, CSHE	0.36	
Pd(111)[199]	(4 × 4)	68	PBE-D3, CSHE	−0.5	0.3,[203] 0.1[225]
Au(111)[199]	(6 × 6)	151	PBE-D3, CSHE	0.2	0.47[226]
Au(111)[202]	(3 × 4)	48	PBE-D3, WF	0.52	0.53[227]
Ag(111)[199]	(4 × 4)	69	PBE-D3, CSHE	−0.6	−0.45[228]

[a]Two different methods have been employed to derive the pzc, using either the work function (WF) or the computational standard hydrogen electrode (CSHE).[36,211]

orthogonal (3 × 4) Au(111) surface unit cell.[202] On Pt(111), the oxygen distribution profile again allows one to differentiate between the solvation water layers of watA and watB molecules. Furthermore, a strong electronic polarization of the first water layer on Pt(111) is observed that closely resembles the results obtained from the icelike bilayers on Pt(111)[22] shown in Figure 8. Thus, there is a significant charge transfer from the watA and watB water layer region toward the Pt(111) surface also in the more disordered water layers at room temperature. This strong electronic polarization of the water/Pt(111) interface has also been obtained in another AIMD study.[23]

However, as Figure 15b demonstrates, the polarization of the water/Au(111) is significantly weaker. This is also reflected in the work function changes of Pt(111) and Au(111) upon introducing the water film. Whereas on Pt(111) the work function is reduced by 1.07 eV due to the presence of water, it is only 0.22 eV for Au(111).[202] These results are also consistent with the corresponding work function changes for adsorbed water bilayers[22] presented earlier. Thus, the amount of polarization obviously reflects the strength of the interaction of the water molecules with these two metal surfaces. These differences can also be identified by comparing the oxygen concentration distribution profiles at both surfaces shown in Figures 15e and f. For Pt(111), two distinct peaks are visible corresponding to the strongly bound watA molecules and the more weakly bound watB molecules in the solvation layer. In contrast, on Au(111) there is a diffuse broad peak, and the more strongly bound watA molecules are only visible as a small shoulder peak.

Finally, we summarize the results of the AIMD simulations on the metal (111) surfaces presented in this section in Table 1, where the size of the unit cell, the number of water molecules, the functional used in the AIMD simulations, and the method to derive the potential of zero charge (pzc) are listed, and the calculated pzc is compared with the experimental values. Here we include an additional AIMD study[223] in which the pzc of Pt(111) was derived from the determination of the work function (WF) and by employing the CSHE, both using the PBE-D3 functional as well as nonlocal van der Waals correction including rVV10 functional.[224]

Except for Pd(111),[199] the pzc values derived from the AIMD simulations are in reasonable agreement with the experimental values. Note that, with respect to the measured pzc of Pt(111), there is some experimental spread. This is mainly caused by the fact that the experimental determination is hampered by the fact that Pt(111) strongly interacts with the ions present in the electrolyte.[207] Apparently, the size of the unit cells is not a very critical parameter, at least as far as the pzc is concerned; the same appears to be true for the exact choice of the functional. Hence, the pzc does not seem to be a very sensitive parameter reflecting the quality of an AIMD simulation of water/metal interfaces. Still, considering the study by Bramley et al.,[223] in which the pzc was derived both from the work function and using the CSHE, the latter approach yields values that are ∼0.2 V lower than those derived from the work function.

4.3. Water Layers on Adsorbate-Covered Metal Surfaces

It is important to realize that liquid water typically contains not only water molecules but also a certain concentration of ions, as already mentioned earlier when discussing the electrochemical aspects of water layers. Even in pure water, the autoionization of water produces H^+ proton and OH^- hydroxide anion with a concentration given by the autoionization constant pK_w of water, which at room temperature is pK_w = pH + pOH = 14. This leads to pH = pOH = 7 for any solvent not containing any acid or base. Furthermore, even low ion concentrations in water can lead to a high coverage of these species on metal surfaces[9] when the interaction of the ions with the metal surface is strong enough. While the presence of strongly interacting anions such as halides leads to highly covered metal surfaces, the products of the autoionization of water, namely, the H^+ proton and the OH^- hydroxide anion, also strongly interact with specific metal surfaces and thus cover metal surfaces. For example, it is well-known in electrochemistry that Pt electrodes become hydrogen-covered at low electrode potentials, at which the metal electrode surface is negatively charged, whereas at high electrode potentials, the adsorption of OH or other anions that are present in the electrolyte starts.[173,229] There is only a narrow potential window, the so-called double layer region that is dependent also on the pH value, at which Pt(111) in contact with water is not covered by any adsorbate. Hence, rigorously speaking, the AIMD simulations of liquid water on clean

https://doi.org/10.1021/acs.chemrev.1c00679
Chem. Rev. XXXX, XXX, XXX−XXX

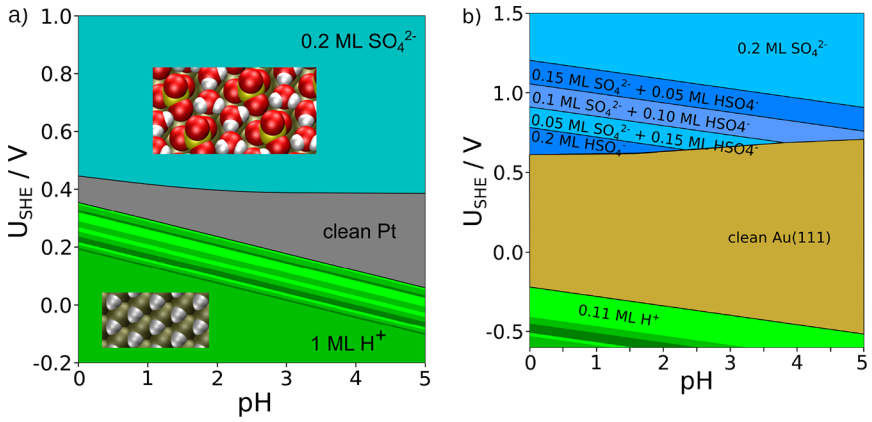

Figure 16. Pourbaix diagrams derived within the concept of the computational hydrogen electrode of adsorbed sulfate (SO_4^{2-}), bisulfate (HSO_4^-), and protons (H^+) on Pt(111) (a) and Au(111) (b) for a temperature of T = 298 K and a fixed sulfate activity of $a(SO_4^{2-})$ = 0.1. The green area denotes the hydrogen-covered phases, whereas the blue areas indicate SO_4^{2-} and HSO_4^- adsorbate phases. Adapted from ref 176 under the Creative Commons Attribution License (CC BY).

Pt(111) presented in this Review so far are only valid for a specific, rather narrow range of electrochemical conditions.

Hence, before starting any numerically expensive AIMD run of metal−water interfaces, one needs to carefully reflect what kind of metal−water interfaces shall be considered and whether adsorbed species might be present at the thermodynamic conditions to which the simulations correspond. AIMD simulations are still too time-consuming to derive stable adsorbate configurations at surfaces, for example, using thermodynamic integration methods. However, there are grand-canonical schemes that allow one to address this issue[25,39,230−232] very conveniently.

The first applications of this scheme were done in the field of heterogeneous catalysis,[230,233] where this approach was coined ab initio thermodynamics. If the free energies entering the grand-canonical scheme were all correctly determined, then the results of this scheme would correctly identify the equilibrium structure of the considered interfaces. Still, the evaluation of free energies is rather complex and time-consuming. Therefore, usually in these calculations the thermodynamic control parameter such as temperature and pressure only enters the properties of the species in the gas-phase reservoir. However, at solid−gas interfaces the presence of the gas phase and temperature, pressure, and entropy effects can often be safely neglected in the determination of the free energies of the surface structure.[230] Hence, good agreement between theory and experiment has been obtained in the description of reactions in heterogeneous catalysis.[234,235]

At metal−water interfaces, in contrast to metal−gas interfaces, typically the adsorbates originate from the solvated species. Hence, as the reference in the determination of the adsorption energies, the solvation energies of these species have to be employed. Again, the evaluation of solvation energies is rather complex and typically requires demanding methods such as thermodynamic integration schemes.[236] Their evaluation in fact can be avoided elegantly by utilizing the fact that many solvated species are connected to corresponding gas-phase species through their redox potential. This is the basis of the concept of the computational hydrogen electrode (CHE).[231,232] For example, at standard conditions the H_2 molecule is in equilibrium with the proton H^+ and the electron in solution. In addition, it is also well-known how the electrochemical potential of the proton changes with the electrode potential and the proton concentration, i.e., the pH value. Hence, the H_2 molecule in the gas phase can be used as the reference for the electrochemical potential of the solvated proton.

To determine the free energies of adsorption entering the CHE approach, in principle the free energies of the adsorbed species in the presence of the solvent need to be calculated, which, again, is computationally very demanding. Hence, in applications of the CHE concept, often the presence of the solvent is neglected in the first-principles calculations of adsorbate structures.[231,232,237] In fact, in the adsorption of small species strongly interacting with metal surfaces such as halogen and hydrogen atoms, indeed the presence of water and varying electrode potentials often can be neglected safely. Stable halide structures on metal electrodes as a function of the electrochemical control parameters[9] have been correctly identified in first-principles calculations,[174] and even more complex phenomena such as the competitive adsorption of halides and protons[238] have been semiquantitatively reproduced.[175]

However, for larger adsorbates such as sulfates, the presence of water can no longer be neglected. Experimentally, it is well-known that at high electrode potential sulfate forms rowlike $\sqrt{3} \times \sqrt{7}$ structures on Pt(111)[239,240] and Au(111).[241,242] DFT studies showed that such a rowlike $\sqrt{3} \times \sqrt{7}$ structure can be stabilized by water molecules that are situated in between the sulfate rows.[243,244] First-principles calculations using the concept of the computational hydrogen electrode confirmed that the existence of the striped sulfate phase on Pt(111) can only be reproduced if explicit water molecules are appropriately taken into account.[176,242] The phase diagrams resulting from such calculations are shown in Figure 16, where so-called Pourbaix diagrams of adsorbed sulfate (SO_4^{2-}), bisulfate (HSO_4^-), and protons (H^+) on Pt(111) and Au(111) are shown. Pourbaix diagrams correspond to phase diagrams as a function of the pH value and the electrode potentials.

Figure 16a illustrates that, at low electrode potentials with respect to the standard hydrogen electrode (SHE), Pt(111) is hydrogen-covered; then there is a small potential window, the so-called double layer region mentioned earlier, in which Pt(111) is uncovered. At an electrode potential slightly above 0.4 V vs SHE, sulfate adsorption in the rowlike $\sqrt{3} \times \sqrt{7}$ structure becomes thermodynamically stable, in agreement

https://doi.org/10.1021/acs.chemrev.1c00679
Chem. Rev. XXXX, XXX, XXX−XXX

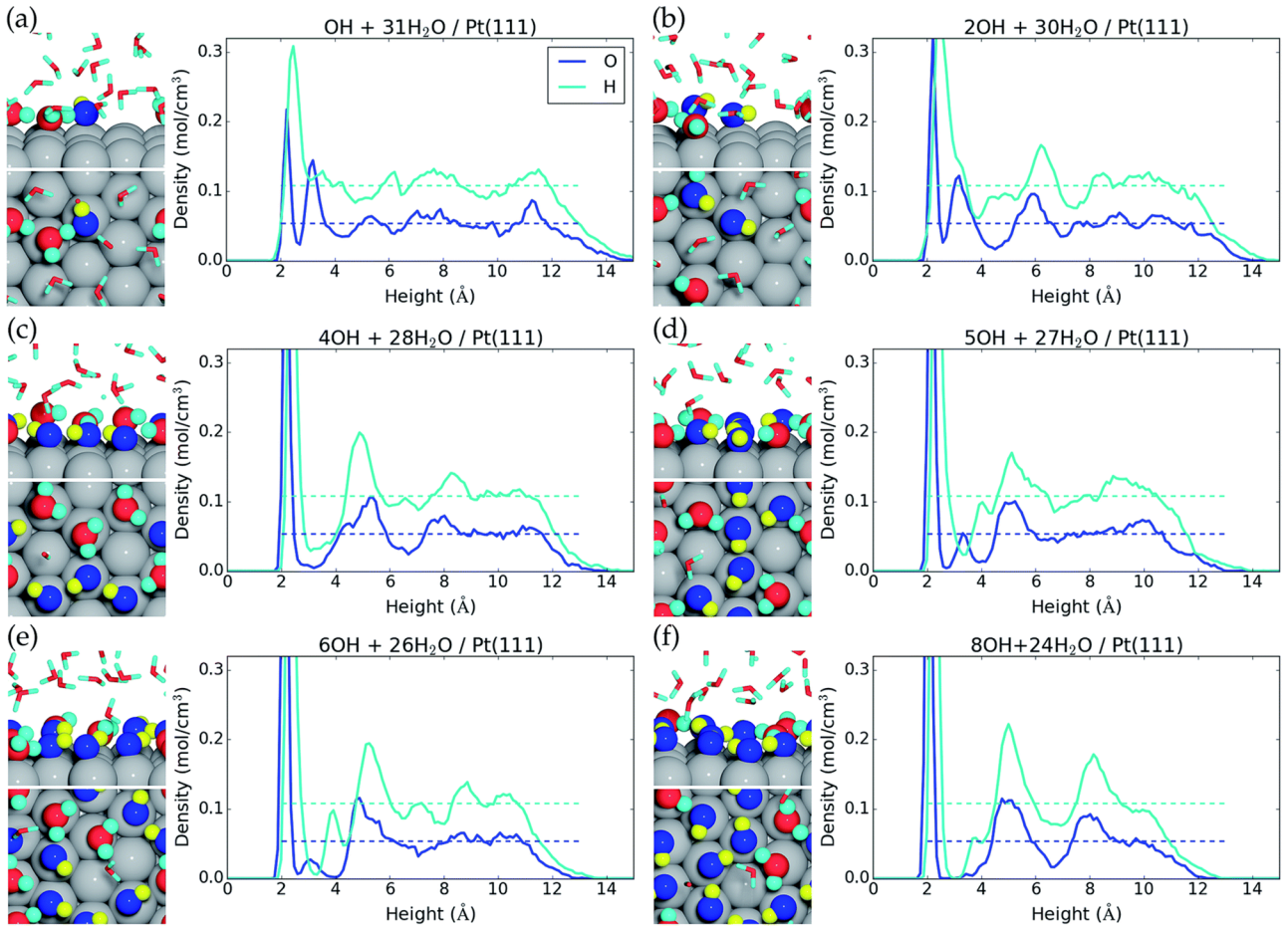

Figure 17. Snapshots in side and top view and averaged atomic density of AIMD simulations, in which (a) one, (b) two, (c) four, (d) five, (e) six, and (f) eight water molecules at the Pt(111)/water interface are replaced by adsorbed OH. The snapshots have been taken at the end of the AIMD runs, which lasted at least for 30 ps. The oxygen atoms of the adsorbed hydroxide are colored in blue. Reprinted from ref 248 under a Creative Commons Attribution 3.0 Unported License.

with the experiment.[239,240] This structure is illustrated in the inset of Figure 16a. The adsorbed sulfate forms rows that are interlocked and stabilized by strongly adsorbed water molecules. Without the explicit consideration of the water molecules, this structure would only appear at conditions that are rather different from those observed in the experiment, stressing the importance of the explicit inclusion of these molecules.

On Au(111) (Figure 16b), there is a much wider potential window in which the clean metal surface is thermodynamically stable in the presence of a sulfate-containing electrolyte. This is due to the weaker interaction of gold with adsorbates than that of, e.g., platinum. Above 0.6 V, a series of mixed bisulfate/sulfate adsorbate structures appears. Experimentally, cyclic voltammograms in this potential are rather featureless, but above 1 V, a spike in the cyclic voltammograms appears and a disorder−order transition in the surface structure becomes observable in STM measurements.[241,242] This structural transition agrees nicely with the occurrence of the pure $\sqrt{3} \times \sqrt{7}$ sulfate phase obtained in DFT calculations within a grand-canonical approach,[176,242] as illustrated in Figure 16b. Again, this structure is significantly stabilized in the calculations through the presence of the explicit water molecules between the sulfate rows; without their consideration, the experimentally observed $\sqrt{3} \times \sqrt{7}$ sulfate phase would not even show up as thermodynamically stable in the Pourbaix diagrams.[176]

Note that, in the calculations presented in Figure 16, no hydroxide or oxygen adsorption has been considered. However, it is well-known that, even in the presence of anions such as sulfate in the electrolyte, at higher potentials first hydroxide adsorption and then oxygen adsorption and surface oxidation occur.[245,246] This has been confirmed in grand-canonical calculations yielding Pourbaix diagrams for Ag(111), Pt(111), and Ni(111).[229] In this work, only H, OH, and O were considered as adsorbates. According to this study, for low pH values Ag dissolves and then oxidizes, whereas for Pt(111) the pH value does not influence the sequence of oxide phases. Ni(111), on the other hand, dissolves at low electrode potential and pH values that correspond to both acidic and alkaline solutions.[229] The findings for Pt(111) were later reproduced to a large extent in a study based on the concept of the generalized computational hydrogen electrode.[247]

In AIMD simulations of water on adsorbate-covered metal surfaces, so far mainly the native adsorbates hydrogen and hydroxide have been considered,[20,23,171,201,247−249] but phenol-covered surfaces have also been considered.[250] On Pt(111), hydrogen adsorption is thermodynamically stable at low electrode potentials, as illustrated in Figure 16a. This hydrogen coverage passivates the Pt(111) surface to a certain extent and lowers the water adsorption energies. In one of the first AIMD

https://doi.org/10.1021/acs.chemrev.1c00679
Chem. Rev. XXXX, XXX, XXX−XXX

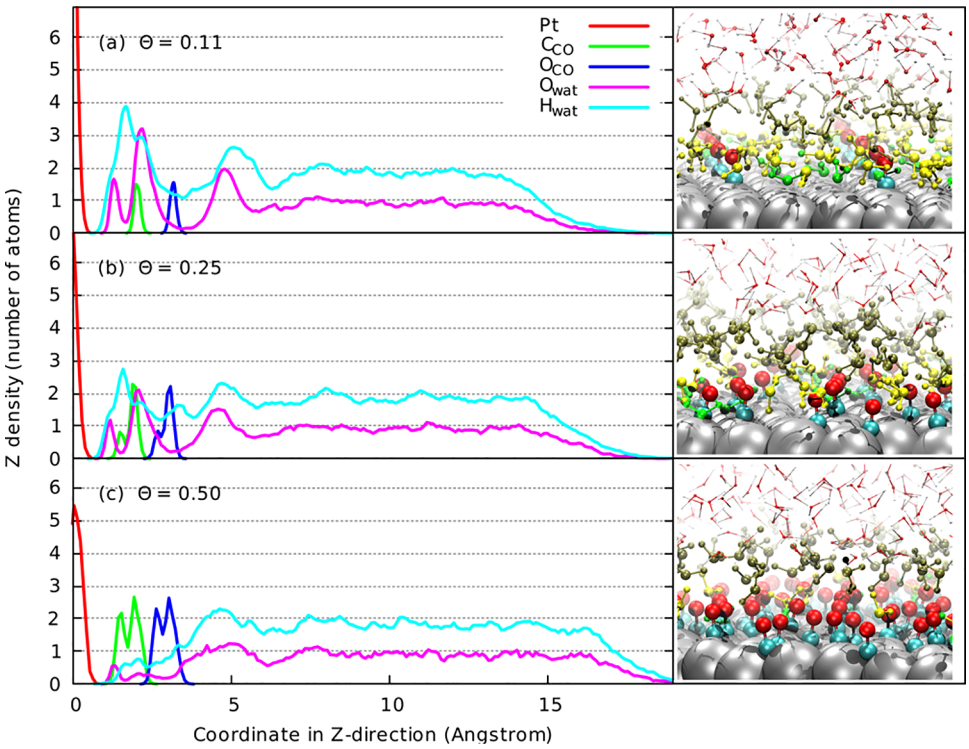

Figure 18. Atomic density profiles and snapshots of first-principles molecular dynamics simulation of the water/CO/Pt(111) interface with 134 water molecules within a (6 × 6) surface unit cell and CO coverages of (a) 0.11 ML, (b) 0.25 ML, and (c) 0.50 ML. The differences in the color coding of the water molecules indicate their distance from the surface. Reprinted with permission from ref 251. Copyright 2018 American Chemical Society.

studies addressing water on H/Pt(111), the simulations were performed for two water layers within a $2\sqrt{3} \times 2\sqrt{3}R30°$ geometry initially in the structure of icelike bilayers[171] with a relatively short simulation time of 11 ps at a temperature of 300 K. The weaker interaction strength of Pt(111) through the passivating hydrogen layers leads to an increase of the distance of the first water layer by ∼1 Å.

The repulsion of water from the Pt(111) surface upon the formation of the hydrogen layer is also illustrated in Figure 13B, where the water distribution of six water layers within a 6 × 6 surface unit cell on hydrogen-covered Pt(111) averaged over a 40 ps AIMD run time[20] is shown. Still, the oxygen atoms of two water molecules penetrate into the SolA region for a short period of time. According to a thorough analysis of the trajectories, these events correspond to the formation of a H_3O^+ cation after the detachment of a proton from the surface that then remains close to the detachment site temporarily. The oxygen atoms of the watB molecules above hydrogen-covered Pt(111) show a larger variation in their location than the watB molecules above clean Pt(111). Furthermore, the density or coverage of the watB water molecules above H/Pt(111) is smaller than that above Pt(111) and close to the corresponding value for liquid water.[20] This can be attributed to the weaker interaction of the water molecules with H/Pt(111) leading to a less densely packed solvation layer. The effect of an increasing number of adsorbed hydrogen atoms on Pt(111) on the water structure was considered in an AIMD study with 32 water molecules within a 3 × 4 orthogonal surface unit cell.[248] These simulations found that the hydrogen atom competed with the chemisorbed water molecules for adsorption sites and effectively replaced these water molecules.

The fact that a saturation hydrogen coverage on Pt(111) basically eliminates the chemisorption of water, as indicated in Figure 13B, has also been confirmed in two further AIMD studies[201,252] with basically the same setup that is illustrated in Figure 12a. In the second study,[201] the electrode potential was varied between −0.03 and −0.84 V vs SHE by including between one and five sodium atoms in the solution, which immediately became Na^+ ions in the solution, with their electrons being transferred to the Fermi energy of the metal. Thus, the differential Helmholtz capacitance also could be derived as a function of the electrode potential. It turns out that this capacitance for the hydrogen-covered Pt(111) electrode depends only very weakly on the electrode potential, which has been explained by the compensation between charge polarization and water-reorientation effects.[201]

The effect of adsorbed hydroxyl on Pt(111) on the water structure was studied by successively replacing water molecules with OH in the AIMD study already mentioned earlier.[248] The results of this study are presented in Figure 17. In addition, the internal energies of the particular configurations have been determined from the time-averaged DFT energy plus the time-averaged kinetic energy of the AIMD simulations. In fact, if the OH formation energy is calculated with respect to the dissociation of water molecules and the formation of a corresponding amount of gas-phase hydrogen molecules, then the OH formation at the Pt(111)/water interface turns out to be endothermic.[248] Among the considered systems, the energy cost per hydroxide is the lowest for OH coverages of 0.08 and 0.42 ML. This was considered to be surprising because DFT studies of OH formation at the interface of Pt(111) with a static water bilayer[253] found an OH coverage of 1/3 to be the most stable. Still, one has to take into account

https://doi.org/10.1021/acs.chemrev.1c00679
Chem. Rev. XXXX, XXX, XXX−XXX

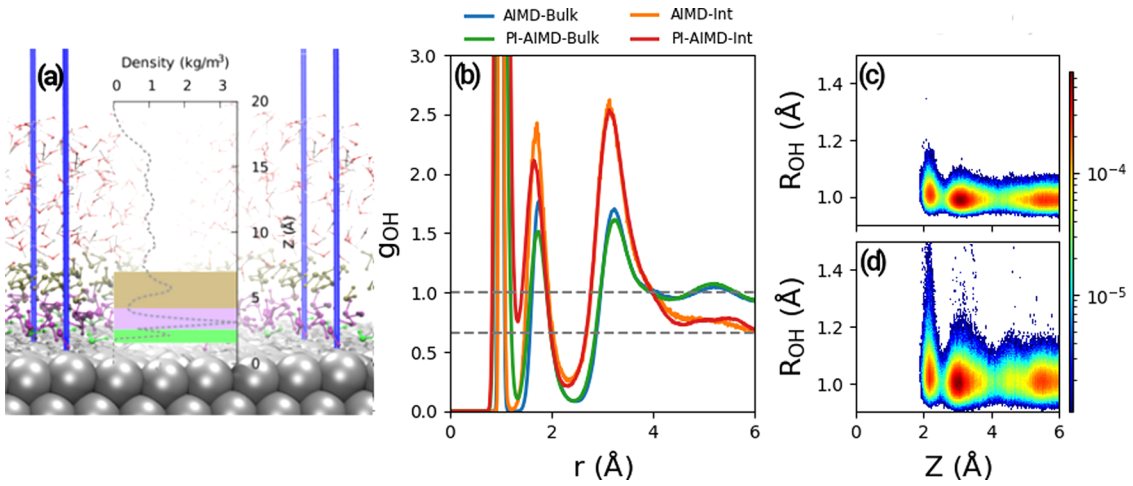

Figure 19. Path-integral AIMD (PI-AIMD) simulations of a liquid water film on a Pt(111) surface. (a) Illustration of the simulation box together with a plot of the density of water as a function of the distance from the surface. (b) O−H radial distribution functions derived from both the AIMD and PI-AIMD simulations, separately for the water molecules in the bulk and at the interface. (c, d) Distribution of the O−H obtained from the AIMD (c) and PI-AIMD (d) simulations in the whole considered water systems. Probabilities rise from blue to red in the false-color representation. Reprinted with permission from ref 116. Copyright 2020 American Chemical Society.

that it is not the formation energy per adsorbate that determines the stability of the corresponding adsorbate phase but rather the formation energy per surface area. This would yield an OH coverage of 0.75 ML to be most stable based on the formation energies per OH as a function of coverage reported in this study. Note that DFT calculations with the presence of water on Pt(111) modeled by an implicit solvent found an OH coverage of 2/3 to be the most stable.[254]

Interestingly, according to this AIMD study[248] with 32 water molecules above a (3 × 4) Pt(111) surface, the pure $32H_2O$/Pt(111) interface is not particularly dynamic; only a few events of water adsorption and desorption are observed during the AIMD run time of >30 ps. In fact, it is hard to judge whether this is consistent or inconsistent with the water distribution shown in Figure 13A, which in fact suggests a frequent exchange of water molecules at the clean Pt(111)/interface.[20] In contrast, in the AIMD simulations with OH coverages of 0.08 and 0.17 ML,[248] protons are transferred between adsorbed H_2O and OH species on a time scale of <1 ps, and water molecules adsorb and desorb on a time scale of 5 ps. For higher OH coverages, the H_2O and OH species at the surface become more detached from the water in the subsequent layers. This is reflected in the more pronounced minima in the atomic density at larger distances after the large peaks corresponding to the first water layer for increasing OH coverage in Figure 17. This spatial separation obviously reduces the number of water-exchange events. Obviously, the dynamic nature of water layers at metal surfaces still needs to be scrutinized in more detail.

The aqueous Pt(111)/CO/water interface at different CO coverages was studied by the second-generation Car−Parrinello molecular dynamics scheme.[251] Snapshots of the simulations together with the averaged atomic density profiles for CO coverages of 0.11, 0.25, and 0.5 ML are shown in Figure 18. The simulations were performed at room temperature in a (6 × 6) Pt (111) surface unit cell with 134 water molecules, and the production runs were performed for 30 ps. CO adsorbed in an upright fashion at the on-top positions of Pt(111) at low coverages,[255] but with only a slight energetic preference, whereas at high coverages of 0.75 ML, CO adsorbate structures with a coexistence of on-top and 3-fold hollow sites exist.[256] In the first-principles simulations illustrated in Figure 18, the CO molecules increasingly populate Pt bridge sites at higher coverages; for Θ = 0.5, both adsorption sites are almost equally possible in the presence of water. For higher CO coverages, the density profile of water becomes much smoother, indicating that the water becomes more liquid-like above the CO molecules, which indicates a passivating of the surface by the CO molecules. Upon increasing the CO coverage, the C−O stretch frequencies increase, both in vacuum and in the presence of water, apparently due to the higher CO−CO repulsion, which weakens the interaction with the metal surface. The presence of water leads to a red-shift of the vibrational frequencies, which, however, vanishes for the CO coverage of 0.5 ML, at which the water molecules are practically all above the CO layer, which reduces the water−CO interaction.

4.4. Nuclear Quantum Effects at Water/Metal Interfaces

As already mentioned in the Theoretical Description of the Water−Water and Water−Metal Interactions section, nuclear quantum effects might play a role in the description of water due to the light mass of the hydrogen atoms. However, the consideration of nuclear quantum effects on a first-principles level is numerically rather demanding as they require, e.g., performing path-integral (PI) molecular dynamics techniques.[109] Still, PI-AIMD studies are possible, as demonstrated in a PI-AIMD study of the effect of quantum delocalization on the ionization of water at water/metal interfaces.[116] The PI simulations have been performed at room temperature with six beads per atom for water at Pt(111) and Au(111) using a (6 × 6) surface unit cell containing 134 water molecules, as illustrated in Figure 19a.

The calculated O−H radial distribution functions for water in the bulk and at the Pt(111) interface are plotted in Figure 19b. The distributions in the bulk derived from the AIMD and PI-AIMD simulations (blue and green lines in Figure 19b, respectively) are rather similar. Only the first peak is slightly more broadened in the quantum simulations compared to that in the classical simulations. At the interface, the situation is different. The quantum simulations yield a higher probability

https://doi.org/10.1021/acs.chemrev.1c00679
Chem. Rev. XXXX, XXX, XXX−XXX

of finding the hydrogen atom at distances between 1.2 and 1.5 Å from the oxygen atom. Note that these distances are between those of the O−H bond in water and the hydrogen bond. These distances have been associated with proton-transfer events.[116]

This broadening becomes more obvious in Figure 19c and d, where the distribution in the intramolecular O−H distance R_{OH}, i.e., the distance between the oxygen atoms and the closest hydrogen atoms, is plotted as a function of the distance from the surface. Close to the surface, this distribution is significantly broader in the quantum simulations (Figure 19c) than in the classical simulations (Figure 19d). The quantum simulations yield a much larger delocalization in the O−H distances, suggesting a higher tendency toward ionization. Indeed, along the quantum PI-AIMD trajectories, water dissociation is much more frequent than that along the classical AIMD trajectories: whereas in the classical simulations within 25 ps practically no dissociation events occur, in the quantum simulations dissociated water molecules are present in 7% of the sampled configurations. There is also an isotope effect in the ionization probability. Running the PI-AIMD simulations for D_2O yields ionization of the water molecules for only 3.5% of the time. In contrast to Pt(111), on Au(111) no enhancement of the ionization probability is observed in the quantum simulations compared to the classical simulations. Hence, there is a clear correlation of the ionization probability with the strength of the metal−water interaction.

The comparison between AIMD and PI-AIMD simulations[116] yields rather interesting insights into the role of nuclear quantum effects in the interaction of water with metal surfaces. At the same time, chemical trends in the variation of the metal surfaces presented in this Review appear to induce more significant changes than the inclusion of quantum nuclear effects. Hence, it should be appropriate to neglect nuclear quantum effects to obtain a first general understanding of structures and processes at water/metal interfaces.

4.5. Experimental Validation of Ab Initio Studies of Water−Metal Interfaces

As far as the validation of the results of AIMD studies with respect to the properties of water/metal interfaces is concerned, we already noted earlier that the potential of zero charge does not appear to be a very sensitive parameter. However, one faces the additional problem that the arsenal of experimental tools to characterize these properties is limited. This is mainly due to the fact that electron beams cannot be used to probe the properties of these interfaces because their penetration length into water is limited. Surface X-ray scattering has been used to probe the distribution of water molecules at the Ag(111)/electrolyte interface.[257,258] These studies found a significant compression of the first water layer on Ag(111), which was explained by the strong electric field at the charged Ag(111) electrode.[258] However, such a strong compression could not be reproduced in DFT calculations,[15] and in principle it is also inconsistent with the fact that water is typically regarded as being incompressible.

As already mentioned earlier, vibrational spectra can be derived from molecular dynamics simulations. Methods such as sum-frequency generation (SFG) are only sensitive to regions that have no inversion symmetry; hence, they are well-suited to probe the vibrational properties at interfaces.[10,197,259] The difference between the vibrational spectra of the bulk liquid and a system including a metal−water interface also can be used to identify interface-specific modes. This has been done, for example, for the Pt−water interface employing surface-enhanced infrared absorption spectroscopy in the attenuated total reflection mode (ATR-SEIRAS) in which the bulk background has been derived from measurements of a CO-covered Pt electrode.[197] Furthermore, we already saw in Figure 14 how the number of hydrogen-bond donors at the Au(111)/water interface derived from AIMD simulations compared to measured Raman O−H frequencies.[213]

In fact, from molecular dynamics simulations, vibrational spectra can be derived through the Fourier transform of the velocity autocorrelation function, as already mentioned earlier, so that calculated and measured vibrational spectra at water/metal interfaces can be directly compared. Recall that, at water/metal interfaces, typically two vibrational bands related to water vibrations can be identified in the measured spectra. First, the O−H stretch vibration is observed with peaks at about 3200 and 3400 cm^{-1} that are associated with more strongly adsorbed water molecules and more weakly bonded, liquid water molecules, respectively.[197] Whereas on Au(111) the peak at 3400 cm^{-1} is more pronounced, on Pt(111) the peak at 3200 cm^{-1} is dominant, reflecting the stronger interaction of Pt with water than that of Au. Second, at ∼1600 cm^{-1} the HOH bending mode is observed.[189] However, on Pt[189,222] and Ag,[259] a broad peak at ∼3000 cm^{-1} also has been observed, and its assignment was controversially discussed. This particular peak was addressed in AIMD simulations of water on Pt(111) and Au(111);[18] the calculated vibrational spectra are shown in Figure 20. On Au(111), the computed vibrational spectra clearly peaked at 3400 and 1600 cm^{-1}, close to the results for bulk water. On Pt(111), in contrast, an additional peak in the vibrational spectra related to the watA molecules appears, whereas the OH stretch frequency of the watB molecules is close to 3400 cm^{-1}. The assignment of the vibrational frequencies to the watA and watB molecules on Pt(111) is also illustrated in Figure 20. In this sketch, the highest occupied molecular orbital of the watA molecule is shown, indicating the chemisorption of the watA molecule on Pt. This chemisorption is also associated with a charge transfer from the oxygen atom toward the surface, and it has been proposed that this charge transfer leads to strong hydrogen bonds of the watA molecules.[18]

Still, one should admit that the comparison of the center of two rather broad vibrational peaks at water/metal interfaces is certainly a necessary condition to judge the reliability of AIMD simulations but not a sufficient one. The same shifts might also be caused by a different structural arrangement of the water molecules at the metal surfaces. Still, due to the lack of experimental tools with an atomic resolution at water/metal interfaces, computer experiments based on reliable AIMD simulations are an indispensable tool to clarify the properties of these interfaces.

5. IMPLICIT SOLVENT MODELS

The proper treatment of the liquid side of water/metal interfaces requires one to perform statistical averages over sufficiently many different atomic configurations, i.e., microstates, leading to a considerable computational effort in order to obtain a reliable statistical sampling. One way to avoid this effort is to describe the electrode and any adsorbate layer atomistically but to describe the liquid through an implicit solvent model in which the liquid is modeled as a polarizable dielectric medium. Such an approach has been used widely to

https://doi.org/10.1021/acs.chemrev.1c00679
Chem. Rev. XXXX, XXX, XXX−XXX

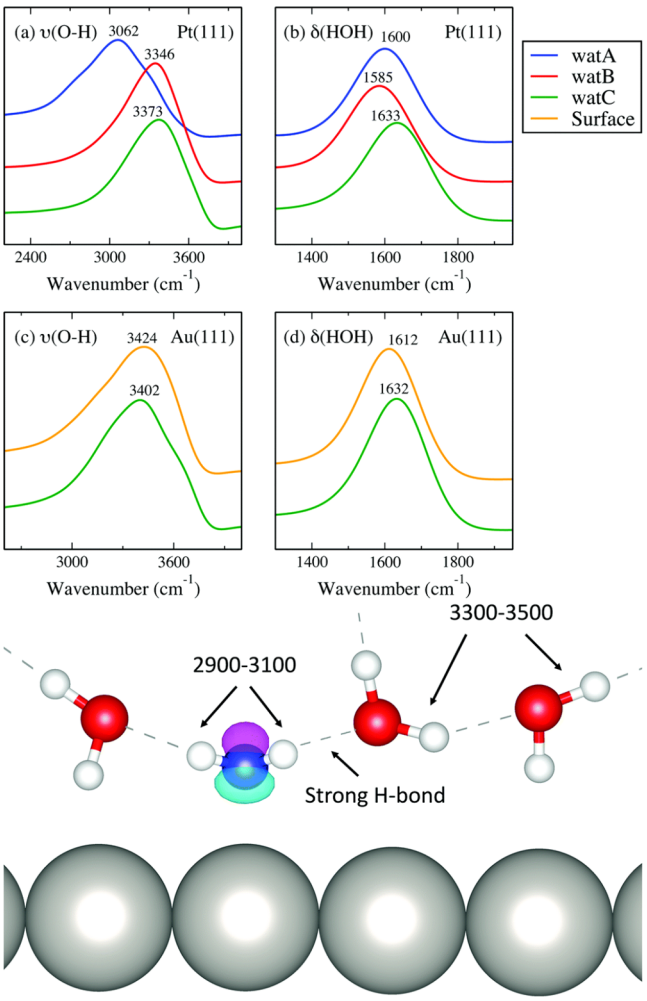

Figure 20. Vibrational frequencies of water molecules at Pt(111)−water and Au(111)−water interfaces derived from AIMD simulations determined for watA, watB, and watC molecules.[18] (a, c) Vibrational spectrum of the O−H stretching modes. (b, d) H−O−H bending modes. Furthermore, the assignment of vibrational OH stretch frequencies to the different water species at Pt(111) is illustrated in the extra panel. The weaker bound watB molecules have higher OH stretch frequencies than the more strongly bound watA molecule. For the watA molecule, the highest occupied molecular orbital (HOMO) is indicated by the pink and cyan isosurfaces. Reprinted with permission from ref 18. Copyright 2018 PCCP Owner Societies.

address solvation phenomena of isolated molecules.[261−263] However, this approach had not been implemented for a relatively long time in periodic codes. Only recently, on the basis of the groundbreaking work of Fattebert and Gygi,[264,265] has there been a number of implementations of implicit solvent models into periodic DFT codes,[198,266−277] which have been used quite frequently to describe structures and processes at metal−water interfaces.[176,254,278−282]

Indeed, implicit solvent models are computationally very attractive, taking the polarizable nature of electrolytes into account. Still, they correspond to an approximate description of the liquid nature of the electrolyte. Typically, in the implicit solvent models the parametrization is based on averaged bulk solvation data. Especially, they do not take any directional bonding and steric interactions of the solvent molecules into account, which is particularly critical in the description of polar solvents such as water.[260] Although the approximative nature of implicit solvent models is well-known,[283] it is still often hard to judge the severity of these approximations. This is especially caused by the lack of direct comparisons of the results of implicit and explicit solvent models for solid/electrolyte interfaces. The comparison with experimental results usually only allows one to qualitatively judge the reliability of implicit solvent models. For example, qualitative trends in the differential capacity of metal electrode surfaces are correctly reproduced,[283] and selectivity trends in electrocatalytic reactions at metal−water interfaces involving hydrophilic reaction intermediates are well-reproduced.[254,284]

Thus, there is certainly a need for AIMD benchmark studies that allow the validation of computationally less demanding but more approximative approaches to describe metal−water interfaces. There is one example presented in Figure 21 with respect to the adsorption energies of the small molecules and radicals CO, CHO, COH, OCCHO, and OH on metal−water interfaces.[260] The upper panels show the calculated adsorption energies ΔE_{ads} of these molecules on Cu(211), Cu(111), Au(111), and Pt(111) in vacuum and at metal−water interfaces with the water represented by either an implicit solvent model or explicit water molecules through AIMD simulations. As the reference for all of these adsorption energies, the gas-phase energies of the considered species have been taken. With regard to this gas-phase reference, one would naively expect that adsorption in the presence of water would be stronger than that in the gas phase because, in addition to the direct metal−adsorbate bonding, attractive water−adsorbate interactions would contribute to the adsorption energies. This is indeed the case for the adsorption on the flat Cu(111), Au(111), and Pt(111) surfaces. Interestingly, the AIMD simulations yield a destabilization of the considered adsorbates in the presence of water on the stepped Cu(211) surface. However, one also has to take into account that the molecular adsorbate replaces adsorbed water molecules, and obviously the replacement of more strongly bound water molecules at the stepped surface leads to this destabilization.[260] In implicit solvent models, this effect cannot be properly reproduced. Therefore, the presence of implicit water leads to a stabilization in all considered systems.

The solvation energies ΔE_{solv} plotted in the lower panels of Figure 21 correspond to the difference between the adsorption energies in either implicit or explicit water and the adsorption energies in vacuum. In fact, the comparison shows large differences of up to 0.6 eV, which are most pronounced for OH adsorption on the (111) surfaces. There is also no clear qualitative trend with respect to the order in the adsorption energies between the two solvent models. On Cu(211), the presence of explicit water leads to a weaker adsorption than seen in the presence of implicit water, whereas it is the other way around for most adsorbates on the (111) metal surfaces. Given the rather large differences in the adsorption energies in implicit and explicit water and the nonuniform qualitative trends between these two approaches, it is certainly fair to say that further work is needed in order to improve the reliability of implicit solvent models for the description of metal−water interfaces.

6. CONCLUSIONS AND OUTLOOK

In this Review, we have attempted to yield an overview of the growing field of ab initio simulations of water/metal interfaces. Water/metal interfaces play a ubiquitous role in many technologically relevant areas such as electrochemical energy

https://doi.org/10.1021/acs.chemrev.1c00679
Chem. Rev. XXXX, XXX, XXX−XXX

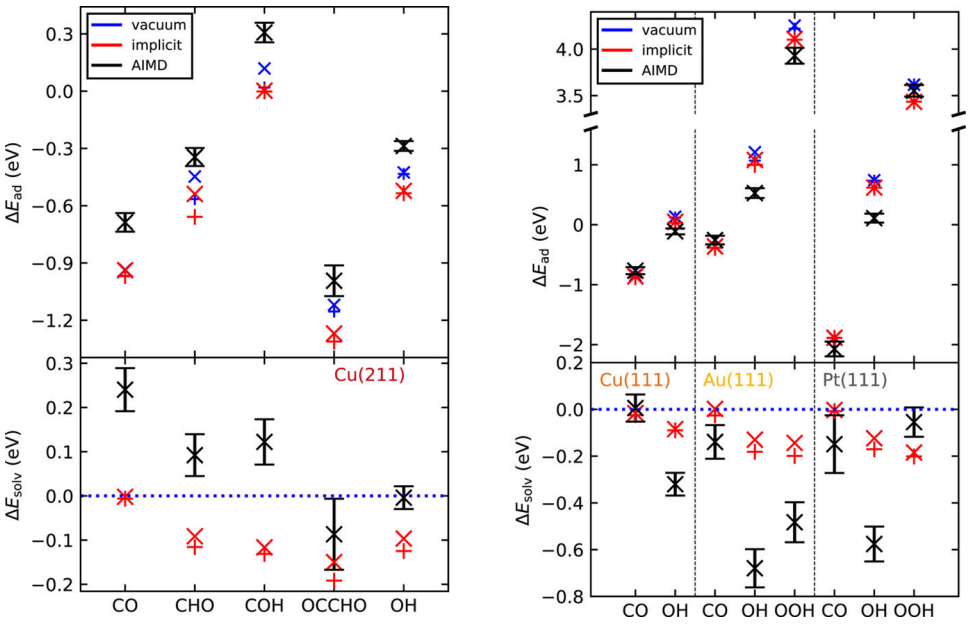

Figure 21. Comparison of the adsorption energies of various small molecules on Cu(211), Cu(111), Au(111), and Pt(111) derived from DFT calculations for the metal−vacuum interface (blue symbols), with the water represented by either an implicit solvent (red symbols) or explicit water molecules through AIMD simulations. Reprinted with permission from ref 260. Copyright 2020 AIP Publishing.

conversion and storage, electro- and photocatalysis, lubrication, and corrosion, as well as in the life sciences, which explains the interest in these interfaces. Although the interaction of water molecules with metal surfaces is in general not particularly strong and similar to the water−water interaction, water molecules can exhibit a significant electronic polarization close to the surface with a sizable electron transfer toward the metal surface. Due to this considerable electronic rearrangement, which strongly influences the properties of water/metal interfaces, in principle electronic structure methods are needed for a reliable modeling of water/metal interfaces.

However, water layers at metal surfaces do not exhibit a strong ordering at ambient conditions, at which their structures are rather liquid-like instead of icelike. This liquid nature of the water layers requires one to perform numerically demanding statistical averages, for example, those based on molecular dynamics simulation for sufficiently long times and adequately large system sizes. Fortunately, due to the ongoing improvement in computer power and advances in first-principles codes, it has become possible to run ab initio molecular dynamics simulations that are suitable to derive statistically meaningful results.

In this Review, we have presented recent AIMD studies of water/metal interfaces that provided detailed insights into the structure and properties of these interfaces. Whereas at more strongly interacting metal surfaces such as Pt(111) the first water solvation layer above the metal surface is characterized by the occurrence of water molecules that are relatively tightly bound through their oxygen atom to the Pt surface, at more weakly interacting metal surfaces such as Au(111) a more diffuse water layer results directly at the surface. From the second water layer on, the structure of the water films is already rather liquid-like, independent of the particular metal.

Most of the studies presented in this Review indeed focused on only a few benchmark systems, with Pt(111) and Au(111) being the most prominent ones. This is understandable, as still some basic concepts and features related to structures and processes at water/metal surfaces need to be identified and established. Still, the powerful approach of the AIMD methodology is well-suited to scrutinize the properties of other, more complex water/metal interfaces, for example, stepped surfaces or adsorbate-covered surfaces. It is undoubtedly true that AIMD studies of water/metal surfaces are still numerically demanding and require high-performance computing resources. Still, in principle such AIMD studies only need the identification of an interesting scientific question and the selection of the appropriate initial conditions. The corresponding computer experiment then provides a wealth of data and information that only needs to be appropriately harvested.

These computer experiments are also rather important in order to understand atomistic details of water/metal interfaces because the experimental tools to monitor structures and processes at water/metal interfaces are rather limited. The structure of water molecules and single water layers adsorbed on metal surfaces at low temperatures can still be determined by scanning probe techniques, but with respect to liquid water layers, mainly vibrational spectroscopy techniques provide data to which the results of AIMD simulations can be compared. Still, the vibrational bands at water/metal surfaces are rather broad, so that in principle only the consistency between simulations and experiment can be deduced from an agreement between calculated and measured results. On the other hand, the lack of experimental data regarding the atomistic details of water/metal interfaces makes the information derived from AIMD simulation even more valuable, of course under the assumption that the AIMD simulations yield reliable results.

Water/metal interfaces also play a central role in electrochemistry, and it is this interface at which most electrocatalytic reactions occur. In the theoretical description of electrochemical interfaces between aqueous electrolytes and metal electrodes, additional control parameters, such as the electrode

https://doi.org/10.1021/acs.chemrev.1c00679
Chem. Rev. XXXX, XXX, XXX−XXX

potential or the pH value, become essential. It is the long-term goal of theoretical electrochemistry to perform simulations under potential control, and there are promising approaches; however, there is no constant-potential method yet that is generally accepted. As far as electrocatalytic reactions at water/metal interfaces are concerned, little is known about the direct influence of the aqueous electrolyte, for example, with respect to the height of the reaction barriers. Their determination requires one to derive free activation energies, which is numerically even more demanding than plain AIMD simulations, as it necessitates the use of thermodynamic integration schemes. In general, true free energies have not been determined in any of the AIMD studies presented in this Review, so this still remains a challenge for the future.

The high numerical demand of AIMD simulations of course also calls for the identification of more approximate methods that still allow for an adequate description of water/metal interfaces. As far as adsorbates on surfaces are concerned, at least for strongly interacting and small adsorbates such as hydrogen or halogen atoms, there is some evidence that the influence of the aqueous environment can be neglected in the determination of adsorption energies, which then can enter a grand-canonical approach to derive equilibrium adsorbate structures. For the determination of the adsorption energy of larger adsorbates at water/metal interfaces, however, the explicit presence of water molecules cannot be safely neglected anymore. Here, the use of implicit solvent models offers a numerically attractive alternative to the explicit consideration of water molecules in the liquid phase. However, in principle implicit solvent models are not well-suited to describe polar solvents such as water. Note that AIMD simulations can be used to provide benchmark results in order to assess the reliability of implicit solvent models in the description of water/metal surfaces. For now, implicit solvent models are apparently able to provide qualitatively correct trends, but their quantitative accuracy needs to be further improved. It remains to be seen whether combinations of implicit and explicit solvent models might provide a suitable route to reduce the numerical effort of AIMD simulations without significantly compromising their reliability.

Overall, ab initio studies of water/metal interfaces are a suitable tool to provide reliable insights into structures and processes at these interfaces. They are numerically still demanding, but considering the progress in the efficiency of first-principles electronic structure methods and the ongoing increase in computer power, we anticipate a growing number of these ab initio studies, further deepening our understanding of water/metal interfaces.

AUTHOR INFORMATION

Corresponding Author

Axel Groß − *Institute of Theoretical Chemistry, Ulm University, 89069 Ulm, Germany; Electrochemical Energy Storage, Helmholtz Institute Ulm (HIU), 89069 Ulm, Germany;* orcid.org/0000-0003-4037-7331; Email: Axel.Gross@uni-ulm.de

Author

Sung Sakong − *Institute of Theoretical Chemistry, Ulm University, 89069 Ulm, Germany;* orcid.org/0000-0001-9777-7489

Complete contact information is available at: https://pubs.acs.org/10.1021/acs.chemrev.1c00679

Notes

The authors declare no competing financial interest.

Biographies

Axel Groß obtained his Diploma in Physics from the University of Göttingen in 1990 and his Ph.D. 1993 in Theoretical Physics at the Technical University of Munich. After five years as a staff scientist in the Theory Department of the Fritz-Haber-Institute of the Max-Planck-Society in Berlin, he became Associate Professor in Theoretical Physics/Surface Physics at the Technical University of Munich. In 2004 he was appointed as a Full Professor in Theoretical Chemistry at Ulm University; furthermore, in 2011 he became PI at Helmholtz Institute Ulm (HIU) Electrochemical Energy Storage. His research interests focus on the first-principles modelling of atomistic structures and processes at surfaces and at solid−gas and electrochemical electrode−electrolyte interfaces, reactions in heterogeneous and electrocatalysis, and materials modelling related to electrochemical energy storage.

Sung Sakong obtained his B.Sc. and M.Sc. in Physics at the Sogang University (Seoul) and Ph.D. in Theoretical Physics at the Technical University of Munich in 2005. Afterward, he worked as a researcher at the University of Duisburg-Essen and Ulm University. He has been studying elementary processes and phenomena at solid−gas and solid−liquid interfaces with first-principles atomistic modeling and numerical simulation techniques. His research interests cover structures and reactions in heterogeneous catalysis and electrocatalysis and the modeling of electrode−electrolyte interfaces.

ACKNOWLEDGMENTS

This research has been supported by the German Research Foundation (DFG) through Contract GR 1503/39-1 and Project ID 390 874 152 (POLiS Cluster of Excellence) and by the Dr. Barbara Mez-Starck Foundation. The authors acknowledge computer time provided by the state of Baden-Württemberg through the ForHLR and bwHPC programs and the German Research Foundation (DFG) through Grant no. INST 40/575-1 FUGG (JUSTUS 2 cluster). This work contributes to the research performed at CELEST (Center for Electrochemical Energy Storage Ulm-Karlsruhe).

REFERENCES

(1) Shi, R.; Tanaka, H. The Anomalies and Criticality of Liquid Water. *Proc. Natl. Acad. Sci. U. S. A.* **2020**, *117*, 26591−26599.

(2) Pettersson, L. G. M.; Henchman, R. H.; Nilsson, A. Water-The Most Anomalous Liquid. *Chem. Rev.* **2016**, *116*, 7459−7462.

(3) Björneholm, O.; Hansen, M. H.; Hodgson, A.; Liu, L.-M.; Limmer, D. T.; Michaelides, A.; Pedevilla, P.; Rossmeisl, J.; Shen, H.; Tocci, G.; Tyrode, E.; Walz, M.-M.; Werner, J.; Bluhm, H. Water at Interfaces. *Chem. Rev.* **2016**, *116*, 7698−7726.

(4) Seh, Z. W.; Kibsgaard, J.; Dickens, C. F.; Chorkendorff, I.; Nørskov, J. K.; Jaramillo, T. F. Combining Theory and Experiment in Electrocatalysis: Insights into Materials Design. *Science* **2017**, *355*, 146.

(5) Carrasco, J.; Hodgson, A.; Michaelides, A. A Molecular Perspective of Water at Metal Interfaces. *Nat. Mater.* **2012**, *11*, 667−674.

(6) Thiel, P. A.; Madey, T. E. The Interaction of Water with Solid Surfaces: Fundamental Aspects. *Surf. Sci. Rep.* **1987**, *7*, 211.

(7) Schmickler, W. Electronic Effects in the Electric Double Layer. *Chem. Rev.* **1996**, *96*, 3177−3200.

(8) Henderson, M. A. The Interaction of Water with Solid Surfaces: Fundamental Aspects Revisited. *Surf. Sci. Rep.* **2002**, *46*, 1.

(9) Magnussen, O. M. Ordered Anion Adlayers on Metal Electrode Surfaces. *Chem. Rev.* **2002**, *102*, 679−725.
(10) Shen, Y. R.; Ostroverkhov, V. Sum-Frequency Vibrational Spectroscopy on Water Interfaces: Polar Orientation of Water Molecules at Interfaces. *Chem. Rev.* **2006**, *106*, 1140−1154.
(11) Hodgson, A.; Haq, S. Water Adsorption and the Wetting of Metal Surfaces. *Surf. Sci. Rep.* **2009**, *64*, 381−451.
(12) Ceriotti, M.; Fang, W.; Kusalik, P. G.; McKenzie, R. H.; Michaelides, A.; Morales, M. A.; Markland, T. E. Nuclear Quantum Effects in Water and Aqueous Systems: Experiment, Theory, and Current Challenges. *Chem. Rev.* **2016**, *116*, 7529−7550.
(13) Brini, E.; Fennell, C. J.; Fernandez-Serra, M.; Hribar-Lee, B.; Lukšič, M.; Dill, K. A. How Water's Properties Are Encoded in its Molecular Structure and Energies. *Chem. Rev.* **2017**, *117*, 12385−12414.
(14) Michaelides, A.; Alavi, A.; King, D. A. Insight into H_2O-Ice Adsorption and Dissociation on Metal Surfaces from First-Principles Simulations. *Phys. Rev. B* **2004**, *69*, 113404.
(15) Roudgar, A.; Groß, A. Water Bilayer on the Pd/Au(111) Overlayer System: Coadsorption and Electric Field Effects. *Chem. Phys. Lett.* **2005**, *409*, 157.
(16) Michaelides, A. Density Functional Theory Simulations of Water-Metal Interfaces: Waltzing Waters, a Novel 2D Ice Phase, and More. *Appl. Phys. A: Mater. Sci. Process.* **2006**, *85*, 415.
(17) Groß, A.; Gossenberger, F.; Lin, X.; Naderian, M.; Sakong, S.; Roman, T. Water Structures at Metal Electrodes Studied by Ab Initio Molecular Dynamics Simulations. *J. Electrochem. Soc.* **2014**, *161*, E3015−E3020.
(18) Le, J.; Fan, Q.; Perez-Martinez, L.; Cuesta, A.; Cheng, J. Theoretical Insight into the Vibrational Spectra of Metal−Water Interfaces from Density Functional Theory Based Molecular Dynamics. *Phys. Chem. Chem. Phys.* **2018**, *20*, 11554−11558.
(19) Kristoffersen, H. H.; Chan, K.; Vegge, T.; Hansen, H. A. Energy−Entropy Competition in Cation−Hydroxyl Interactions at the Liquid Water−Pt(111) Interface. *Chem. Commun.* **2020**, *56*, 427−430.
(20) Sakong, S.; Groß, A. Water Structures on a Pt(111) Electrode from ab initio Molecular Dynamic Simulations for a Variety of Electrochemical Conditions. *Phys. Chem. Chem. Phys.* **2020**, *22*, 10431−10437.
(21) Le, J.-B.; Cheng, J. Modeling Electrified Metal/Water Interfaces from ab initio Molecular Dynamics: Structure and Helmholtz Capacitance. *Curr. Opin. Electrochem.* **2021**, *27*, 100693.
(22) Schnur, S.; Groß, A. Properties of Metal−Water Interfaces Studied from First Principles. *New J. Phys.* **2009**, *11*, 125003.
(23) Sakong, S.; Groß, A. The Electric Double Layer at Metal-Water Interfaces Revisited Based on a Charge Polarization Scheme. *J. Chem. Phys.* **2018**, *149*, 084705.
(24) Clabaut, P.; Staub, R.; Galiana, J.; Antonetti, E.; Steinmann, S. N. Water Adlayers on Noble Metal Surfaces: Insights from Energy Decomposition Analysis. *J. Chem. Phys.* **2020**, *153*, 054703.
(25) Groß, A.; Sakong, S. Modelling the Electric Double Layer at Electrode/Electrolyte Interfaces. *Curr. Opin. Electrochem.* **2019**, *14*, 1−6.
(26) Le, J.-B.; Cheng, J. Modeling Electrochemical Interfaces from ab initio Molecular Dynamics: Water Adsorption on Metal Surfaces at Potential of Zero Charge. *Curr. Opin. Electrochem.* **2020**, *19*, 129−136.
(27) Natarajan, S. K.; Behler, J. Neural Network Molecular Dynamics Simulations of Solid−Liquid Interfaces: wWater at Low-Index Copper Surfaces. *Phys. Chem. Chem. Phys.* **2016**, *18*, 28704−28725.
(28) Iyemperumal, S. K.; Deskins, N. A. Evaluating Solvent Effects at the Aqueous/Pt(111) Interface. *ChemPhysChem* **2017**, *18*, 2171−2190.
(29) Izvekov, S.; Mazzolo, A.; Van Opdorp, K.; Voth, G. A. Ab initio Molecular Dynamics Simulation of the Cu(110)-Water Interface. *J. Chem. Phys.* **2001**, *114*, 3248.
(30) Izvekov, S.; Voth, G. A. Ab initio Molecular Dynamics Simulation of the Ag(111)-Water Interface. *J. Chem. Phys.* **2001**, *115*, 7196.
(31) Helmholtz, H. Studien über elektrische Grenzschichten. *Ann. Phys.* **1879**, *243*, 337−382.
(32) Gouy, L. G. Sur la Constitution de la Charge Électrique à la Surface d'un Électrolyte. *J. Phys. Theor. Appl.* **1910**, *9*, 457.
(33) Chapman, D. L. A Contribution to the Theory of Electrocapillarity. *Philos. Mag. Series 6* **1913**, *25*, 475−481.
(34) Stern, O. Zur Theorie der Elektrolytischen Doppelschicht. *Z. Elektrochem. Angew. Phys.* **1924**, *30*, 508−516.
(35) Calle-Vallejo, F.; Koper, M. T. First-Principles Computational Electrochemistry: Achievements and Challenges. *Electrochim. Acta* **2012**, *84*, 3−11.
(36) Cheng, J.; Sprik, M. Alignment of Electronic Energy Levels at Electrochemical Interfaces. *Phys. Chem. Chem. Phys.* **2012**, *14*, 11245−11267.
(37) Magnussen, O. M.; Groß, A. Toward an Atomic-Scale Understanding of Electrochemical Interface Structure and Dynamics. *J. Am. Chem. Soc.* **2019**, *141*, 4777−4790.
(38) Schwarz, K.; Sundararaman, R. The Electrochemical Interface in First-Principles Calculations. *Surf. Sci. Rep.* **2020**, *75*, 100492.
(39) Groß, A. Grand-Canonical Approaches to Understand Structures and Processes at Electrochemical Interfaces From an Atomistic Perspective. *Curr. Opin. Electrochem.* **2021**, *27*, 100684.
(40) Siepmann, J. I.; Sprik, M. Influence of Surface Topology and Electrostatic Potential on Water/Electrode Systems. *J. Chem. Phys.* **1995**, *102*, 511−524.
(41) Crozier, P. S.; Rowley, R. L.; Henderson, D. Molecular Dynamics Calculations of the Electrochemical Properties of Electrolyte Systems Between Charged Electrodes. *J. Chem. Phys.* **2000**, *113*, 9202.
(42) Bukowski, R.; Szalewicz, K.; Groenenboom, G. C.; van der Avoird, A. Predictions of the Properties of Water from First Principles. *Science* **2007**, *315*, 1249.
(43) Spohr, E. Computer Simulations of the Water/Platinum Interface. *J. Phys. Chem.* **1989**, *93*, 6171.
(44) Spohr, E. Effect of Electrostatic Boundary Conditions and System Size on the Interfacial Properties of Water and Aqueous Solutions. *J. Chem. Phys.* **1997**, *107*, 6342−6348.
(45) Raghavan, K.; Foster, K.; Motakabbir, K.; Berkowitz, M. Structure and Dynamics of Water at the Pt(111) Interface: Molecular Dynamics Study. *J. Chem. Phys.* **1991**, *94*, 2110−2117.
(46) Xia, X.; Berkowitz, M. L. Electric-Field Induced Restructuring of Water at a Platinum-Water Interface: A Molecular Dynamics Computer Simulation. *Phys. Rev. Lett.* **1995**, *74*, 3193−3196.
(47) Heinz, H.; Vaia, R. A.; Farmer, B. L.; Naik, R. R. Accurate Simulation of Surfaces and Interfaces of Face-Centered Cubic Metals Using 12−6 and 9−6 Lennard-Jones Potentials. *J. Phys. Chem. C* **2008**, *112*, 17281−17290.
(48) Goddard, W. A., III.; Merinov, B. V.; van Duin, A. C. T.; Jacob, T.; Blanco, M.; Molinero, V.; Jang, S. S.; Jang, Y. H. Multi-Paradigm Multi-Scale Simulations for Fuel Cell Catalysts. *Mol. Simul.* **2006**, *32*, 251−268.
(49) Kirchhoff, B.; Braunwarth, L.; Jung, C.; Jonsson, H.; Fantauzzi, D.; Jacob, T. Simulations of the Oxidation and Degradation of Platinum Electrocatalysts. *Small* **2020**, *16*, 1905159.
(50) Braunwarth, L.; Jung, C.; Jacob, T. Exploring the Structure−Activity Relationship on Platinum Nanoparticles. *Top. Catal.* **2020**, *63*, 1647−1657.
(51) Daw, M. S.; Baskes, M. I. Embedded-Atom Method: Derivation and Applications to Impurities, Surfaces, and Other Defects in Metals. *Phys. Rev. B* **1984**, *29*, 6443.
(52) Daw, M. S.; Foiles, S. M.; Baskes, M. I. The Embedded-Atom Method − a Review of Theory and Applications. *Mater. Sci. Rep.* **1993**, *9*, 251−310.
(53) Lorenz, S.; Scheffler, M.; Groß, A. Descriptions of Surface Chemical rReactions Using a Neural Network Representation. *Phys. Rev. B* **2006**, *73*, 115431.

https://doi.org/10.1021/acs.chemrev.1c00679
Chem. Rev. XXXX, XXX, XXX−XXX

(54) Carbogno, C.; Behler, J.; Reuter, K.; Groß, A. Signatures of Nonadiabatic O_2 Dissociation at Al(111): First-Principles Fewest-Switches Study. *Phys. Rev. B* **2010**, *81*, 035410.
(55) Morawietz, T.; Behler, J. A Density-Functional Theory-Based Neural Network Potential for Water Clusters Including van der Waals Corrections. *J. Phys. Chem. A* **2013**, *117*, 7356−7366.
(56) Behler, J. Perspective: Machine Learning Potentials for Atomistic Simulations. *J. Chem. Phys.* **2016**, *145*, 170901.
(57) Morawietz, T.; Singraber, A.; Dellago, C.; Behler, J. How van der Waals interactions determine the unique properties of water. *Proc. Natl. Acad. Sci. U. S. A.* **2016**, *113*, 8368−8373.
(58) Le, T. C.; Winkler, D. A. Discovery and Optimization of Materials Using Evolutionary Approaches. *Chem. Rev.* **2016**, *116*, 6107−6132.
(59) Li, X.; Paier, W.; Paier, J. Machine Learning in Computational Surface Science and Catalysis: Case Studies on Water and Metal-Oxide Interfaces. *Front. Chem.* **2020**, *8*, 601029.
(60) Warshel, A.; Weiss, R. M. An Empirical Valence Bond Approach for Comparing Reactions in Solutions and in Enzymes. *J. Am. Chem. Soc.* **1980**, *102*, 6218−6226.
(61) Wilhelm, F.; Schmickler, W.; Nazmutdinov, R. R.; Spohr, E. A Model for Proton Transfer to Metal Electrodes. *J. Phys. Chem. C* **2008**, *112*, 10814−10826.
(62) Wilhelm, F.; Schmickler, W.; Nazmutdinov, R. R.; Spohr, E. Modeling Proton transfer to Charged Silver Electrodes. *Electrochim. Acta* **2011**, *56*, 10632−10644.
(63) Schmickler, W.; Wilhelm, F.; Spohr, E. Probing the Temperature Dependence of Proton Transfer to Charged Platinum Electrodes by Reactive Molecular Dynamics Trajectory Studies. *Electrochim. Acta* **2013**, *101*, 341−346.
(64) Wiebe, J.; Kravchenko, K.; Spohr, E. Electrolyte Effects in a Model of Proton Discharge on Charged Electrodes. *Surf. Sci.* **2015**, *631*, 35−41.
(65) Lin, H.; Truhlar, D. G. QM/MM: What Have We Learned, Where Are wWe, and Where Do We Go from Here? *Theor. Chem. Acc.* **2007**, *117*, 185.
(66) Groß, A. The Virtual Chemistry Lab for Reactions at Surfaces: Is It Possible? Will It Be Helpful? *Surf. Sci.* **2002**, *500*, 347.
(67) Hafner, J.; Wolverton, C.; Ceder, G. Toward Computational Material Design: the Impact of Density Functional Theory on Materials Research. *MRS Bull.* **2006**, *31*, 659.
(68) Burke, K. Perspective on Density Functional Theory. *J. Chem. Phys.* **2012**, *136*, 150901.
(69) Tsatsoulis, T.; Sakong, S.; Groß, A.; Grüneis, A. Reaction Energetics of Hydrogen on Si(100) Surface: A Periodic Many-Electron Theory Study. *J. Chem. Phys.* **2018**, *149*, 244105.
(70) Perdew, J. P.; Chevary, J. A.; Vosko, S. H.; Jackson, K. A.; Pederson, M. R.; Singh, D. J.; Fiolhais, C. Atoms, Molecules, Solids, and Surfaces: Applications of the Generalized Gradient Approximation for Exchange and Correlation. *Phys. Rev. B* **1992**, *46*, 6671.
(71) Perdew, J. P.; Burke, K.; Ernzerhof, M. Generalized Gradient Approximation Made Simple. *Phys. Rev. Lett.* **1996**, *77*, 3865.
(72) Hammer, B.; Hansen, L. B.; Nørskov, J. K. Improved Adsorption Energetics Within Density-Functional Theory Using Revised Perdew-Burke-Ernzerhof Functionals. *Phys. Rev. B* **1999**, *59*, 7413.
(73) Do, H.; Besley, N. A. Structural Optimization of Molecular Clusters with Density Functional Theory Combined with Basin Hopping. *J. Chem. Phys.* **2012**, *137*, 134106.
(74) Paier, J.; Marsman, M.; Kresse, G. Why Does the B3LYP Hybrid Functional Fail for Metals? *J. Chem. Phys.* **2007**, *127*, 024103.
(75) Soper, A. K. The Radial Distribution Functions of Water as Derived from Radiation Total Scattering Experiments: Is There Anything We Can Say for Sure? *ISRN Phys. Chem.* **2013**, *2013*, 279463.
(76) Sakong, S.; Forster-Tonigold, K.; Groß, A. The Structure of Water at a Pt(111) Electrode and the Potential of Zero Charge Studied from First Principles. *J. Chem. Phys.* **2016**, *144*, 194701.
(77) Fernández-Serra, M. V.; Artacho, E. Network Equilibration and First-Principles Liquid Water. *J. Chem. Phys.* **2004**, *121*, 11136−11144.
(78) VandeVondele, J.; Mohamed, F.; Krack, M.; Hutter, J.; Sprik, M.; Parrinello, M. The Influence of Temperature and Density Functional Models in ab initio Molecular Dynamics Simulation of Liquid Water. *J. Chem. Phys.* **2005**, *122*, 014515.
(79) Liu, L.-M.; Krack, M.; Michaelides, A. Interfacial Water: A First Principles Molecular Dynamics Study of a Nanoscale Water Film on Salt. *J. Chem. Phys.* **2009**, *130*, 234702.
(80) Soper, A. K. Joint Structure Refinement of X-Ray and Neutron Diffraction Data on Disordered Materials: Application to Liquid Water. *J. Phys.: Condens. Matter* **2007**, *19*, 335206.
(81) Kelkkanen, A. K.; Lundqvist, B. I.; Nørskov, J. K. Density Functional for van der Waals Forces Accounts for Hydrogen Bond in Benchmark Set of Water Hexamers. *J. Chem. Phys.* **2009**, *131*, 046102.
(82) Klimes, J.; Bowler, D. R.; Michaelides, A. Chemical Accuracy for the van der Waals Density Functional. *J. Phys.: Condens. Matter* **2010**, *22*, 022201.
(83) Klimes, J.; Michaelides, A. Perspective: Advances and Challenges in Treating van der Waals Dispersion Forces in Density Functional Theory. *J. Chem. Phys.* **2012**, *137*, 120901.
(84) Møgelhøj, A.; Kelkkanen, A. K.; Wikfeldt, K. T.; Schiøtz, J.; Mortensen, J. J.; Pettersson, L. G. M.; Lundqvist, B. I.; Jacobsen, K. W.; Nilsson, A.; Nørskov, J. K. Ab Initio van der Waals Interactions in Simulations of Water Alter Structure from Mainly Tetrahedral to High-Density-Like. *J. Phys. Chem. B* **2011**, *115*, 14149−14160.
(85) Zhang, C.; Spanu, L.; Galli, G. Entropy of Liquid Water from Ab Initio Molecular Dynamics. *J. Phys. Chem. B* **2011**, *115*, 14190−14195.
(86) Wang, J.; Román-Pérez, G.; Soler, J. M.; Artacho, E.; Fernández-Serra, M.-V. Density, Structure, and Dynamics of Water: The Effect of van der Waals Interactions. *J. Chem. Phys.* **2011**, *134*, 024516.
(87) Lin, I.-C.; Seitsonen, A. P.; Coutinho-Neto, M. D.; Tavernelli, I.; Rothlisberger, U. Importance of van der Waals Interactions in Liquid Water. *J. Phys. Chem. B* **2009**, *113*, 1127−1131.
(88) Lin, I.-C.; Seitsonen, A. P.; Tavernelli, I.; Rothlisberger, U. Structure and Dynamics of Liquid Water from ab Initio Molecular Dynamics−Comparison of BLYP, PBE, and revPBE Density Functionals with and without van der Waals Corrections. *J. Chem. Theory Comput.* **2012**, *8*, 3902−3910.
(89) Forster-Tonigold, K.; Groß, A. Dispersion Corrected RPBE Studies of Liquid Water. *J. Chem. Phys.* **2014**, *141*, 064501.
(90) Grimme, S.; Antony, J.; Ehrlich, S.; Krieg, H. A Consistent and Accurate ab initio Parametrization of Density Functional Dispersion Correction (DFT-D) for the 94 Elements H-Pu. *J. Chem. Phys.* **2010**, *132*, 154104.
(91) Grimme, S.; Hansen, A.; Brandenburg, J. G.; Bannwarth, C. Dispersion-Corrected Mean-Field Electronic Structure Methods. *Chem. Rev.* **2016**, *116*, 5105−5154.
(92) Dion, M.; Rydberg, H.; Schröder, E.; Langreth, D. C.; Lundqvist, B. I. Van der Waals Density Functional for General Geometries. *Phys. Rev. Lett.* **2004**, *92*, 246401.
(93) Román-Pérez, G.; Soler, J. M. Efficient Implementation of a van der Waals Density Functional: Application to Double-Wall Carbon Nanotubes. *Phys. Rev. Lett.* **2009**, *103*, 096102.
(94) Schmidt, J.; VandeVondele, J.; Kuo, I.-F. W.; Sebastiani, D.; Siepmann, J. I.; Hutter, J.; Mundy, C. J. Isobaric-Isothermal Molecular Dynamics Simulations Utilizing Density Functional Theory: An Assessment of the Structure and Density of Water at Near-Ambient Conditions. *J. Phys. Chem. B* **2009**, *113*, 11959−11964.
(95) Jonchiere, R.; Seitsonen, A. P.; Ferlat, G.; Saitta, A. M.; Vuilleumier, R. Van der Waals Effects in ab initio Water at Ambient and Supercritical Conditions. *J. Chem. Phys.* **2011**, *135*, 154503.
(96) Gillan, M. J.; Alfè, D.; Michaelides, A. Perspective: How Good is DFT for Water? *J. Chem. Phys.* **2016**, *144*, 130901.

https://doi.org/10.1021/acs.chemrev.1c00679
Chem. Rev. XXXX, XXX, XXX−XXX

(97) Miceli, G.; de Gironcoli, S.; Pasquarello, A. Isobaric First-Principles Molecular Dynamics of Liquid Water With Nonlocal van der Waals Interactions. *J. Chem. Phys.* **2015**, *142*, 034501.
(98) Mahlberg, D.; Sakong, S.; Forster-Tonigold, K.; Groß, A. Improved DFT Adsorption Energies with Semiempirical Dispersion Corrections. *J. Chem. Theory Comput.* **2019**, *15*, 3250−3259.
(99) Schienbein, P.; Marx, D. Assessing the properties of Supercritical Water in Terms of Structural Dynamics and Electronic Polarization Effects. *Phys. Chem. Chem. Phys.* **2020**, *22*, 10462−10479.
(100) Schienbein, P.; Marx, D. Supercritical Water is not Hydrogen Bonded. *Angew. Chem., Int. Ed.* **2020**, *59*, 18578−18585.
(101) Sun, J.; Ruzsinszky, A.; Perdew, J. P. Strongly Constrained and Appropriately Normed Semilocal Density Functional. *Phys. Rev. Lett.* **2015**, *115*, 036402.
(102) Chen, M.; Ko, H.-Y.; Remsing, R. C.; Calegari Andrade, M. F.; Santra, B.; Sun, Z.; Selloni, A.; Car, R.; Klein, M. L.; Perdew, J. P.; Wu, X. Ab initio Theory and Modeling of Water. *Proc. Natl. Acad. Sci. U. S. A.* **2017**, *114*, 10846−10851.
(103) Carrasco, J.; Santra, B.; Klimeš, J.; Michaelides, A. To Wet or Not to Wet? Dispersion Forces Tip the Balance for Water Ice on Metals. *Phys. Rev. Lett.* **2011**, *106*, 026101.
(104) Tonigold, K.; Groß, A. Dispersive Interactions in Water Bilayers at Metallic Surfaces: A Comparison of the PBE and RPBE Functional Including Semiempirical Dispersion Corrections. *J. Comput. Chem.* **2012**, *33*, 695−701.
(105) Carrasco, J.; Klimeš, J.; Michaelides, A. The Role of van der Waals Forces in Water Adsorption on Metals. *J. Chem. Phys.* **2013**, *138*, 024708.
(106) Groß, A. Reactions at Surfaces Studied by ab initio Dynamics Calculations. *Surf. Sci. Rep.* **1998**, *32*, 291.
(107) Berta, D.; Ferenc, D.; Bako, I.; Madarasz, A. Nuclear Quantum Effects from the Analysis of Smoothed Trajectories: Pilot Study for Water. *J. Chem. Theory Comput.* **2020**, *16*, 3316−3334.
(108) Lie, G. C.; Clementi, E. Molecular-Dynamics Simulation of Liquid Water with an ab initio Flexible Water-Water Interaction Potential. *Phys. Rev. A* **1986**, *33*, 2679−2693.
(109) Marx, D.; Hutter, J. Ab Initio Molecular Dynamics—Theory and Implementation. In *Modern Methods and Algorithms of Quantum Chemistry*; John von Neumann-Institute for Computing: Jülich, 2000; pp 329−477.
(110) Marx, D. Proton Transfer 200 Years after von Grotthuss: Insights from Ab Initio Simulations. *ChemPhysChem* **2006**, *7*, 1848−1870.
(111) Morrone, J. A.; Car, R. Nuclear Quantum Effects in Water. *Phys. Rev. Lett.* **2008**, *101*, 017801.
(112) Chen, B.; Ivanov, I.; Klein, M. L.; Parrinello, M. Hydrogen Bonding in Water. *Phys. Rev. Lett.* **2003**, *91*, 215503.
(113) Fritsch, S.; Potestio, R.; Donadio, D.; Kremer, K. Nuclear Quantum Effects in Water: A Multiscale Study. *J. Chem. Theory Comput.* **2014**, *10*, 816−824.
(114) Habershon, S.; Markland, T. E.; Manolopoulos, D. E. Competing Quantum Effects in the Dynamics of a Flexible Water Model. *J. Chem. Phys.* **2009**, *131*, 024501.
(115) Groß, A.; Scheffler, M. Role of Zero-Point Effects in Catalytic Reactions Involving Hydrogen. *J. Vac. Sci. Technol. A* **1997**, *15*, 1624.
(116) Lan, J.; Rybkin, V. V.; Iannuzzi, M. Ionization of Water as an Effect of Quantum Delocalization at Aqueous Electrode Interfaces. *J. Phys. Chem. Lett.* **2020**, *11*, 3724−3730.
(117) Naderian, M.; Groß, A. From Single Molecules to Water Networks: Dynamics of Water Adsorption on Pt(111). *J. Chem. Phys.* **2016**, *145*, 094703.
(118) Sanchez, C. G. Molecular Reorientation of Water Adsorbed on Charged Ag(111) Surfaces. *Surf. Sci.* **2003**, *527*, 1−11.
(119) Meng, S.; Wang, E. G.; Gao, S. Water Adsorption on Metal Surfaces: A General Picture from Density Functional Theory Studies. *Phys. Rev. B* **2004**, *69*, 195404.
(120) Ranea, V. A.; Michaelides, A.; Ramírez, R.; Vergés, J. A.; de Andres, P. L.; King, D. A. Density Functional Theory Study of the Interaction of Monomeric Water with the Ag\\{111\\} Surface. *Phys. Rev. B* **2004**, *69*, 205411.
(121) Sebastiani, D.; Delle Site, L. Adsorption of Water Molecules on Flat and Stepped Nickel Surfaces from First Principles. *J. Chem. Theory Comput.* **2005**, *1*, 78−82.
(122) Vassilev, P.; van Santen, R. A.; Koper, M. T. M. Ab initio Studies of a Water Layer at Transition Metal Surfaces. *J. Chem. Phys.* **2005**, *122*, 054701.
(123) Carrasco, J.; Michaelides, A.; Scheffler, M. Insight from First Principles into the Nature of the Bonding between Water Molecules and 4d Metal Surfaces. *J. Chem. Phys.* **2009**, *130*, 184707.
(124) Árnadóttir, L.; Stuve, E. M.; Jónsson, H. Adsorption of Water Monomer and Clusters on Platinum(111) Terrace and Related Steps and Kinks: I. Configurations, Energies, and hHydrogen Bonding. *Surf. Sci.* **2010**, *604*, 1978−1986.
(125) Fajin, J. L. C.; Cordeiro, M. N. D. S.; Gomes, J. R. B. Density Functional Theory Study of the Water Dissociation on Platinum Surfaces: General Trends. *J. Phys. Chem. A* **2014**, *118*, 5832−5840.
(126) Huzayyin, A.; Chang, J. H.; Lian, K.; Dawson, F. Interaction of Water Molecule with Au(111) and Au(110) Surfaces under the Influence of an External Electric Field. *J. Phys. Chem. C* **2014**, *118*, 3459−3470.
(127) Fischer, J. M.; Mahlberg, D.; Roman, T.; Groß, A. Water Adsorption on Bimetallic PtRu/Pt(111) Surface Alloys. *Proc. R. Soc. A* **2016**, *472*, 20160618.
(128) Cahyanto, W. T.; Zulaehah, S.; Abdullatif, F.; Widanarto, W.; Effendi, M.; Kasai, H. A First-Principles Study of the Adsorption of H_2O on Ru- and Mo-Alloyed Pt(111) Surfaces. *J. Electron. Mater.* **2020**, *49*, 2642−2650.
(129) Haq, S.; Harnett, J.; Hodgson, A. Growth of Thin Crystalline Ice Films on Pt(111). *Surf. Sci.* **2002**, *505*, 171−182.
(130) Lew, W.; Crowe, M. C.; Karp, E.; Lytken, O.; Farmer, J. A.; Árnadóttir, L.; Schoenbaum, C.; Campbell, C. T. The Energy of Adsorbed Hydroxyl on Pt(111) by Microcalorimetry. *J. Phys. Chem. C* **2011**, *115*, 11586−11594.
(131) Meng, S.; Xu, L. F.; Wang, E. G.; Gao, S. Vibrational Recognition of Hydrogen-Bonded Water Networks on a Metal Surface. *Phys. Rev. Lett.* **2002**, *89*, 176104.
(132) Ranea, V. A.; Michaelides, A.; Ramírez, R.; de Andres, P. L.; Vergés, J. A.; King, D. A. Water Dimer Diffusion on Pd(111) Assisted by an H-Bond Donor-Acceptor Tunneling Exchange. *Phys. Rev. Lett.* **2004**, *92*, 136104.
(133) Santra, B.; Michaelides, A.; Fuchs, M.; Tkatchenko, A.; Filippi, C.; Scheffler, M. On the Accuracy of Density-Functional Theory Exchange-Correlation Functionals for H Bonds in Small Water Clusters. II. The Water Hexamer and van der Waals Interactions. *J. Chem. Phys.* **2008**, *129*, 194111.
(134) Mitsui, T.; Rose, M. K.; Fomin, E.; Ogletree, D. F.; Salmeron, M. Water Diffusion and Clustering on Pd(111). *Science* **2002**, *297*, 1850−1852.
(135) Morgenstern, K.; Nieminen, J. Intermolecular Bond Length of Ice on Ag(111). *Phys. Rev. Lett.* **2002**, *88*, 066102.
(136) Michaelides, A.; Morgenstern, K. Ice Nanoclusters at Hydrophobic Metal Surfaces. *Nat. Mater.* **2007**, *6*, 597−601.
(137) Nauta, K.; Miller, R. E. Formation of Cyclic Water Hexamer in Liquid Helium: The Smallest Piece of Ice. *Science* **2000**, *287*, 293−295.
(138) Schnur, S.; Groß, A. Challenges in the First-Principles Description of Reactions in Electrocatalysis. *Catal. Today* **2011**, *165*, 129−137.
(139) Xantheas, S. S. Ab initio Studies of Cyclic Water Clusters $(H_2O)_n$, n = 1−6. III. Comparison of Density Functional with MP2 Results. *J. Chem. Phys.* **1995**, *102*, 4505−4517.
(140) Roudgar, A.; Groß, A. Hydrogen Adsorption Energies on Bimetallic Overlayer Systems at the Solid-Vacuum and the Solid-Liquid Interface. *Surf. Sci.* **2005**, *597*, 42.
(141) Gohda, Y.; Schnur, S.; Groß, A. Influence of Water on Elementary Reaction Steps in Electrocatalysis. *Faraday Discuss.* **2009**, *140*, 233−244.

https://doi.org/10.1021/acs.chemrev.1c00679
Chem. Rev. XXXX, XXX, XXX−XXX

(142) Lin, X.; Evers, F.; Groß, A. First-Principles Study of the Structure of Water Layers on Flat and Stepped Pb Electrodes. *Beilstein J. Nanotechnol.* **2016**, *7*, 533−543.
(143) Gibson, K. D.; Viste, M.; Sibener, S. J. The Adsorption of Water on Clean and Oxygen Predosed Rh(111): Surface Templating via (1*times*1)-O/Rh(111) Induces Formation of a Novel High-Density Interfacial Ice Structure. *J. Chem. Phys.* **2000**, *112*, 9582−9589.
(144) Feibelman, P. J. Reactive Wetting: H_2O/Rh(111). *Phys. Rev. Lett.* **2003**, *90*, 186103.
(145) Feibelman, P. J. Comment on "Vibrational Recognition of Hydrogen-Bonded Water Networks on a Metal Surface. *Phys. Rev. Lett.* **2003**, *91*, 059601.
(146) Glebov, A.; Graham, A. P.; Menzel, A.; Toennies, J. P. Orientational Ordering of Two-Dimensional Ice on Pt(111). *J. Chem. Phys.* **1997**, *106*, 9382−9385.
(147) Meng, S.; Xu, L. F.; Wang, E. G.; Gao, S.; et al. Reply. *Phys. Rev. Lett.* **2003**, *91*, 059602.
(148) Feibelman, P. J. Partial Dissociation of Water on Ru(0001). *Science* **2002**, *295*, 99.
(149) Michaelides, A.; Alavi, A.; King, D. A. Different Surface Chemistries of Water on Ru\\{0001\\}: From Monomer Adsorption to Partially Dissociated Bilayers. *J. Am. Chem. Soc.* **2003**, *125*, 2746−2755.
(150) Doering, D. L.; Madey, T. E. The Adsorption of Water on Clean and Oxygen-Dosed Ru(001). *Surf. Sci.* **1982**, *123*, 305−337.
(151) Held, G.; Menzel, D. The Structure of the p($\sqrt{3} \times \sqrt{3}$)R30° Bilayer of D_2O on Ru(001). *Surf. Sci.* **1994**, *316*, 92−102.
(152) Materzanini, G.; Tantardini, G. F.; Lindan, P. J. D.; Saalfrank, P. Water Adsorption at Metal Surfaces: A First-Principles Study of the $p(\sqrt{3} \times \sqrt{3})R30°$ H_2O Bilayer on Ru(0001). *Phys. Rev. B* **2005**, *71*, 155414.
(153) Maroun, F.; Ozanam, F.; Magnussen, O. M.; Behm, R. J. The Role of Atomic Ensembles in the Reactivity of Bimetallic Catalysts. *Science* **2001**, *293*, 1811.
(154) Groß, A. Tailoring the Reactivity of Bimetallic Overlayer and Surface Alloy Systems. *J. Phys.: Condens. Matter* **2009**, *21*, 084205.
(155) Zhang, B.-W.; Yang, H.-L.; Wang, Y.-X.; Dou, S.-X.; Liu, H.-K. A Comprehensive Review on Controlling Surface Composition of Pt-Based Bimetallic Electrocatalysts. *Adv. Energy Mater.* **2018**, *8*, 1703597.
(156) Carrasco, J.; Michaelides, A.; Forster, M.; Haq, S.; Raval, R.; Hodgson, A. A One-Dimensional Ice structure Built from Pentagons. *Nat. Mater.* **2009**, *8*, 427−431.
(157) Baghbanpourasl, A.; Hingerl, K.; Wippermann, S.; Schmidt, W. G. Copper(110) Surface in Thermodynamic Equilibrium with Water Vapor Studied from First Principles. *Surf. Sci.* **2013**, *612*, 82−89.
(158) Bange, K.; Grider, D.; Madey, T.; Sass, J. The Surface Chemistry of H_2O on Clean and Oxygen-Covered Cu(110). *Surf. Sci.* **1984**, *137*, 38−64.
(159) Polak, M. On the Structure and Bonding of H_2O Adsorbed on Cu(110). *Surf. Sci.* **1994**, *321*, 249−260.
(160) Schiros, T.; Haq, S.; Ogasawara, H.; Takahashi, O.; Öström, H.; Andersson, K.; Pettersson, L. G. M.; Hodgson, A.; Nilsson, A. Structure of Water Adsorbed on the Open Cu(110) Surface: H-up, H-down, or Both? *Chem. Phys. Lett.* **2006**, *429*, 415−419.
(161) Yamada, T.; Tamamori, S.; Okuyama, H.; Aruga, T. Anisotropic Water Chain Growth on Cu(110) Observed with Scanning Tunneling Microscopy. *Phys. Rev. Lett.* **2006**, *96*, 036105.
(162) Ren, J.; Meng, S. First-Principles Study of Water on Copper and Noble Metal (110) Surfaces. *Phys. Rev. B* **2008**, *77*, 054110.
(163) Forster, M.; Raval, R.; Carrasco, J.; Michaelides, A.; Hodgson, A. Water-Hydroxyl Phases on an Open Metal Surface: Breaking the Ice Rules. *Chem. Sci.* **2012**, *3*, 93−102.
(164) Forster, M.; Raval, R.; Hodgson, A.; Carrasco, J.; Michaelides, A. *c*(2 × 2) Water-Hydroxyl Layer on Cu(110): A Wetting Layer Stabilized by Bjerrum Defects. *Phys. Rev. Lett.* **2011**, *106*, 046103.
(165) Bjerrum, N. Structure and Properties of Ice. *Science* **1952**, *115*, 385−390.
(166) Ibach, H. Vibration Spectroscopy of Water on Stepped Gold Surfaces. *Surf. Sci.* **2010**, *604*, 377.
(167) Ibach, H. Electron Energy Loss Spectroscopy of the Vibration Modes of Water on Ag(100) and Ag(115) Surfaces and Comparison to Au(100), Au(111) and Au(115). *Surf. Sci.* **2012**, *606*, 1534.
(168) Lin, X.; Groß, A. First-Principles Study of the Water Structure on Flat and Stepped Gold Surfaces. *Surf. Sci.* **2012**, *606*, 886−891.
(169) Schmitz, M.; Tavan, P. Vibrational Spectra from Atomic Fluctuations in Dynamics Simulations. II. Solvent-Induced frequency Fluctuations at Femtosecond Time resolution. *J. Chem. Phys.* **2004**, *121*, 12247−12258.
(170) Kolb, M. J.; Calle-Vallejo, F.; Juurlink, L. B. F.; Koper, M. T. M. Density Functional Theory Study of Adsorption of H_2O, H, O, and OH on Stepped Platinum Surfaces. *J. Chem. Phys.* **2014**, *140*, 134708.
(171) Roman, T.; Groß, A. Structure of Water Layers on Hydrogen-Covered Pt Electrodes. *Catal. Today* **2013**, *202*, 183−190.
(172) Schmidt, T. J.; Ross, P. N., Jr.; Markovic, N. M. Temperature Dependent Surface Electrochemistry on Pt Single Crystals in Alkaline Electrolytes: Part 2. The Hydrogen Evolution/Oxidation Reaction. *J. Electroanal. Chem.* **2002**, *524*, 252−260.
(173) Marković, N. M.; Ross, P. N., Jr. Surface Science Studies of Model Fuel Cell Electrocatalysts. *Surf. Sci. Rep.* **2002**, *45*, 117.
(174) Gossenberger, F.; Roman, T.; Groß, A. Equilibrium Coverage of Halides on Metal Electrodes. *Surf. Sci.* **2015**, *631*, 17−22.
(175) Gossenberger, F.; Roman, T.; Groß, A. Hydrogen and Halide Co-Adsorption on Pt(111) in an Electrochemical Environment: a Computational Perspective. *Electrochim. Acta* **2016**, *216*, 152−159.
(176) Gossenberger, F.; Juarez, F.; Groß, A. Sulfate, Bisulfate, and Hydrogen Co-adsorption on Pt(111) and Au(111) in an Electrochemical Environment. *Front. Chem.* **2020**, *8*, 634.
(177) Algara-Siller, G.; Lehtinen, O.; Wang, F.; Nair, R.; Kaiser, U.; Wu, H.; Grigorieva, I.; Geim, A. Square Ice in Graphene Nanocapillaries. *Nature* **2015**, *519*, 443.
(178) Freitas, R. R. Q.; Rivelino, R.; Mota, F. d. B.; de Castilho, C. M. C. DFT Studies of the Interactions of a Graphene Layer with Small Water Aggregates. *J. Phys. Chem. A* **2011**, *115*, 12348−12356.
(179) Achtyl, J. L.; Unocic, R. R.; Xu, L.; Cai, Y.; Raju, M.; Zhang, W.; Sacci, R. L.; Vlassiouk, I. V.; Fulvio, P. F.; Ganesh, P.; Wesolowski, D. J.; Dai, S.; van Duin, A. C. T.; Neurock, M.; Geiger, F. M. Aqueous Proton transfer across Single-Layer Graphene. *Nature Comm* **2015**, *6*, 6539.
(180) Soper, A. K. Physical chemistry: Square Ice in a Graphene Sandwich. *Nature* **2015**, *519*, 417−418.
(181) Zhou, W.; Yin, K.; Wang, C.; Zhang, Y.; Xu, T.; Borisevich, A.; Sun, L.; Idrobo, J. C.; Chisholm, M. F.; Pantelides, S. T.; Klie, R. F.; Lupini, A. R. The Observation of Square Ice in Graphene Questioned. *Nature* **2015**, *528*, E1−E2.
(182) Corsetti, F.; Matthews, P.; Artacho, E. Structural and Configurational Properties of Nanoconfined Monolayer Ice from First Principles. *Sci. Rep.* **2016**, *6*, 18651.
(183) Corsetti, F.; Zubeltzu, J.; Artacho, E. Enhanced Configurational Entropy in High-Density Nanoconfined Bilayer Ice. *Phys. Rev. Lett.* **2016**, *116*, 085901.
(184) Chen, J.; Schusteritsch, G.; Pickard, C. J.; Salzmann, C. G.; Michaelides, A. Two Dimensional Ice from First Principles: Structures and Phase Transitions. *Phys. Rev. Lett.* **2016**, *116*, 025501.
(185) Roman, T.; Groß, A. Polymorphism of Water in Two Dimensions. *J. Phys. Chem. C* **2016**, *120*, 13649−13655.
(186) Chen, J.; Schusteritsch, G.; Pickard, C. J.; Salzmann, C. G.; Michaelides, A. Double-layer Ice from First Principles. *Phys. Rev. B* **2017**, *95*, 094121.
(187) Trasatti, S. The Absolute Electrode Potential: an Explanatory Note. *Pure Appl. Chem.* **1986**, *58*, 955−966.
(188) Filhol, J. S.; Bocquet, M. L. Charge Control of the Water Monolayer/Pd Interface. *Chem. Phys. Lett.* **2007**, *438*, 203−207.

https://doi.org/10.1021/acs.chemrev.1c00679
Chem. Rev. XXXX, XXX, XXX−XXX

(189) Osawa, M.; Tsushima, M.; Mogami, H.; Samjeske, G.; Yamakata, A. Structure of Water at the Electrified Platinum-Water Interface: A Study by Surface-Enhanced Infrared Absorption Spectroscopy. *J. Phys. Chem. C* **2008**, *112*, 4248−4256.
(190) Heras, J. M.; Viscido, L. Work Function Changes Upon Water Contamination of Metal Surfaces. *Appl. Surf. Sci.* **1980**, *4*, 238−241.
(191) Langenbach, E.; Spitzer, A.; Lüth, H. The Adsorption of Water on Pt(111) Studied by Irreflection and UV-Photoemission Spectroscopy. *Surf. Sci.* **1984**, *147*, 179−190.
(192) Kiskinova, M.; Pirug, G.; Bonzel, H. Adsorption and Decomposition of H_2O on a K-Covered Pt(111) Surface. *Surf. Sci.* **1985**, *150*, 319−338.
(193) Hoffmann, W.; Benndorf, C. Investigations on the Influence of Substrate Geometry of Flat and Stepped Ruthenium Surfaces Ru(0001) and Ru($10\bar{1}8$) on the Adsorption Kinetics of H_2O and D_2O. *Surf. Sci.* **1997**, *377−379*, 681−686.
(194) Lilach, Y.; Romm, L.; Livneh, T.; Asscher, M. The First Layers of Water on Ru(001). *J. Phys. Chem. B* **2001**, *105*, 2736−2742.
(195) Car, R.; Parrinello, M. Unified Approach for Molecular Dynamics and Density-Functional Theory. *Phys. Rev. Lett.* **1985**, *55*, 2471.
(196) Jacobi, K.; Bedürftig, K.; Wang, Y.; Ertl, G. From Monomers to Ice - New Vibrational Characteristics of H_2O Adsorbed on Pt(111). *Surf. Sci.* **2001**, *472*, 9−20.
(197) Noguchi, H.; Okada, T.; Uosaki, K. Molecular Structure at Electrode/Electrolyte Solution Interfaces Related to Electrocatalysis. *Faraday Discuss.* **2009**, *140*, 125.
(198) Otani, M.; Hamada, I.; Sugino, O.; Morikawa, Y.; Okamoto, Y.; Ikeshoji, T. Structure of the Water/Platinum Interface−a First Principles Simulation under Bias Potential. *Phys. Chem. Chem. Phys.* **2008**, *10*, 3609−3612.
(199) Le, J.; Iannuzzi, M.; Cuesta, A.; Cheng, J. Determining Potentials of Zero Charge of Metal Electrodes versus the Standard Hydrogen Electrode from Density-Functional-Theory-Based Molecular Dynamics. *Phys. Rev. Lett.* **2017**, *119*, 016801.
(200) Le, J.; Cuesta, A.; Cheng, J. The Structure of Metal-Water Interface at the Potential of Zero Charge from Density Functional theory-Based Molecular Dynamics. *J. Electroanal. Chem.* **2018**, *819*, 87−94.
(201) Le, J.-B.; Chen, A.; Li, L.; Xiong, J.-F.; Lan, J.; Liu, Y.-P.; Iannuzzi, M.; Cheng, J. Modeling Electrified Pt(111)-H_{ad}/Water Interfaces from Ab Initio Molecular Dynamics. *JACS Au* **2021**, *1*, 569−577.
(202) Li, P.; Huang, J.; Hu, Y.; Chen, S. Establishment of the Potential of Zero Charge of Metals in Aqueous Solutions: Different Faces of Water Revealed by Ab Initio Molecular Dynamics Simulations. *J. Phys. Chem. C* **2021**, *125*, 3972−3979.
(203) Petrii, O. A. Zero Charge Potentials of Platinum Metals and Electron Work Functions (Review). *Russ. J. Electrochem.* **2013**, *49*, 401−422.
(204) Schmickler, W.; Santos, E. *Interfacial Electrochemistry*, 2nd ed.; Springer: Berlin, 2010.
(205) Chen, L. D.; Bajdich, M.; Martirez, J. M. P.; Krauter, C. M.; Gauthier, J. A.; Carter, E. A.; Luntz, A. C.; Chan, K.; Nørskov, J. K. Understanding the Apparent Fractional Charge of Protons in the Aqueous Electrochemical Double Layer. *Nat. Commun.* **2018**, *9*, 3202.
(206) Rizo, R.; Sitta, E.; Herrero, E.; Climent, V.; Feliu, J. M. Towards the Understanding of the Interfacial pH Scale at Pt(111) Electrodes. *Electrochim. Acta* **2015**, *162*, 138−145.
(207) Ojha, K.; Arulmozhi, N.; Aranzales, D.; Koper, M. T. M. Double Layer at the Pt(111)-Aqueous Electrolyte Interface: Potential of Zero Charge and Anomalous Gouy-Chapman Screening. *Angew. Chem., Int. Ed.* **2020**, *59*, 711−715.
(208) Rossmeisl, J.; Chan, K.; Ahmed, R.; Tripkovic, V.; Bjorketun, M. E. pH in Atomic Scale Simulations of Electrochemical Interfaces. *Phys. Chem. Chem. Phys.* **2013**, *15*, 10321−10325.
(209) Hansen, M. H.; Jin, C.; Thygesen, K. S.; Rossmeisl, J. Finite Bias Calculations to Model Interface Dipoles in Electrochemical Cells at the Atomic Scale. *J. Phys. Chem. C* **2016**, *120*, 13485−13491.
(210) Hansen, M. H.; Rossmeisl, J. pH in Grand Canonical Statistics of an Electrochemical Interface. *J. Phys. Chem. C* **2016**, *120*, 29135−29143.
(211) Cheng, J.; Sulpizi, M.; Sprik, M. Redox Potentials and pKa for Benzoquinone from Density Functional Theory Based Molecular Dynamics. *J. Chem. Phys.* **2009**, *131*, 154504.
(212) Pedroza, L. S.; Poissier, A.; Fernández-Serra, M.-V. Local Order of Liquid Water at Metallic Electrode Surfaces. *J. Chem. Phys.* **2015**, *142*, 034706.
(213) Li, C.-Y.; Le, J.-B.; Wang, Y.-H.; Chen, S.; Yang, Z.-L.; Li, J.-F.; Cheng, J.; Tian, Z.-Q. In situ Probing Electrified Interfacial Water Structures at Atomically Flat Surfaces. *Nat. Mater.* **2019**, *18*, 697−701.
(214) Lozovoi, A. Y.; Alavi, A.; Kohanoff, J.; Lynden-Bell, R. M. Ab initio Simulation of Charged Slabs at Constant Chemical Potential. *J. Chem. Phys.* **2001**, *115*, 1661.
(215) Taylor, C. D.; Wasileski, S. A.; Filhol, J.-S.; Neurock, M. First Principles Reaction Modeling of the Electrochemical Interface: Consideration and Calculation of a Tunable Surface Potential from Atomic and Electronic Structure. *Phys. Rev. B* **2006**, *73*, 165402.
(216) Skúlason, E.; Karlberg, G. S.; Rossmeisl, J.; Bligaard, T.; Greeley, J.; Jónsson, H.; Nørskov, J. K. Density Functional theory Calculations for the Hydrogen Evolution Reaction in an Electrochemical Double Layer on the Pt(111) Electrode. *Phys. Chem. Chem. Phys.* **2007**, *9*, 3241−3250.
(217) Bonnet, N.; Morishita, T.; Sugino, O.; Otani, M. First-Principles Molecular Dynamics at a Constant Electrode Potential. *Phys. Rev. Lett.* **2012**, *109*, 266101.
(218) Surendralal, S.; Todorova, M.; Finnis, M. W.; Neugebauer, J. First-Principles Approach to Model Electrochemical Reactions: Understanding the Fundamental Mechanisms behind Mg Corrosion. *Phys. Rev. Lett.* **2018**, *120*, 246801.
(219) Tang, M. T.; Liu, X.; Ji, Y.; Norskov, J. K.; Chan, K. Modeling Hydrogen Evolution Reaction Kinetics through Explicit Water−Metal Interfaces. *J. Phys. Chem. C* **2020**, *124*, 28083−28092.
(220) Goldsmith, Z. K.; Calegari Andrade, M. F.; Selloni, A. Effects of Applied Voltage on Water at a Gold Electrode Interface from ab initio Molecular Dynamics. *Chem. Sci.* **2021**, *12*, 5865−5873.
(221) Pedroza, L. S.; Brandimarte, P.; Rocha, A. R.; Fernandez-Serra, M.-V. Bias-Dependent Local Structure of Water Molecules at a Metallic Interface. *Chem. Sci.* **2018**, *9*, 62−69.
(222) Iwasita, T.; Xia, X. Adsorption of Water at Pt(111) Electrode in $HClO_4$ Solutions. The Potential of Zero Charge. *J. Electroanal. Chem.* **1996**, *411*, 95−102.
(223) Bramley, G.; Nguyen, M.-T.; Glezakou, V.-A.; Rousseau, R.; Skylaris, C.-K. Reconciling Work Functions and Adsorption Enthalpies for Implicit Solvent Models: A Pt(111)/Water Interface Case Study. *J. Chem. Theory Comput.* **2020**, *16*, 2703−2715.
(224) Vydrov, O. A.; Van Voorhis, T. Nonlocal van der Waals Density Functional: The Simpler the Better. *J. Chem. Phys.* **2010**, *133*, 244103.
(225) El-Aziz, A.; Kibler, L.; Kolb, D. The Potentials of Zero Charge of Pd(111) and thin Pd Overlayers on Au(111). *Electrochem. Commun.* **2002**, *4*, 535−539.
(226) Kolb, D.; Schneider, J. Surface Reconstruction in Electrochemistry: Au(100)-(5 × 20), Au(111)- (1 × 23) and Au(110)-(1 × 2). *Electrochim. Acta* **1986**, *31*, 929−936.
(227) Hamm, U.; Kramer, D.; Zhai, R.; Kolb, D. The pzc of Au(111) and Pt(111) in a Perchloric Acid Solution: an ex situ Approach to the Immersion Technique. *J. Electroanal. Chem.* **1996**, *414*, 85−89.
(228) Valette, G. Double Layer on Silver Single Crystal Electrodes in Contact with Electrolytes Having Anions which are Slightly Specifically Adsorbed: Part III. The (111) face. *J. Electroanal. Chem.* **1989**, *269*, 191−203.
(229) Hansen, H. A.; Rossmeisl, J.; Nørskov, J. K. Surface Pourbaix Diagrams and Oxygen Reduction Activity of Pt, Ag and Ni(111) Surfaces Studied by DFT. *Phys. Chem. Chem. Phys.* **2008**, *10*, 3722−3730.

https://doi.org/10.1021/acs.chemrev.1c00679
Chem. Rev. XXXX, XXX, XXX−XXX

(230) Reuter, K.; Scheffler, M. Composition, Structure, and Stability of RuO_2(110) as a Function of Oxygen Pressure. *Phys. Rev. B* **2001**, *65*, 035406.
(231) Nørskov, J. K.; Rossmeisl, J.; Logadottir, A.; Lindqvist, L.; Kitchin, J. R.; Bligaard, T.; Jónsson, H. Origin of the Overpotential for Oxygen Reduction at a Fuel-Cell Cathode. *J. Phys. Chem. B* **2004**, *108*, 17886−17892.
(232) Peterson, A. A.; Abild-Pedersen, F.; Studt, F.; Rossmeisl, J.; Nørskov, J. K. How Copper Catalyzes the Electroreduction of Carbon Dioxide into Hydrocarbon Fuels. *Energy Environ. Sci.* **2010**, *3*, 1311−1315.
(233) Rogal, J.; Reuter, K.; Scheffler, M. CO Oxidation at Pd(100): A First-Principles Constrained Thermodynamics Study. *Phys. Rev. B* **2007**, *75*, 205433.
(234) Lundgren, E.; Gustafson, J.; Mikkelsen, A.; Andersen, J. N.; Stierle, A.; Dosch, H.; Todorova, M.; Rogal, J.; Reuter, K.; Scheffler, M. Kinetic Hindrance during the Initial Oxidation of Pd(100) at Ambient Pressures. *Phys. Rev. Lett.* **2004**, *92*, 046101.
(235) Stampfl, C. Surface Processes and Phase Transitions from ab initio Atomistic thermodynamics and Statistical Mechanics. *Catal. Today* **2005**, *105*, 17−35.
(236) Leach, A. R. *Molecular Modelling: Principles and Applications*, 2nd ed.; Pearson Education: Harlow, 2001; Chapter 11, pp 563−584.
(237) Halck, N. B.; Petrykin, V.; Krtil, P.; Rossmeisl, J. Beyond the Volcano Limitations in Electrocatalysis - Oxygen Evolution Reaction. *Phys. Chem. Chem. Phys.* **2014**, *16*, 13682−13688.
(238) Garcia-Araez, N.; Climent, V.; Herrero, E.; Feliu, J.; Lipkowski, J. Thermodynamic Studies of Chloride Adsorption at the Pt(111) Electrode Surface from 0.1 M \\{HClO4\\} Solution. *J. Electroanal. Chem.* **2005**, *576*, 33−41.
(239) Funtikov, A.; Stimming, U.; Vogel, R. Anion Adsorption from Sulfuric Acid Solutions on Pt(111) Single Crystal Electrodes. *J. Electroanal. Chem.* **1997**, *428*, 147−153.
(240) Garcia-Araez, N.; Climent, V.; Rodriguez, P.; Feliu, J. M. Elucidation of the Chemical Nature of Adsorbed Species for Pt(111) in H_2SO_4 Solutions by Thermodynamic Analysis. *Langmuir* **2010**, *26*, 12408−12417.
(241) Sato, K.; Yoshimoto, S.; Inukai, J.; Itaya, K. Effect of Sulfuric Acid Concentration on the Structure of Sulfate Adlayer on Au(111) Electrode. *Electrochem. Commun.* **2006**, *8*, 725−730.
(242) Fang, W.; Chen, J.; Pedevilla, P.; Li, X.-Z.; Richardson, J. O.; Michaelides, A. Origins of Fast Diffusion of Water Dimers on Surfaces. *Nat. Commun.* **2020**, *11*, 1689.
(243) Santana, J. A.; Cabrera, C. R.; Ishikawa, Y. A Density-Functional Theory Study of Electrochemical adsorption of Sulfuric Acid Anions on Pt(111). *Phys. Chem. Chem. Phys.* **2010**, *12*, 9526−9534.
(244) Comas-Vives, A.; Bandlow, J.; Jacob, T. Ab initio Study of the Electrochemical H_2SO_4/Pt(111) Interface. *Phys. Chem. Chem. Phys.* **2013**, *15*, 992−997.
(245) Jerkiewicz, G.; Vatankhah, G.; Lessard, J.; Soriaga, M. P.; Park, Y.-S. Surface-Oxide Growth at Platinum Electrodes in Aqueous H_2SO_4: Reexamination of its Mechanism Through Combined Cyclic-Voltammetry, Electrochemical Quartz-Crystal Nanobalance, and Auger Electron Spectroscopy Measurements. *Electrochim. Acta* **2004**, *49*, 1451−1459.
(246) Eslamibidgoli, M. J.; Eikerling, M. H. Electrochemical Formation of Reactive Oxygen Species at Pt(111) - A Density Functional Theory Study. *ACS Catal.* **2015**, *5*, 6090−6098.
(247) Hansen, M. H.; Nilsson, A.; Rossmeisl, J. Modelling pH and Potential in Dynamic Structures of the Water/Pt(111) Interface on the Atomic Scale. *Phys. Chem. Chem. Phys.* **2017**, *19*, 23505−23514.
(248) Kristoffersen, H. H.; Vegge, T.; Hansen, H. A. OH Formation and H_2 Adsorption at the Liquid Water−Pt(111) Interface. *Chem. Sci.* **2018**, *9*, 6912−6921.
(249) Surendralal, S.; Todorova, M.; Neugebauer, J. Impact of Water Coadsorption on the Electrode Potential of H-Pt(111)-Liquid Water Interfaces. *Phys. Rev. Lett.* **2021**, *126*, 166802.
(250) Yoon, Y.; Rousseau, R.; Weber, R. S.; Mei, D.; Lercher, J. A. First-Principles Study of Phenol Hydrogenation on Pt and Ni Catalysts in Aqueous Phase. *J. Am. Chem. Soc.* **2014**, *136*, 10287−10298.
(251) Lan, J.; Hutter, J.; Iannuzzi, M. First-Principles Simulations of an Aqueous CO/Pt(111) Interface. *J. Phys. Chem. C* **2018**, *122*, 24068−24076.
(252) Kronberg, R.; Laasonen, K. Coupling Surface Coverage and Electrostatic Effects on the Interfacial Adlayer-Water Structure of Hydrogenated Single-Crystal Platinum Electrodes. *J. Phys. Chem. C* **2020**, *124*, 13706−13714.
(253) Tripkovic, V.; Vegge, T. Potential- and Rate-Determining Step for Oxygen Reduction on Pt(111). *J. Phys. Chem. C* **2017**, *121*, 26785−26793.
(254) Sakong, S.; Groß, A. The Importance of the Electrochemical Environment in the Electro-Oxidation of Methanol on Pt(111). *ACS Catal.* **2016**, *6*, 5575−5586.
(255) Wasileski, S. A.; Koper, M. T. M.; Weaver, M. J. Field-Dependent Chemisorption of Carbon Monoxide on Platinum-Group (111) Surfaces: Relationships between Binding Energetics, Geometries, and Vibrational Properties as Assessed by Density Functional Theory. *J. Phys. Chem. B* **2001**, *105*, 3518−3530.
(256) Wei, J.; Amirbeigiarab, R.; Chen, Y.-X.; Sakong, S.; Gross, A.; Magnussen, O. M. The Dynamic Nature of CO Adlayers on Pt(111) Electrodes. *Angew. Chem., Int. Ed.* **2020**, *59*, 6182−6186.
(257) Toney, M. F.; Howard, J. N.; Richer, J.; Borges, G. L.; Gordon, J. G.; Melroy, O. R.; Wiesler, D. G.; Yee, D.; Sorensen, L. B. Voltage-Dependent Ordering of Water-Molecules at an Electrode-Electrolyte Interface. *Nature* **1994**, *368*, 444.
(258) Toney, M. F.; Howard, J. N.; Richer, J.; Borges, G. L.; Gordon, J. G.; Melroy, O. R.; Wiesler, D. G.; Yee, D.; Sorensen, L. B. Distribution of Water Molecules at Ag(111)/Electrolyte Interface as Studied with Surface X-Ray Scattering. *Surf. Sci.* **1995**, *335*, 326.
(259) Schultz, Z. D.; Shaw, S. K.; Gewirth, A. A. Potential Dependent Organization of Water at the Electrified Metal-Liquid Interface. *J. Am. Chem. Soc.* **2005**, *127*, 15916−15922.
(260) Heenen, H. H.; Gauthier, J. A.; Kristoffersen, H. H.; Ludwig, T.; Chan, K. Solvation at Metal/Water Interfaces: An ab initio Molecular Dynamics Benchmark of Common Computational Approaches. *J. Chem. Phys.* **2020**, *152*, 144703.
(261) Klamt, A. Conductor-like Screening Model for Real Solvents: A New Approach to the Quantitative Calculation of Solvation Phenomena. *J. Phys. Chem.* **1995**, *99*, 2224−2235.
(262) Barone, V.; Cossi, M. Quantum Calculation of Molecular Energies and Energy Gradients in Solution by a Conductor Solvent Model. *J. Phys. Chem. A* **1998**, *102*, 1995−2001.
(263) Sen, A.; Groß, A. Does Involving Additional Linker Always Increase the Efficiency of an Organic Dye for p-Type Dye-Sensitized Solar Cells? *ACS Appl. Energy Mater.* **2019**, *2*, 6341−6347.
(264) Fattebert, J.-L.; Gygi, F. Density Functional Theory for Efficient ab initio Molecular Dynamics Simulations in Solution. *J. Comput. Chem.* **2002**, *23*, 662−666.
(265) Fattebert, J.-L.; Gygi, F. First-Principles Molecular Dynamics Simulations in a Continuum Solvent. *Int. J. Quantum Chem.* **2003**, *93*, 139−147.
(266) Petrosyan, S. A.; Rigos, A. A.; Arias, T. A. Joint Density-Functional Theory: Ab Initio Study of Cr_2O_3 Surface Chemistry in Solution. *J. Phys. Chem. B* **2005**, *109*, 15436−15444.
(267) Otani, M.; Sugino, O. First-Principles Calculations of Charged Surfaces and Interfaces: A Plane-Wave Nonrepeated Slab Approach. *Phys. Rev. B* **2006**, *73*, 115407.
(268) Sugino, O.; Hamada, I.; Otani, M.; Morikawa, Y.; Ikeshoji, T.; Okamoto, Y. First-Principles Molecular Dynamics Simulation of Biased Electrode/Solution Interface. *Surf. Sci.* **2007**, *601*, 5237−5240.
(269) Petrosyan, S. A.; Briere, J.-F.; Roundy, D.; Arias, T. A. Joint Density-Functional Theory for Electronic Structure of Solvated Systems. *Phys. Rev. B* **2007**, *75*, 205105.

https://doi.org/10.1021/acs.chemrev.1c00679
Chem. Rev. XXXX, XXX, XXX−XXX

(270) Andreussi, O.; Dabo, I.; Marzari, N. Revised Self-Consistent Continuum Solvation in Electronic-Structure Calculations. *J. Chem. Phys.* **2012**, *136*, 064102.
(271) Sundararaman, R.; Letchworth-Weaver, K.; Arias, T. A. A Computationally Efficacious Free-Energy Functional for Studies of Inhomogeneous Liquid Water. *J. Chem. Phys.* **2012**, *137*, 044107.
(272) Letchworth-Weaver, K.; Arias, T. A. Joint Density Functional theory of the Electrode-Electrolyte Interface: Application to Fixed Electrode Potentials, Interfacial Capacitances, and Potentials of Zero Charge. *Phys. Rev. B* **2012**, *86*, 075140.
(273) Sundararaman, R.; Gunceler, D.; Arias, T. A. Weighted-Density Functionals for Cavity Formation and Dispersion Energies in Continuum Solvation Models. *J. Chem. Phys.* **2014**, *141*, 134105.
(274) Andreussi, O.; Marzari, N. Electrostatics of Solvated Systems in Periodic Boundary Conditions. *Phys. Rev. B* **2014**, *90*, 245101.
(275) Mathew, K.; Sundararaman, R.; Letchworth-Weaver, K.; Arias, T. A.; Hennig, R. G. Implicit Solvation Model for Density-Functional Study of Nanocrystal Surfaces and Reaction Pathways. *J. Chem. Phys.* **2014**, *140*, 084106.
(276) Sundararaman, R.; Goddard, W. A.; Arias, T. A. Grand Canonical Electronic Density-Functional Theory: Algorithms and Applications to Electrochemistry. *J. Chem. Phys.* **2017**, *146*, 114104.
(277) Mathew, K.; Kolluru, V. S. C.; Mula, S.; Steinmann, S. N.; Hennig, R. G. Implicit Self-Consistent Electrolyte Model in Plane-Wave Density-Functional Theory. *J. Chem. Phys.* **2019**, *151*, 234101.
(278) Sakong, S.; Naderian, M.; Mathew, K.; Hennig, R. G.; Groß, A. Density Functional Theory Study of the Electrochemical Interface Between a Pt Electrode and an Aqueous Electrolyte Using an Implicit Solvent Method. *J. Chem. Phys.* **2015**, *142*, 234107.
(279) Kastlunger, G.; Lindgren, P.; Peterson, A. A. Controlled-Potential Simulation of Elementary Electrochemical Reactions: Proton Discharge on Metal Surfaces. *J. Phys. Chem. C* **2018**, *122*, 12771−12781.
(280) Melander, M. M.; Kuisma, M. J.; Christensen, T. E. K.; Honkala, K. Grand-Canonical Approach to Density Functional Theory of Electrocatalytic Systems: Thermodynamics of Solid-Liquid Interfaces at Constant Ion and Electrode Potentials. *J. Chem. Phys.* **2019**, *150*, 041706.
(281) Hörmann, N. G.; Andreussi, O.; Marzari, N. Grand Canonical Simulations of Electrochemical Interfaces in Implicit Solvation Models. *J. Chem. Phys.* **2019**, *150*, 041730.
(282) Hörmann, N. G.; Reuter, K. Thermodynamic Cyclic Voltammograms Based on Ab Initio Calculations: Ag(111) in Halide-Containing Solutions. *J. Chem. Theory Comput.* **2021**, *17*, 1782−1794.
(283) Nattino, F.; Truscott, M.; Marzari, N.; Andreussi, O. Continuum Models of the Electrochemical Diffuse Layer in Electronic-Structure Calculations. *J. Chem. Phys.* **2019**, *150*, 041722.
(284) Sakong, S.; Groß, A. Methanol Oxidation on Pt(111) from First-Principles in Heterogeneous and Electrocatalysis. *Electrocatal* **2017**, *8*, 577−586.

https://doi.org/10.1021/acs.chemrev.1c00679
Chem. Rev. XXXX, XXX, XXX−XXX